

**STUDIES ON TWO PHOTON ABSORPTIONS
IN CERTAIN LASER DYES
USING PULSED PHOTOACOUSTICS AND
FLUORESCENCE TECHNIQUES**

P. SATHY

THESIS SUBMITTED
IN PARTIAL FULFILMENT OF THE REQUIREMENTS
FOR THE DEGREE OF
DOCTOR OF PHILOSOPHY

LASER DIVISION
DEPARTMENT OF PHYSICS
COCHIN UNIVERSITY OF SCIENCE AND TECHNOLOGY
KOCHI - 682 022
INDIA


1992

CERTIFICATE

Certified that the work presented in this thesis entitled "Studies on two photon absorptions in certain laser dyes using pulsed photoacoustics and fluorescence techniques" is based on the bonafide research work done by Ms.P.Sathy under my guidance, at the department of Physics, Cochin University of Science and Technology, and has not been included in any other thesis submitted previously for the award of any degree.

Cochin - 682 022
5-11-92




Dr. V P N Nampoori
Professor of Physics

DECLARATION

Certified that the work presented in this thesis entitled "Studies on two photon absorptions in certain laser dyes using pulsed photoacoustics and fluorescence techniques" is based on the original research work done by me under the guidance of Professor V P N Nampoori, Department of Physics, Cochin University of Science and Technology, and has not been included in any other thesis submitted previously for the award of any degree.

Cochin - 682 022
5-11-92


P. Sathy

PREFACE

Light and its various interactions with matter have been a subject of interest and fascination for mankind from the early stages of human civilization. As time passed on, various theories were proposed about the intrinsic nature of light many often leading to a better understanding of the phenomenon. Theoretical speculations on nonlinear optical phenomena had been initiated in the first half of the present century itself; however, it was only after the advent of lasers that experimental studies took a crucial turn. It was soon realized that this new branch of optics offered many prospects for exploration, and research work still goes on with ever increasing momentum in various laboratories around the world.

In general, interaction of light with matter depends on various parameters like intensity of light, nature of the molecules, their energy level structure etc. The electric dipole moment induced in a medium due to interaction with the electromagnetic field is given by the relation,

$$P = \chi_1 E + \chi_2 E^2 + \chi_3 E^3 + \dots$$

and the influence of higher order terms in the above expansion can be augmented by increasing the light intensity or selecting a proper medium with larger values of higher order coefficients. As compared to lasers, ordinary light sources suffer from the drawback of much lower bandwidth - throughput products. This

necessitates the use of lasers for observing nonlinear phenomena. Different terms in the above expansion give rise to distinct nonlinear effects; for example the term $\chi_2 E^2$ will give rise to second harmonic generation and parametric oscillation while $\chi_3 E^3$ to effects like two photon absorption, stimulated Raman scattering, Optical phase conjugation, four wave mixing etc.

The objectives of the present work are (a) an in-depth study of one of these nonlinear effects viz. the two photon absorption (TPA) process occurring in organic media and (b) development of the pulsed photoacoustic (PA) technique as an alternative to the nonlinear fluorescence (NLF) method for revealing multiphoton transitions occurring in these media. Laser dyes, due to their importance in the field of laser technology, are selected as samples for study.

A dye molecule, on irradiation by a light beam, absorbs a single photon or less frequently two or more photons provided the energy of the incident radiation is high and gets excited to a higher state. These excited states will subsequently relax through a combination of radiative and nonradiative pathways. The radiative part can be detected using the fluorescence technique and the nonradiative part by photoacoustic technique as it is a direct monitor of the nonradiative relaxation channel. Both methods can provide data on the nature of absorption, and the relative convenience of either method depends on certain external factors. One notes that in commercial and laboratory models of dye lasers, an implicit assumption is that losses due to nonlinear processes is a minimum during operation, which is

quite a good approximation. However this does not imply a complete absence of such phenomena in dyes, and the present work has been motivated from the fact that detailed investigations in this direction have been scarce in the past. In the course of this work we also had the opportunity to undertake a comparative evaluation of the relative capabilities of photoacoustic and fluorescence techniques for use in such studies. The thesis, in eight chapters, will describe the details of the work carried out and results obtained there from.

In the first chapter of the thesis a general introduction of the work is given. A detailed discussion on multiphoton excitation with special emphasis on two photon absorption (TPA) is presented. The utility of PA and NLF for probing the multiphoton excitation dynamics is discussed with relevant theory. Photophysical aspects and lasing characteristics of laser dyes are also discussed in this chapter.

The instrumental aspects of the work are discussed in the second chapter. The design and fabrication of the PA cell, transducer chamber and their calibrations are given. A description of the laser source and detection systems employed for the photoacoustic and fluorescence measurements is also included in this chapter.

The two dyes that are studied in detail are Rhodamine 6G (R6G) and Fluorescein belonging to the class of Xanthene dyes. Results of the PA investigations carried out using the 532 nm radiation from the frequency doubled Nd:YAG laser in these dye

solutions of various concentrations (ranging from 10^{-3} - 10^{-6} moles/lit) in different solvents (water, methanol and ethylene glycol) are discussed in chapters 3 and 4. The variation of the PA signal with pump flux for every concentration in each solvent has been observed. Based on our measurements we have identified two-photon absorption in these dyes, and the dependence of TPA excitation probability on the sample concentration and pump flux is unveiled. Qualitative discussion on the symmetry alterations of the fluorophore due to solute-solvent interactions is also given. Chapter 3 contains results obtained for R6G, and in chapter 4 the same for Fluorescien are given.

The nonlinear fluorescence (Antistokes Fluorescence) resulting from the $S_1 \rightarrow S_0$ transition, subsequent to TP excitation with the 1060 nm pump beam forms the core of chapter 5. Studies show that while photoacoustics is not an appropriate technique to detect TP absorption NLF proves to be very useful when infrared laser source is used as excitation source. An interesting aspect observed is the three photon transitions occurring in the dyes studied viz., R6G and Fluorescien which show a peculiar solvent dependence, details of which are also included in this chapter.

Chapter 6 is an account of experiments carried out to excite NLF from higher excited states of the dyes R6G, DCM and Fluorescien. Detection of NLF from higher excited states requires careful instrumentation to avoid the strong stokes emission from

entering the detector. The dyes are excited to the S_3 and S_2 levels using the 532 nm beam and 532+1060 nm beam of the Nd:YAG laser; however $S_3 \longrightarrow S_0$ transition could not be detected due to the sensitivity limitations of the equipment. $S_2 \longrightarrow S_0$ transitions have been recorded for the three dyes. When a fraction of 1060 nm photons is added to the 532 nm beam the probability of $S_0 \longrightarrow S_2$ transition is found to be enhanced.

Chapter 7 opens with a brief introduction of the various techniques generally used for calculation of fluorescence quantum yields. The lasing efficiency of a dye intimately depends on its quantum efficiency, and a relatively new method for this measurement employing the PA technique is discussed. The basic idea is to quench the fluorescence and measure the corresponding increase in PA signal. In our experiments R6G dissolved in water is taken as the sample. Concentration quenching has been applied. Satisfactory results have been obtained, which are discussed.

Chapter 8 is the concluding part of the thesis. An overview of the work is given in brief and the viability of the techniques (NLF and PA) for the analysis of higher order absorptions in organic media is outlined. Both methods are found to have certain merits and demerits which are discussed at length.

Part of the work presented in this thesis has been published/under publication in the form of the following journal papers :

- (1). Observation of two photon absorption in Rh6G using photoacoustic technique
P.Sathy, Reji philip, VPN Nampoore, CPG Vallabhan
Optics communications, 74 (5), 313 (1990)
- (2). Characteristics of two-photon absorption in methanol solutions of Rh6G using laser induced pulsed photoacoustics
Reji Philip, P Sathy, VPN Nampoore, Jacob Philip, and CPG Vallabhan
J. Phys. B : At. Mol. Opt. Phys., 25, 155 (1992)
- (3). Fluorescence quantum yield of Rh6G using pulsed photoacoustic technique
P.Sathy, Reji philip, VPN Nampoore, CPG Vallabhan
Pramana, J. Phys., 34, 585 (1990)
- (4). Effect of a fluorescing impurity on the characteristics of stimulated Raman scattering from acetone
P.Sathy, Reji Philip, VPN Nampoore, CPG Vallabhan
Pramana, J Phys., 38,(6), 673, (1992)
- (5). An experimental set-up for the study of pulsed laser induced acoustic signals in condensed matter
Reji Philip, P.Sathy, VPN Nampoore, Jacob Philip, CPG Vallabhan
J.Acoust.Soc.Ind.,16, (3&4), 223, (1988)
- (6). Beam profile characterisation of a high energy pulsed laser using photoacoustic technique
Reji philip, P.Sathy, VPN Nampoore, CPG Vallabhan
J.Acoust.Soc.Ind.,17, (3&4), 332, (1989)

- (7). Characteristics of Photoacoustic signal from methanol solutions of the laser dye Rhodamine 6G
Reji Philip, P.Sathy, VPN Nampoori, Jacob Philip and CPG Vallabhan
J.Acoust.Soc.Ind., 18, (3&4), 11 (1990)

- (8). Dependence of laser-induced ultrasonic pulse amplitude in dye solutions on concentration
P.Sathy, Reji Philip, VPN Nampoori, CPG Vallabhan
Journal of Pure and Applied Ultrasonics, 13, 24 (1991)

- (9). Photoacoustic observation of two photon processes in the laser dye Rhodamine 6G
P.Sathy, Reji Philip, VPN Nampoori, Jacob Philip and CPG Vallabhan
Proceedings of the National seminar on lasers in Engineering and Medicine, Nov.-Dec. 1989, Trivandrum, pp. 120-123

- (10). Characteristics of the photoacoustic signal at the lasing threshold of the laser dye Rhodamine 6G
P Sathy, Reji Philip, VPN Nampoori and CPG Vallabhan
(J.Acoust.Soc.Ind. - accepted for publication)

CONTENTS

Page No.

CHAPTER 1 INTRODUCTION

1.1	Absorption of light by matter	3
1.2	Two photon absorption - an outline of the theory	5
1.3	Laser dyes	9
1.4	Introduction to photoacoustics	12
1.5	Multiphoton absorption and PA generation	22
1.6	Detection of the acoustic signal	23
1.7	Introduction to Fluorescence	24
1.8	Laser action in fluorescent dyes	35
1.9	Summary	38
	References	39

CHAPTER 2 INSTRUMENTATION

2.1	Introduction	44
2.2	Photoacoustics	44
2.3	Fluorescence	53
2.4	Summary	60
	References	61

**CHAPTER 3 TWO PHOTON ABSORPTION IN
RHODAMINE 6G : INVESTIGATIONS
BY PULSED PHOTOACOUSTICS**

3.0	Introduction	63
3.1	Absorption and Fluorescence properties	64
3.2	Nonlinear absorption in dyes	68
3.3	Generation of photoacoustic signals in R6G - pumping by 532 nm	69
3.4	Experimental set up	70
3.5	Results	71
3.6	PA generation in R6G : pumping by 1060 nm	79
3.7	Conclusions	79
	References	81

**CHAPTER 4 TWO PHOTON ABSORPTION IN
FLUORESCIEN : INVESTIGATIONS
BY PULSED PHOTOACOUSTICS**

4.0	Introduction	83
4.1	Absorption and Fluorescence properties	85
4.2	Generation of PA signal in Fluorescien - pumping by 532 nm	86
4.3	PA generation in fluorescien : pumping by 1060 nm	91
4.4	Conclusions	91
	References	93

CHAPTER 5 MULTIPHOTON ABSORPTIONS IN XANTHENE
DYES USING 1060 nm RADIATION :



5.0	Introduction	94
5.1	Theory	95
5.2	Experimental set up	98
5.3	Results	99
5.4	Discussion	101
5.5	Conclusions	104
	References	105

CHAPTER 6 MULTIPHOTON ABSORPTIONS IN XANTHENE



6.0	Introduction	107
6.1	Excited state absorption	108
6.2	Experimental set up	112
6.3	Results	112
6.4	Discussion	114
6.5	Conclusions	116
	References	117

**CHAPTER 7 MEASUREMENT OF FLUORESCENCE QUANTUM
YIELD USING PHOTOACOUSTIC TECHNIQUE**

7.1	Conventional methods for the measurement of fluorescence quantum yields	119
7.2	Calorimetric methods	122
7.3	Photoacoustic method	124
7.4	Fluorescence quantum yield measurement of Rhodamine 6G using pulsed photoacoustic technique	126
7.5	Experimental Set up	127
7.6	Results and discussion	128
7.7	Conclusions	129
	References	131

CHAPTER 8 GENERAL CONCLUSIONS 133

CHAPTER - 1

INTRODUCTION

Interaction of light with matter depends on various parameters like intensity of light, nature of the molecules, structure and symmetry of their energy level etc. Basic understanding of the problem can be described in terms of the electric dipole moment induced in a medium due to interaction with electromagnetic field. In general, the induced dipole moment \vec{P} can be written as a function of the electric field associated with the electromagnetic radiation field;

$$\vec{P} = f(\vec{E}) \quad (1.1)$$

which, as a perturbation series can be written as,

$$\vec{P} = \chi^{(1)} : \vec{E} + \chi^{(2)} : \vec{E} \vec{E} + \chi^{(3)} : \vec{E} \vec{E} \vec{E} + \dots \quad (1.2)$$

The terms of the polarization in equation 1.2 higher than first order can be described as the non-linear part $(P)_{NL}$ so that one can write \vec{P} as,

$$\vec{P} = \vec{P}_L + \vec{P}_{NL} \quad (1.3a)$$

$$\text{where, } \vec{P}_L = \chi^{(1)} : \vec{E} \quad (1.3b)$$

$$\text{and } \vec{P}_{NL} = \chi^{(2)} : \vec{E} \vec{E} + \chi^{(3)} : \vec{E} \vec{E} \vec{E} + \dots \quad (1.3c)$$

The perturbation treatment demands the condition that the magnitudes of coefficients decrease as one goes for higher order terms in the above expansion. This means that the contribution to the induced dipole moment is mainly from the lower order terms. The influence of higher order terms can be augmented either by increasing the magnitude of \vec{E} , ie, the intensity of light, (because $I \propto |\vec{E}|^2$) or by selecting proper media with sufficiently large values of higher order coefficients. Whereas the first condition puts forward the restriction of keeping the intensity below the optical damage threshold of the medium, the second condition implies that only a selected class of materials reveal optical nonlinearities. Since the levels of light intensity available from ordinary light sources are very low, the higher order optical phenomena were surfaced only after the advent of coherent and intense optical sources viz., lasers.

The first term on the R.H.S. of the equation 1.2, when inserted in Maxwell's equations, gives the wave equation [1]

$$\nabla^2 \vec{E} - \frac{\partial \eta^2}{\partial c^2} \frac{\partial^2 \vec{E}}{\partial t^2} = \frac{\partial^2 \vec{P}}{\partial t^2} \quad (1.4)$$

Equation 1.4 gives rise to the familiar effects like diffraction, refraction, reflection etc., if one considers only the linear part of the polarization while the higher order terms will result in several nonlinear optical phenomena.

Considering the strength of interaction between the medium and the laser beam, one can describe various nonlinear phenomena resulting from each of the higher order terms. For

example; $\chi^{(2)} \vec{E}^2$ term will give rise to optical Second Harmonic Generation, parametric oscillation etc; while $\chi^{(3)} \vec{E}^3$ will reveal phenomena like two photon absorption, Stimulated Raman and Brillouin processes, Optical phase conjugation, Four wave mixing etc. Considering still higher order terms in equation 1.2, one encounters more of new exciting nonlinear effects. [1,2,3].

An important aspect of nonlinear optical phenomena worth noting is their dependence on the symmetry properties of atoms and molecules involved in the interaction. For example, the second order nonlinear processes occur only in materials which do not possess a centre of symmetry. Such a restriction is not applicable for third order terms. Obviously, materials which exhibit third order nonlinear phenomena will be much larger in number as compared to those showing second order effects.

The objective of the present work is a detailed investigation of one of the nonlinear optical effects, viz two photon absorption in certain Laser Dyes using pulsed photoacoustics (PA) and nonlinear fluorescence (NLF) as the tools. To make the thesis self contained, in the following sections we outline some of the basic aspects of light-matter-interactions. Detailed discussion on two photon process will be given in the subsequent sections of this chapter.

1.1 ABSORPTION OF LIGHT BY MATTER

The total energy (E_t) of a molecule (excluding translational energy and internal nuclear energy) is given by,

$$E_t = E_e + E_v + E_r \quad (1.5)$$

where (E_e) , (E_v) , (E_r) are the electronic, vibrational and rotational energies respectively. Optical absorption raises the molecules to a higher energy level E'_t , so that

$$E'_t = E'_e + E'_v + E'_r \quad (1.6)$$

where the primed terms indicate excited levels. If an absorption transition is defined as

$$\Delta E_x = E'_x - E_x$$

where $x = t, e, v$ or r , then for a typical molecule, [4]

$$\Delta E_r \approx 10 \text{ cm}^{-1}, \quad \Delta E_v \approx 10^3 \text{ cm}^{-1}, \quad \Delta E_e \approx 10^4 \text{ cm}^{-1}.$$

A state involving electronic and vibrational energy is referred to as a vibronic state, and a transition between two such states is a vibronic transition. Each vibronic energy change (ΔE_t) due to an optical absorption gives rise to an absorption band system, each band of which corresponds to different value of ΔE_v . An energy level diagram for a typical normal mode of vibration of a dye molecule is given in fig.1.1.

When the molecular system is irradiated by an intense light source (eg.laser), multiphotonic processes can occur, corresponding to the absorption of the same or different energies, and they may be absorbed at the same time or at different times. Thus in general, a two photon process can involve two distinct photons absorbed by the same molecule

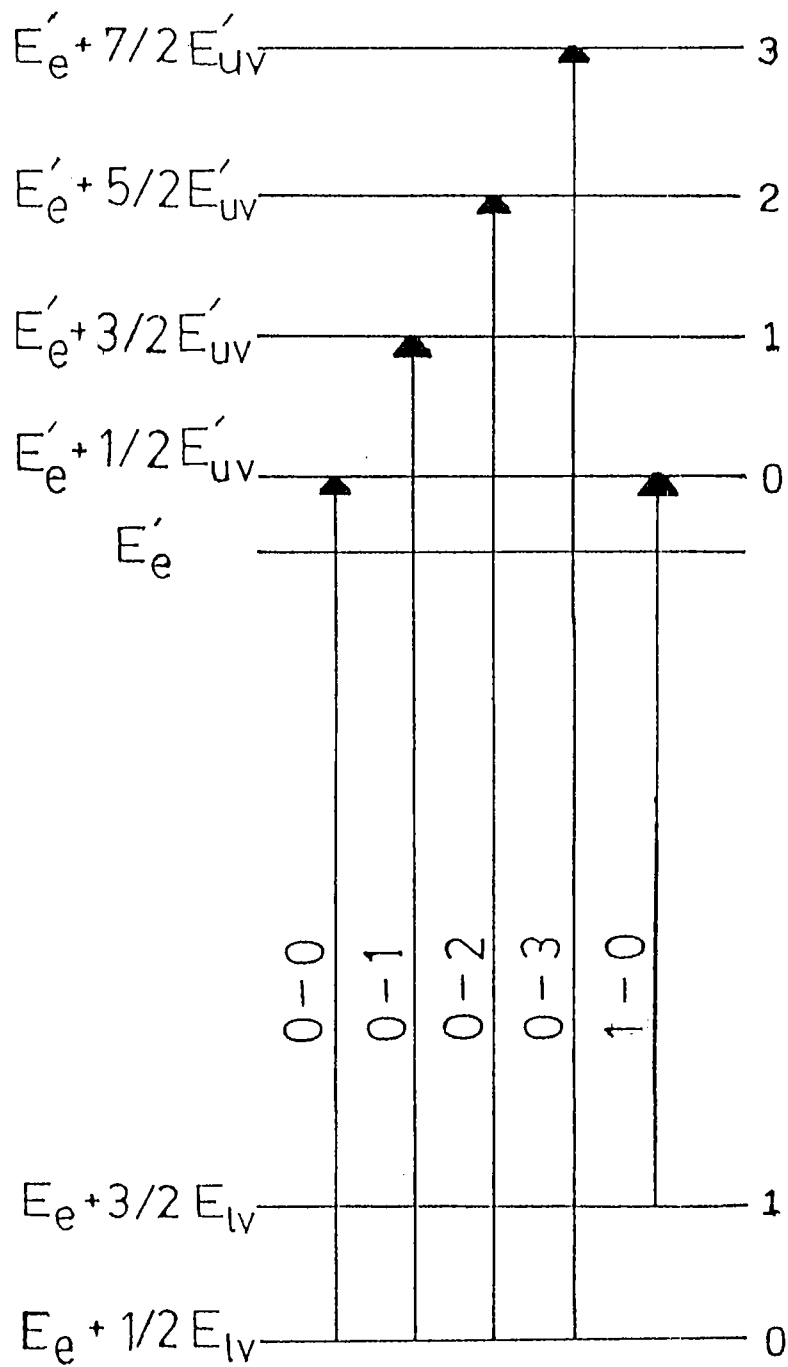


Fig.1.1. Vibronic absorption transitions. The 1-0 transition is a hot band.

E_{lv} - Energy of lower vibrational level

E_{uv} - Energy of upper vibrational level

simultaneously or in succession [5].

1.2 TWO PHOTON ABSORPTION - AN OUTLINE OF THE THEORY

The most general expression for the rate of energy absorption by matter in the presence of electromagnetic fields is given by:

$$\left\langle \frac{d}{dt} \left(\frac{\text{absorbed energy}}{\text{volume}} \right) \right\rangle = \langle \vec{j} \cdot \vec{E} \rangle \quad (1.7)$$

The current \vec{j} induced in the medium by the electromagnetic field includes the electric dipole, magnetic dipole and electric quadrupole polarizations. Each of these induced polarizations can be expanded in terms of a power series of the inducing (incident) electric/magnetic field, through nonlinear electric/magnetic susceptibilities. Hence the absorption coefficient, defined as

$$\alpha = \frac{d}{dt} \left(\frac{\text{absorbed energy}}{\text{volume}} \right) / \text{energy flux} \quad (1.8)$$

can be expanded into the nonlinear form

$$\alpha = \alpha(I) = \alpha^{(1)} + \alpha^{(2)} I + \alpha^{(3)} I^2 + \alpha^{(4)} I^3 + \dots \quad (1.9)$$

It can be seen that the linear (dipolar) absorption coefficient is given by the imaginary part of the linear dipole susceptibility χ_L'' :

$$\alpha = \alpha_L^{(1)} = \frac{4\pi\omega}{c} \chi_L'' \quad (1.10)$$

The magnetic dipole susceptibility also contributes to α_L , but only by a factor 10^{-5} less than the electric dipole susceptibility. There is no direct contribution of the second-order susceptibility to linear absorption.

The two photon absorption (TPA) coefficient is related to the imaginary part of the third order nonlinear susceptibility tensor $\chi_{NL}^{(3)}(\omega_1, \omega_2, -\omega_2)$. The absorption coefficient is obtained as [6]

$$\alpha^{(2)}(\omega_1) = \left(\frac{32 \pi^2 \omega_1}{c^2} \right) \chi_{NL}^{(3)}(\omega_1, \omega_2, -\omega_2) \quad (1.11)$$

In general, TPA is expected to arise from "resonant" contributions of the imaginary part of the third order dipole susceptibility for induced electric and magnetic dipoles and from a first order contribution of the imaginary part of the quadrupole susceptibility. Two photons are involved in this transition, whereas one-photon absorption (OPA) is caused by a transition via one photon from a ground state $|g\rangle$ to a final state $|f\rangle$.

The rate at which energy is absorbed per volume of the material system, i.e., $\langle (d/dt) (\text{absorbed energy} / \text{volume}) \rangle$, is given by the rate per species τ_{gf} at which a single transition $|g\rangle \rightarrow |f\rangle$ with absorption of a quantum $\hbar\omega$ takes place, times the density of species n_0 :

$$\left\langle \frac{d}{dt} \left(\frac{\text{absorbed energy}}{\text{volume}} \right) \right\rangle = \tau_{gf} \hbar \omega n_0 \quad (1.12)$$

For linear absorption we thus get using equation 1.8,

$$\alpha_L = \tau_{gf} \bar{h} \omega n_o / I \quad (1.13)$$

so that by comparing with equation (1.10), the transition rate τ_{gf} for electric dipolar transition is connected with the imaginary part of the susceptibility χ_L through

$$n_o \tau_{gf} = (4 \pi I / c \bar{h}) \chi_L'' \quad (1.14)$$

Similarly in the case of two photon absorption ($\bar{h}\omega = \bar{h}\omega_1 + \bar{h}\omega_2$) for electric dipolar transitions we have τ_{gf} related to the imaginary part of the nonlinear susceptibility tensor $\chi_{NL}^{(3)}$ in the following way [6]:

$$n_o \tau_{gf} = (32 \pi^2 / c^2 \bar{h}) I_1 I_2 \chi_{NL}^{(3)''} = (1/2\bar{h}) |E_1|^2 |E_2|^2 \chi_{NL}^{(3)''} \quad (1.15)$$

Transition rates for quadropole and magnetic dipolar transitions can similarly be connected with the corresponding susceptibilities. The detailed analysis of the theory of two-photon absorption using the perturbation theory is found in several articles [7]. The theory of multi-photon absorption transitions was initiated by Goeppert-Mayer [8], and it has been developed and applied specifically to aromatic hydrocarbons by Elveth and Peticolas [9], Pao and Rentzepis [10], Bebb and Gold [11], Hernandez and Gold [12], Pantell et al [13], and others.

1.2.1 TPA Spectroscopy and OPA Spectroscopy - certain features

In OPA, only a small fraction of the possible eigenstates

of matter can be explored, according to certain selection rules. In gases, many of the forbidden transitions are too weak to be detected by OPA while these can be successfully investigated by means of higher order absorptions. For one photon (OP) absorption only "allowed dipole transitions" can be studied in great detail in most circumstances. Hence only a small subset of the energy eigenstates of matter, namely those belonging to a particular symmetry group of the system are accessible to the OP technique, whereas allowed transitions in two-photon (TP) absorption cover a much wider range of symmetry types. Thus two photon spectroscopy is a better tool as compared to one photon spectroscopy for studying absorption properties in optically dense matter. Whereas the penetration range of light can be as small as $10^{-1} - 10^{-2}$ μm in OP absorption, due to the comparatively smaller two photon cross sections the TP absorption takes place almost uniformly through out a dense sample. Polarization studies in gases and liquids are difficult in one-photon absorption because of an averaging out of polarization effects. On the other hand two photon spectroscopy can identify the symmetry of eigenstates of matter in such experiments where the directions of polarization vectors of both the light beams can be independently varied. These advantages indicate that two photon spectroscopy is a successful alternative that can overcome the limitations of one photon absorption technique.

Various applications of TPA have been identified, such as the duration measurement of picosecond laser pulses by fluorescence trace analysis [14], the analysis of third harmonic generation process [15,16,17] etc. TPA may act as a power limiter in high power lasers [18,19,20]. Dye laser action was also

achieved by two photon excitation [21,22]. Multiphoton absorption phenomena are also found to be particularly useful for the investigation of coherence properties of a pump laser beam [23].

1.3 LASER DYES

Considering their extensive applications in laser technology, laser dyes have been selected for the present studies. An essential constituent of any laser is the amplifying medium which, in the case of a dye laser is a solution of organic dye. Organic dyes are compounds with conjugated double bonds which absorb light in the region extending from far ultraviolet to near infrared. The various classes of dyes and the region of the spectrum they cover are illustrated in fig.1.2 [24].

Frequency tunability in a specified range is the attraction of the dye laser and its fabrication is indigenously possible. The development of the dye laser has been closely associated with the discovery of new and better laser dyes. Eventhough various compounds were reported for use in dye lasers, a survey of approximately one thousand commercial dyes showed only four to be useful [25]. This clearly indicates that very special requirements must be met by a chemical compound to be qualified as a laser dye. Saturated organic compounds absorb at wavelengths less than 160 nm, but this energy being higher than the dissociation energy of most chemical bonds, photochemical decomposition may occur making such compounds not very suitable as laser dyes. The laser dye should have an absorption which matches the spectral distribution of the pump source. The long-wavelength absorption band of dyes is attributed to the

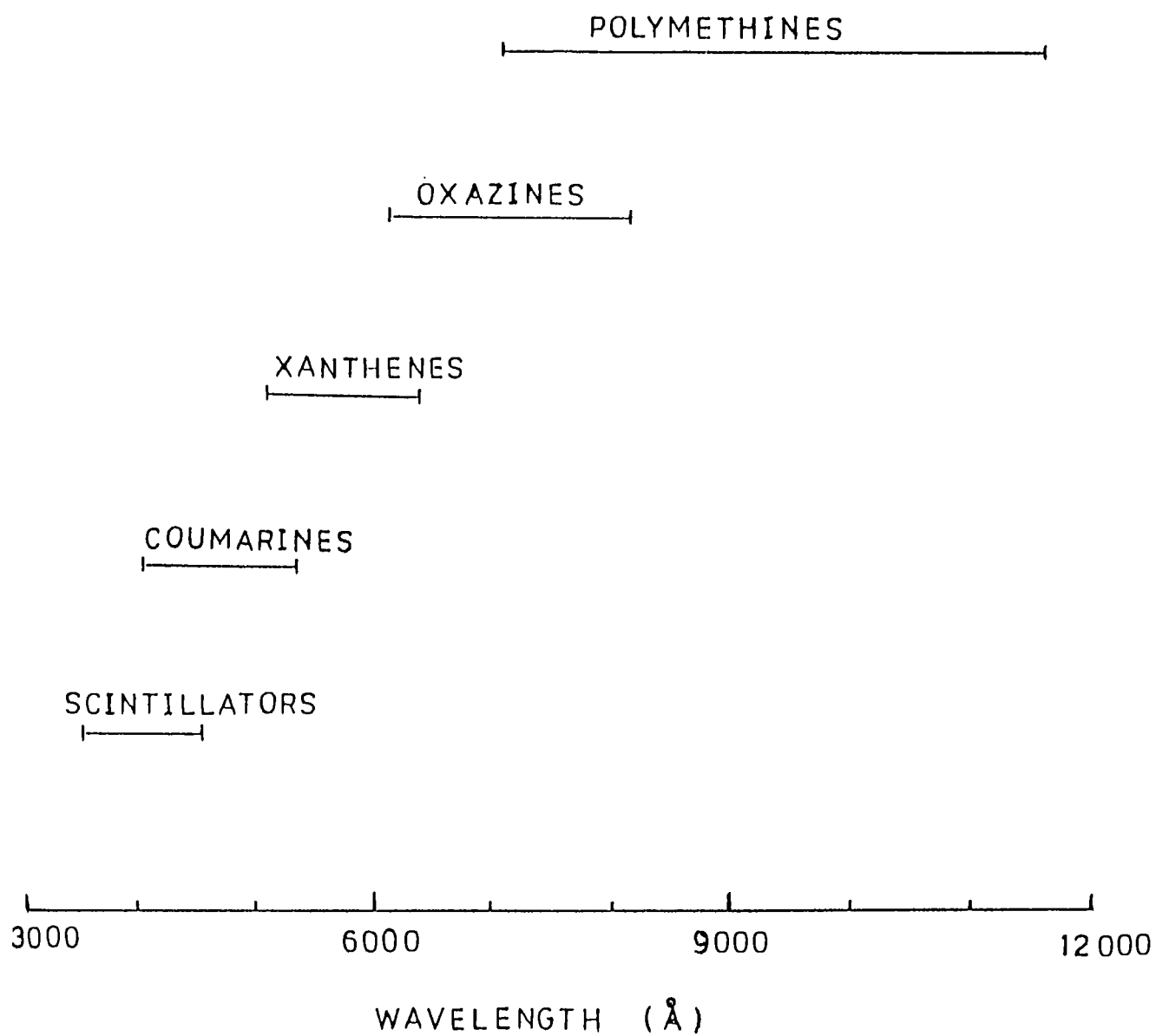


Fig.1.2. Wavelength tunability ranges for various important classes of organic dyes

transitions from the electronic ground state S_0 to the first excited singlet state S_1 . In an *ideal* laser dye the nonradiative processes like internal conversion and intersystem crossing (described in the following sections) should be negligible, so that the quantum yield of fluorescence has the highest possible value, 1. Table 1.1 shows the quantum yields of certain laser dyes [26]. An efficient laser dye in its first excited singlet state should have negligible absorption of the pump and emission wavelengths. The thermal and photochemical stability of dyes is of utmost importance for laser applications. These properties, however, vary so widely with the almost infinite variety of chemical structure, such that practically no general valid rules can be formulated.

1.3.1 Optical interaction in dyes

The energy levels of a typical organic dye in solution and the processes connecting the various electronic states on light absorption are shown in fig.1.3. Each electronic level is a band composed of a continuum of vibrational and rotational levels. When the dye molecules are pumped optically, they are excited to some higher level in a singlet manifold. Some of the processes taking place subsequent to optical excitation from the ground state are discussed below :

(i). Vibrational relaxation : Absorption of a photon by the dye molecule will excite it to a vibrational level in a higher singlet which is called the Franck-Condon (FC) state. This is followed by a rapid relaxation (10^{-14} to 10^{-13} s in non-viscous solvents) to the lowest vibrational level of the singlet

TABLE - 1.1

QUANTUM YIELDS OF A FEW DYES [26]

Compound	Solvent	Useful range (nm)	λ_{fluor} (nm) λ	Excitation (nm)	ϕ_f (+ 0.02)
Fluorescien	0.1 N NaOH	435-515	532.5	488	0.90
Rhodamine 6G	H ₂ O	470-555	565	546	0.81
Acridine yellow	methanol	410-480	517	436	0.57
Rhodamine 6G	methanol	470-555	573	488	0.86
Cresyl violet	methanol	570-635	623	578	0.55
Methylene blue	methanol	570-680	710	633	0.03
Coumarin I	ethanol	320-410	460	404	0.64
Acridine yellow	ethanol	410-480	517	436	0.47
Cresyl violet	ethanol	510-635	623	546	0.5

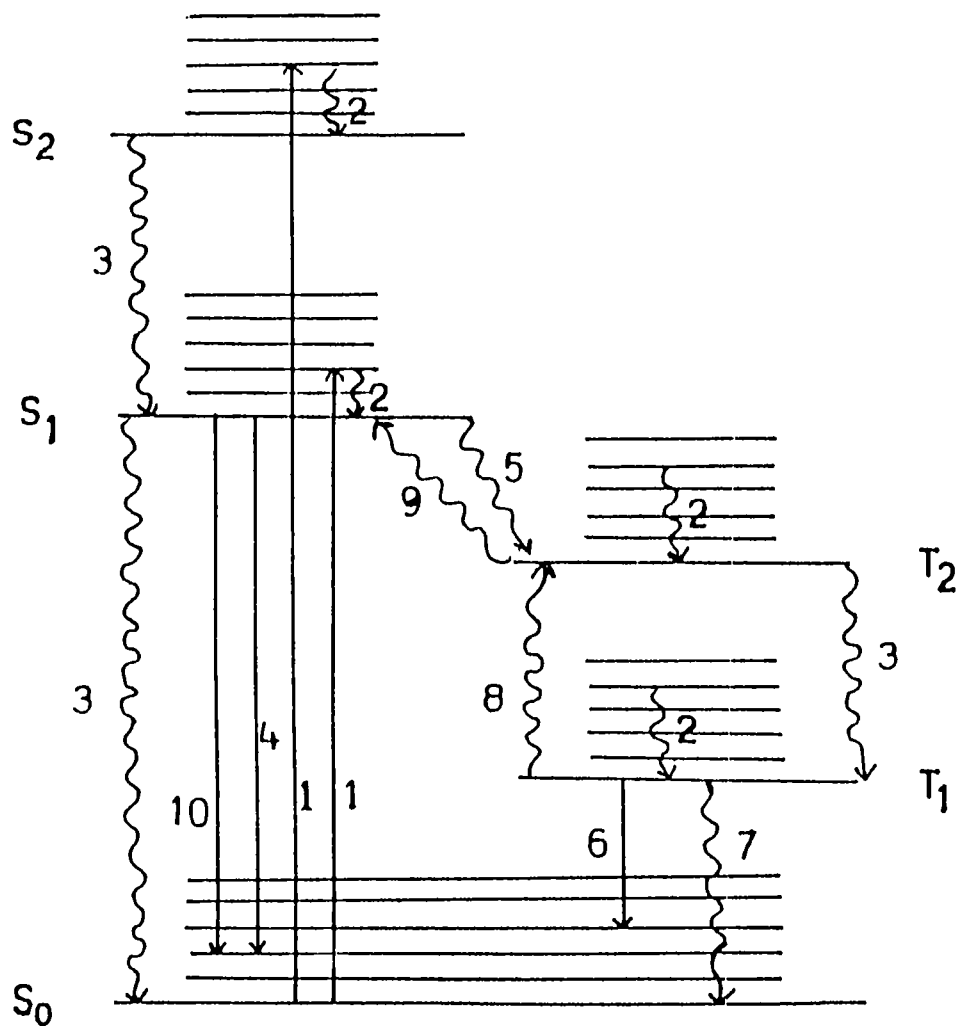


Fig.1.3. The Jablonski diagram for light absorption and the processes connecting different levels in a dye molecule. (1).Absorption, (2).Vibrational relaxation (3).Internal relaxation (4).Fluorescence (5).Intersystem crossing (6).Phosphorescence (7).Quenching (8).Vibrational reactivation (9).Reverse intersystem crossing (10).Delayed fluorescence

manifold, without changing the electronic energy. The mechanism of this process is a collision-like interaction in liquid phase and as a result the excited molecule attains thermal equilibrium with the environment.

(ii). Internal conversion: It is the deactivation process in which the electronic excitation energy is dissipated as thermal energy by collision with another (usually solvent) molecule. This non radiative transition occurs between different electronic states.

(iii). Fluorescence: The emission of optical radiation, which results in a transition of the molecule from an excited state, usually the first excited singlet S_1 , to the singlet ground state S_0 is called fluorescence which occurs typically with a half-life of about 10^{-9} to 10^{-8} sec.

(iv). Intersystem crossing and phosphorescence: Another competitive de-excitation process that can take place is the generally forbidden transition called intersystem crossing, in which there is a change of spin. This occurs through spin-orbit coupling, in which, states with different spin angular momenta and orbital angular momenta mix slightly because they have the same total angular momentum. The loss of energy from the lowest triplet to the ground state may occur by a radiative process called phosphorescence. Since the emission is from a metastable state, phosphorescence lifetimes are large.

Depending on the structure of the dye molecule and its environment, the non radiative processes (internal conversion and

intersystem crossing) compete effectively with the light emission and thus reduce the fluorescence efficiency.

1.3.2 Higher order absorption in dyes

With high pump energies it is possible to excite dye molecules to higher singlets (S_2 , S_3 etc.), followed by a fast relaxation to the S_1 level. The $S_n \rightarrow S_1$ transitions ($n > 1$) have a very strong non radiative character, yielding high amplitude PA signals. This nonradiative de excitation releases thermal energy to the surroundings of the molecule. A modulated light beam will thus induce modulated thermal agitations in the medium, which will in turn generate pressure waves that can be detected by acoustic transducers. On the other hand, radiative de-excitation from S_n to lower levels will give rise to fluorescence emission at a shorter wavelength than the pump wavelength. Such fluorescence emission is termed as nonlinear fluorescence (NLF) or antistokes fluorescence (ASF). However since NLF has a very low probability in $S_n \rightarrow S_1$ transitions, it is generally difficult to probe the higher excitation dynamics in dye molecules by this method. But, as we will see in the following chapters, NLF is ideal for the analysis of $S_1 \rightarrow S_0$ two-photon induced transition. In the following sections we will discuss the basic principles of PA and fluorescence spectroscopy and their applications to the understanding of molecular structure.

1.4 INTRODUCTION TO PHOTOACOUSTICS

Light absorbed by a sample will excite a fraction of the ground state molecular population into higher energy levels.

These excited states will subsequently relax through a combination of radiative and non radiative pathways. Photoacoustic detection is unique in that it is a direct monitor of the non-radiative relaxation channel.

The photoacoustic (PA) effect is the phenomenon of acoustic wave generation in a medium resulting from the absorption of photons. It was discovered by Alexander Graham Bell in 1880 who observed that audible sound is produced when chopped sunlight was incident on optically absorbing materials [27]. The technique saw few applications until about 1968 when an upsurge in its use began due to the availability of laser sources. It has since been used to study a variety of chemical and physical phenomena in a number of fields. With intense pulsed lasers it is possible to observe nonlinear interactions of electromagnetic radiation with matter. PA detection of several nonlinear optical processes have been reported, including two photon (and higher order) electronic absorption [28], infrared multiphoton absorption [29-35] and stimulated scattering [36-41]. Laser can operate as the source and detector of the acoustic waves, and different laser units are used in the coherent analysis of signals in multichannel acoustic data systems.

The basic theory behind PA detection is quite simple. On excitation of the molecule and subsequent de-excitation, the non radiative component will ultimately generate heat in the localized region of the excitation light beam creating a pressure wave that propogates away from the source. The pressure wave is then detected with a suitable sensor such as a microphone or a transducer.

1.4.1 Generation of Photoacoustic signal

The mechanisms of sound generation by the interaction of laser radiation with matter are diverse. In principle, there are five important interaction mechanisms which are responsible for the generation of acoustic waves : dielectric breakdown, vaporization or material ablation, thermoelastic process, electrostriction and radiation pressure. Their contribution depends on the parameters of the incident laser beam as well as on the optical and thermal properties of the medium.

Dielectric breakdown occurs only at laser intensities above $\approx 10^{10} \text{ W cm}^{-2}$ which can quite easily be obtained from a pulsed laser when focussed by a lens. This effect has been investigated experimentally and theoretically in detail for gases [42-45], liquids [46-48] and solids [42,49]. The plasma production related to dielectric breakdown produces a shock wave which propagates initially at supersonic speed in the medium. Dielectric breakdown is the most efficient process for converting optical energy into acoustic energy, with conversion efficiency (η) reaching upto 30% in liquids. This process dominates the interaction at high laser intensities, especially in transparent media where sound generation due to ordinary absorption does not occur.

Material ablation in solids or explosive evaporation in the case of liquids is responsible for the acoustic wave generation if the laser energy density within the absorbing volume of the sample exceeds a certain threshold determined by the thermal properties of the medium. For liquids η in this case

can reach value $\approx 1\%$ [50].

For absorbing media the thermoelastic process is important for sound generation. This process is based on the transient heating of a restricted volume by the absorbed laser energy. The induced temperature gradient produces, as a result of thermal expansion, a strain in the body. This causes an acoustic wave propagating away from the heated zone. The thermoelastic process (heating without phase change) dominates the excitation of sound in absorbing matter at laser energies below the vaporization threshold. Although the conversion efficiency η is rather low, (typically $< 10^{-4}$ for liquids [50,51]), this process has found interesting applications in photoacoustic spectroscopy as a sensitive method for the measurement of small absorptions in solids, liquids, and gases [52]. For example, Patel and Tam [66] have measured absorption coefficients $\approx 10^{-6}$ in liquids, using pulsed photoacoustics.

Electrostriction is always present due to the electric polarizability of molecules in the sample, which causes them to move into or out of regions of higher light intensity depending on whether the polarizability is positive or negative. These motions produce a density gradient and, consequently a sound wave similar to that caused by the thermoelastic process [53]. Electrostriction as a sound generation mechanism is only important in very weakly absorbing media where it may limit the PA detection sensitivity. However by suitable time gated detection of the acoustic signal, suppression of electrostrictive component is possible.

In comparison to other sound generating mechanisms radiation pressure itself is negligible. The amplitude of radiation pressure is given by $p = I/c$, where I is the laser intensity and c the light velocity in vacuum. For a laser intensity of 10^6 W cm^{-2} one obtains $p = 0.3 \text{ mbar}$ compared to a few bars in the case of thermoelastic sound generation under identical conditions.

It may be mentioned here that there are three more mechanisms of acoustic generation which are considered only under specific circumstances: they are (i). photochemical effects (ii). molecular dissociation and (iii). bubble formation.

PA generation can also be classified according to the two types of excitation modes : the continuous wave (cw) modulation mode, whereby the excitation beam is modulated near 50% duty cycle, and the pulsed mode, whereby the excitation beam is of very low duty cycle but high peak power (fig.1.4). In the cw case, the signal is typically analysed in the frequency domain; amplitude and phase of one or several Fourier components are measured and narrow-band filters can be used to suppress noise. Under circumstances when random noise dominates, cw modulation detection is frequently preferable. In the pulsed technique, the signal is acquired and analysed in the time domain, and simple gating techniques make noise suppression possible. When systematic noise (like noise due to window, PA cell wall, or substrate absorption) dominates in the experimental system pulsed PA detection is usually preferred.

In pulsed PA measurements, the excitation pulse is

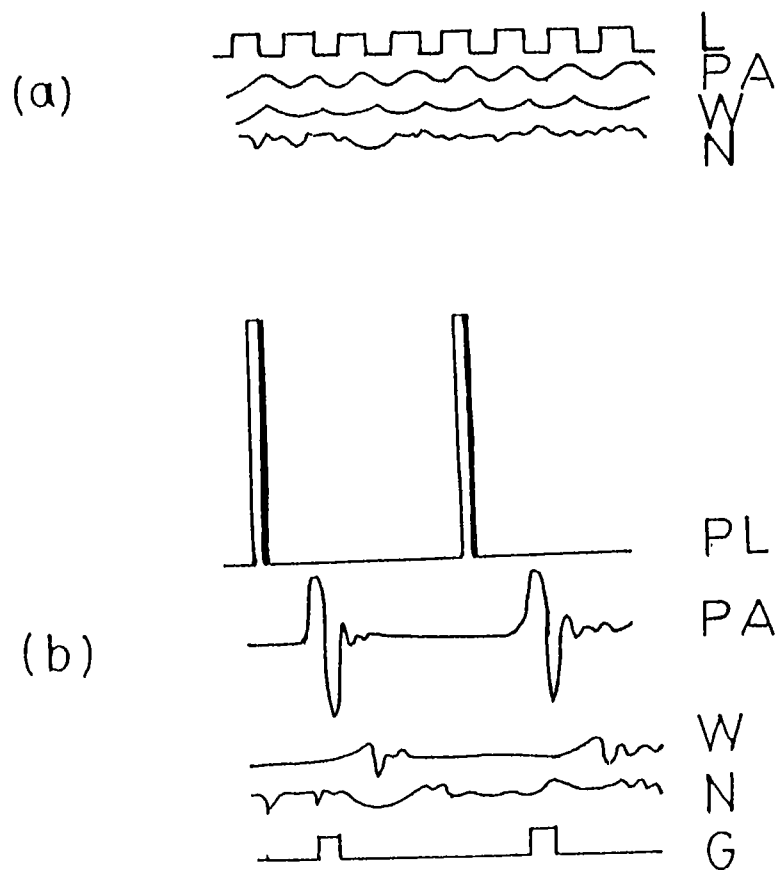


Fig.1.4. Schematic comparison of pulsed and cw modulation techniques in PA detection. (a) cw modulated (b) Pulsed.

L - Modulated light, PL - Pulsed light, PA - Photoacoustic signal, W - Window signal, N - Electromagnetic interference and mechanical resonances or background vibrations D - Detection gate

typically short ($< \mu$ sec) and the acoustic propagation distance during the excitation pulse is typically much smaller than the dimension of the sample; hence, in most cases, the PA pulse shape is independent of the boundary reflections and the sample can often be treated as infinite in extent. In cw modulated PA measurements, the modulation frequency is typically in the $10 - 10^3$ Hz regime.

There are a few factors that make pulsed PA technique preferable to the cw scheme, the most important of which is the inherent higher sensitivity obtained in the former case. A comparison of the two techniques is given in table 1.2.

1.4.2 Theory of Pulsed PA

The generation of a photoacoustic signal relies on the conversion of optical radiation into heat through non radiative relaxation processes. Numerous authors have treated the problem of acoustic generation in a liquid arising from the absorption of a light beam whose intensity varies with time. The case of low optical absorption due to a pulsed excitation resulting in a cylindrical wave has been studied by a few authors [55,56,57]. The thermoelastic generation of spherical or plane acoustic waves in strongly absorbing liquids by pulsed radiation also has been investigated by various authors [58-65]. Here we present the theoretical formulation for calculating the pulsed photoacoustic signal amplitude generated in a weakly absorbing liquid. Absorption of laser radiation along a long, thin liquid column is assumed.

TABLE 1.2

Comparison of cw modulated and pulsed PA techniques [54]

	cw modulated	Pulsed
Modulated intensity	high duty cycle low peak power	low duty cycle high peak power
Acoustic detection	low frequency transducer and lock-in detector usually used	high frequency transducer and boxcar or transient recorder usually used
PA generation efficiency	low	high
Thermal diffusion effects	may be important	usually negligible
Acoustic boundary conditions	important	unimportant
Unmodulated back- ground heating	usually substantial	usually small

Let the laser illumination be provided by a pulsed laser producing pulses of duration τ_p at a repetition rate of f . It is assumed that laser pulse length is longer than the non radiative relaxation time τ_{NR} . For long pulses, ie, τ_p in the microsecond region, the time τ_a for an acoustic pulse to travel across the laser illuminated region in the liquid is less than τ_p , ie.,

$$\tau_p > 2R/v_a = \tau_a \quad (1.16)$$

where v_a is the acoustic velocity in the medium. The rise in temperature of the illuminated volume for weak absorptions of the liquid due to laser irradiation is given by, [66]

$$\Delta T = \frac{E_0 \alpha}{\pi R^2 C_p \rho} \quad (1.17)$$

where E_0 is the input pulse energy, R is the radius of laser beam, α is the absorption coefficient, C_p is the isobaric heat capacity per gram and ρ is the density. The pressure wave created in the system produces a change in pressure, as

$$p = \text{constant} \cdot \frac{\beta v_a}{C_p} E_0 \alpha \quad (1.18)$$

The output voltage V from the acoustic transducer is proportional to p :

$$V = \text{constant} \times p$$

so that,

$$V = K' \frac{\beta v_a}{C_p} E_0 \alpha \quad (1.19)$$

where β is the isobaric compressibility $(\frac{1}{V}) (\frac{-V}{T})_p$ and K' is a constant that includes the geometrical parameters as well as the response properties of the piezoelectric transducer.

In the case of nanosecond excitation, the heated volume of the sample does not undergo a quasi-isobaric expansion and $\tau_p < \tau_a$. The perturbation in temperature due to laser heating is now given by,

$$\Delta T = \frac{E_0 \alpha}{\rho C_v} \quad (1.20)$$

Here C_p (of eqn. (19)) is replaced by C_v because now the heating of laser excited volume takes place at constant volume rather than constant pressure. The pressure change caused by absorption of the pulsed radiation now becomes [67]

$$p = \text{constant.} \frac{\beta v_a^2}{C_p} E_0 \alpha \quad (1.21)$$

so that the output voltage from the acoustic transducer is given by

$$V = K' \frac{\beta v_a^2}{C_p} E_0 \alpha \quad (1.22)$$

The normalised photoacoustic signal S is written as

$$S = \frac{V}{E_0} = K \alpha \quad (1.23)$$

where

$$K = K' \frac{\beta v_a^2}{C_p} \alpha \quad (1.24)$$

Thus a measurement of the normalised photoacoustic signal for a given system gives direct information regarding the absorption coefficient α . The scaling parameters under different conditions are as given below [67]:

$$\begin{aligned} (1). \text{ For } \tau_p \gg \tau_a ; \quad K(\tau_p) &= \frac{\beta v_a}{C_p} \\ (2). \text{ For } \tau_p \ll \tau_a , \tau_r \ll \tau_a ; \quad K(\tau_r) &= \frac{\beta v_a^2}{C_p} \\ (3). \text{ For } \tau_p \ll \tau_a , \tau_r \gg \tau_a ; \quad K(\tau_a) &= \frac{\beta v_a^2}{C_p} \frac{Z_{abs}}{Z_{abs} + Z_{PZT}} \end{aligned} \quad (1.25)$$

Obviously, the time delay between the laser pulse and the arrival of the pressure pulse at the piezoelectric transducer at a distance r from the laser illuminated cylinder is given by $\tau_d = r / v_a$, where v_a is the acoustic velocity in the medium.

The thermoelastic generation of spherical or plane

acoustic waves in strongly absorbing liquids using a pulsed laser has been treated by Sigrist and Chen [68]. Under certain assumptions (homogeneous, isotropic and inviscous medium, neglect of heat diffusion, rate of thermal expansion small with sound speed etc) we consider the regime of surface heating, ie, the generation of plane acoustic waves, which implies that $2a \gg 1/\alpha$ where $2a$ is the laser beam diameter and α is the absorption coefficient. We further assume that the absorption length $1/\alpha$ is much shorter than the sound propagation distance during the laser pulse duration τ_L , ie, $(\alpha)^{-1} \ll c_0 \tau_L$. Now for a laser pulse shape approximated by the equation

$$f(\theta) = \begin{cases} 0 & \text{for } \theta < 0 \\ \theta^3 \exp [3(1-\theta)] & \text{for } \theta \geq 0 \end{cases} \quad (1.26)$$

where $\theta = t/t_R$ is the time normalized by the risetime t_R of the laser pulse, the peak acoustic pressure p^{\max} for a free and rigid boundary are respectively given by

$$p_r^{\max} \propto \beta I_0 c_0 / C_p \quad (1.27a)$$

and

$$p_f^{\max} \propto \frac{\beta I_0}{\alpha \tau_R C_p} \quad (1.27b)$$

where the subscripts r and f stand for rigid and free boundaries respectively. Here I_0 is the laser intensity, C_p is the specific heat at constant pressure of the liquid, c_0 is the acoustic wave velocity, τ_R is the risetime of the laser pulse, and β is the thermal expansion coefficient. According to equations 1.27a and 1.27b, the PA signal is independent of α for rigid boundaries and

proportional to $1/\alpha$ for free boundaries.

Several groups have investigated the thermoelastic source at a liquid surface theoretically, and the properties of the generated acoustic pulse as a function of the laser pulse profile, laser pulse duration etc have been derived [69,70,71,72].

1.5 MULTIPHOTON ABSORPTION AND PA GENERATION

Pulsed lasers are generally used to observe multiphoton absorption in various media because of the high light intensity required. Multiphoton PA spectroscopy, together with multiphoton ionization spectroscopy and multiphoton luminescence spectroscopy are all highly sensitive methods suitable for studying high-lying molecular excited states or other states that are not accessible in a one-photon transition. In a typical experiment done by Cox [35] on SF_6 - Ar mixture using a CO_2 laser it was found that, at low intensity, the pulsed PA signal S increased linearly with the beam intensity I , as expected for linear absorption. At intermediate I , S was proportional to \sqrt{I} , indicating optical saturation of an inhomogeneously broadened absorption. At large I rapid increase of S with I was observed, showing the occurrence of multiphoton absorption.

Several other workers have performed work on multiphoton absorption spectroscopy with PA detection, like Fukumi [73] in ethylene, Brenner et al [74] in propynal, Webb et al [28] in symtriazine, Weulersse and Geneir [75] in CF_3I , Chin et al [76] in gases, and Bass et al [77] and Bae et al [78] in solids. In

their pioneering experiments, Tam and Patel [79] measured the two photon absorption cross-sections in liquids like benzene for the first time.

1.6 DETECTION OF THE ACOUSTIC SIGNAL

The acoustic detector has an important role in PA spectroscopy. The gas-microphone detector for PA signals has been found to be very good in many applications, particularly at low modulation frequencies. However, when one is dealing with large samples, or samples of low surface/volume ratio or samples in which heat flow is only a small fraction of the total heat flow generated within the sample the gas microphone technique proves to be inadequate. Eventhough a piezoelectric transducer is about two orders of magnitude less sensitive than condenser and electret microphones for a given pressure, it is the appropriate detector in such situations, as we will see shortly. (More details of PA signal detection are given in chapter 2).

In an experimental set-up for PA studies acoustic impedance matching has to be maintained between the acoustic source and detector, to ensure efficient coupling of acoustic energy between them. Acoustic impedance Z_a of a medium is given by ρc_o where ρ is the density and c_o is the sound velocity. For most solids, Z_a is in the range of 10^6 g/cm² sec, while for liquids it is about 10^5 g/cm² sec and for gases, 10^2 g/cm² sec. The transmission coefficient of an acoustic wave in a gas going through a solid-gas interface is given by [80]

$$(1 - R) = \frac{4 (Z_{a g}) (Z_{a s})}{[(Z_{a g}) + (Z_{a s})]} \approx 10^{-4} \quad (1.28)$$

where $(Z_{a g})$ is the acoustic impedance of the gas and $(Z_{a s})$ that of the solid.

Similar calculations show that $(1-R)$ for a liquid-solid interface is $\approx 10^{-1}$ and that for solid-solid is ≈ 1 . Thus a piezoelectric transducer is preferable to a gas-microphone detector for observing thermally generated pressure or acoustic fluctuations in condensed matter. Furthermore, piezoelectric sensors can operate at much higher frequencies than microphones, which makes them especially suitable for pulsed PA detection.

1.7 INTRODUCTION TO FLUORESCENCE

When the dye molecules are pumped optically they are excited to some of the higher levels in the singlet manifold, from which they relax within picoseconds (nonradiatively) to the lowest vibronic level of the first excited singlet state S_1 . Fluorescence emission, typically with a half-life of about 10^{-9} to 10^{-8} sec, occurs from here. Fluorescence is generally observed from the lowest excited state of the singlet manifold, since this is the only state in the manifold with a lifetime longer than the time required for the various collision-dependent relaxation and conversion processes.

1.7.1 The Franck-Condon Principle

The potential energy diagram of a diatomic molecule plots the total (electronic and vibrational) energy of the molecule as a function of the nuclear separation r , and the wavefunctions Φ of the vibrational modes approximate to those of a harmonic oscillator (fig.1.5). A similar diagram of E_t and E_t' against a nuclear configuration coordinate Q can be used for the qualitative discussion of more complex molecules, such as the aromatic hydrocarbons, although Q no longer corresponds simply to r .

The *Franck-Condon principle* states that, because the time required for an electronic transition is negligible compared with that of nuclear motion, the most probable vibronic transition is one which involves no change in the nuclear coordinates. This transition, which is referred to as the *Franck-Condon maximum*, represents a vertical transition on the potential energy diagram. In quantum mechanical terms, the Franck-Condon maximum corresponds to maximum overlap between the ground-state vibrational wavefunction and the excited state vibrational wavefunction.

The envelope of the vibronic bands of an absorption band system is referred to as *Franck-Condon envelope*, and its maximum corresponds to the Franck-Condon maximum. This approximates to the position of the most intense vibronic absorption band. If the latter is the 0-0 transition, as in the case of $S_0 \longrightarrow S_1$ absorption of many aromatic hydrocarbons, this indicates that the mean nuclear configuration of the excited electronic state is

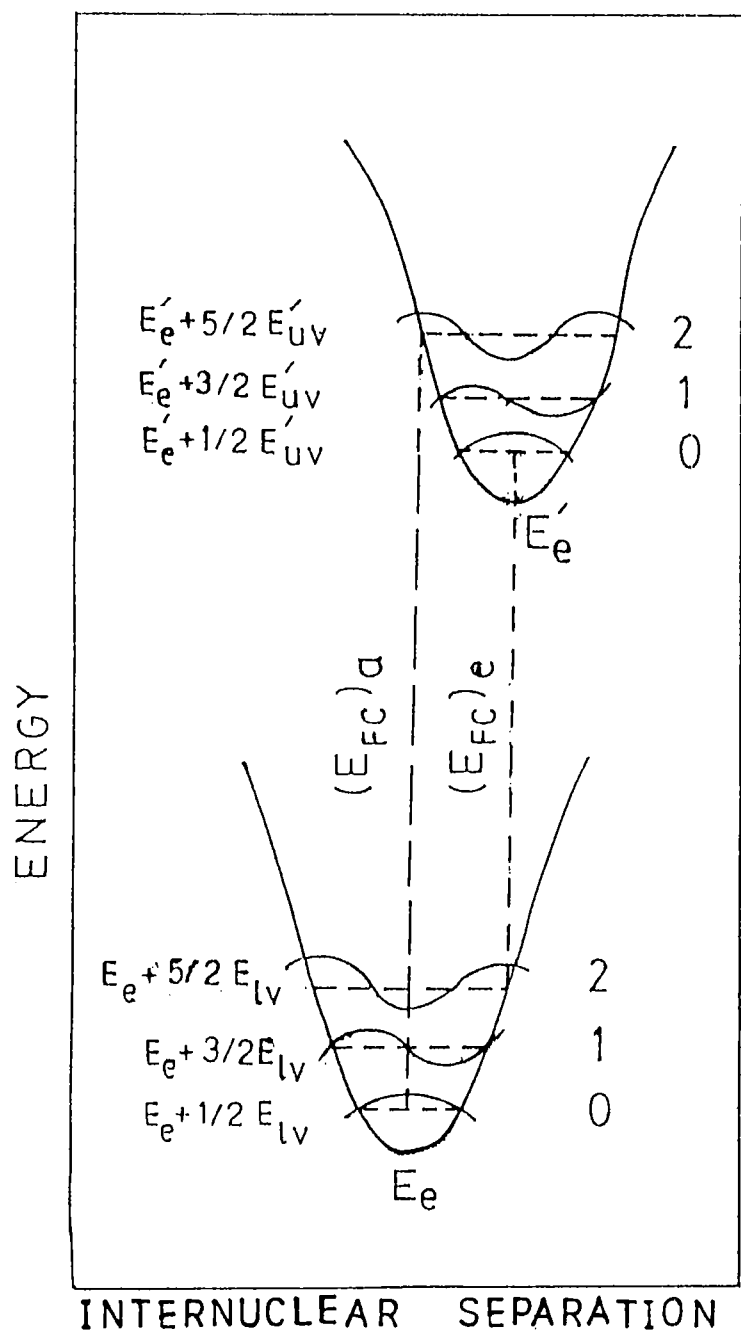


Fig.1.5. Schematic potential energy diagram of a diatomic molecule, showing vibrational wavefunctions of ground and excited electronic states

$(E_{FC})_a$ - Franck-Condon maximum in absorption

$(E_{FC})_e$ - Franck-Condon maximum in emission

similar to that of the ground state.

Information about the nuclear configuration of an electronic excited state and its vibrational modes can be obtained from an analysis of the vibronic structure and the Franck-Condon envelope of the absorption band system, since the latter represents the 'vertical transform' of the ground state zero-point wavefunction.

At room temperature absorption takes place from the lowest vibrational level of the ground state and emission from the lowest vibrational level of the first excited state, making only the 0-0 transition common to both absorption and emission spectra. Frequently the emission spectrum is an approximate mirror-image of the first absorption band because the distribution of vibrational levels in the first excited state, which determines the shape of the first absorption band, is often similar to the distribution of vibrational levels in the ground state, which determines the shape of the fluorescence emission spectrum (fig 1.6). According to *Stoke's law*, the wavelength of fluorescence is always longer than that of the exciting light. However at room temperature a very small proportion of the molecules will be thermally excited to the lower vibrational levels of the ground state and can therefore undergo the transition $0 \leftarrow 1$ which would then be expected to appear in the absorption spectrum as a very weak band. In practice such a band is usually too weak to be observed in the absorption spectrum, but by taking special precautions it is possible to excite molecules at this wavelength and to observe emission corresponding to the $0 \rightarrow 0$ transition, which is of shorter

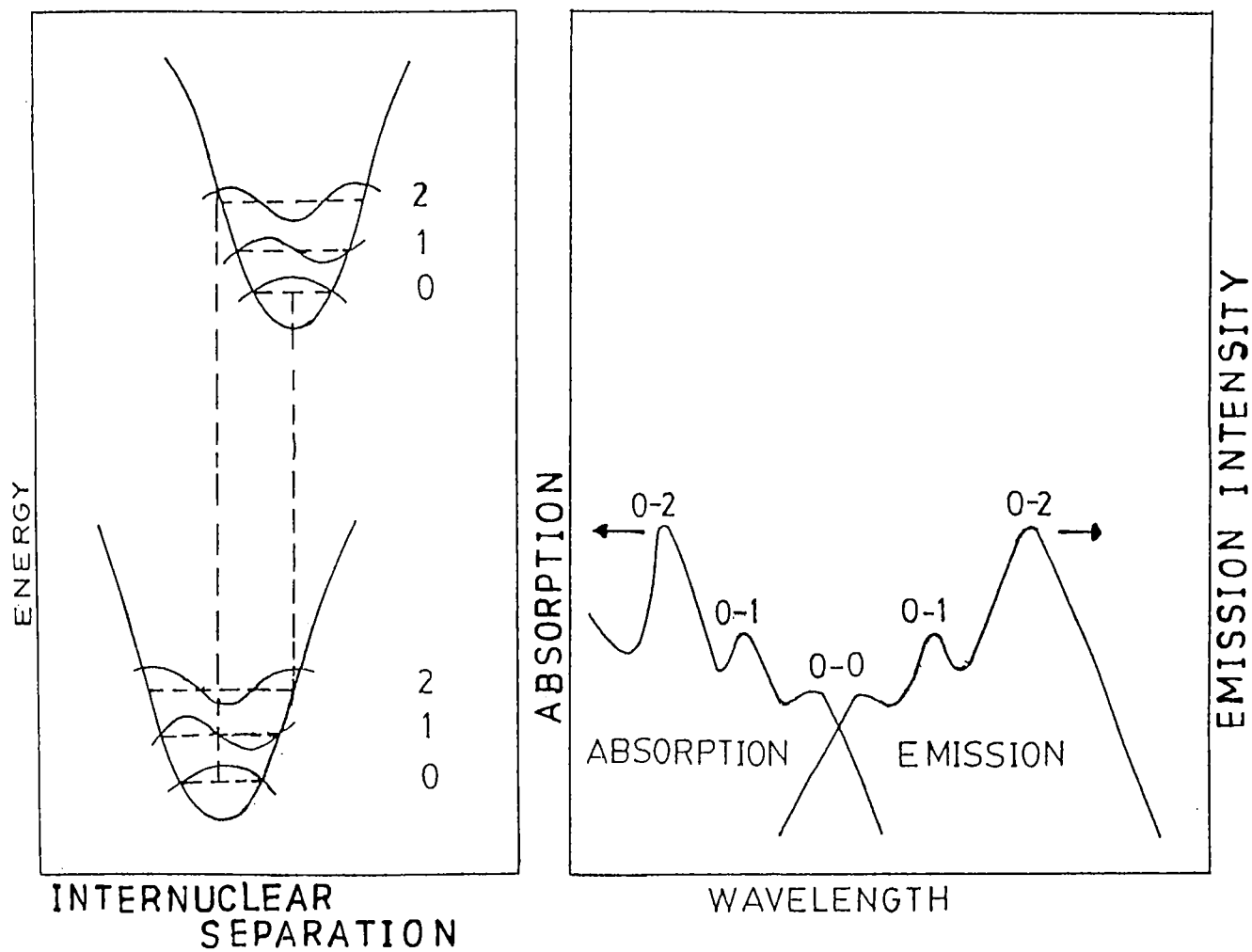


Fig.1.6. Mirror image rule and Franck-Condon factors

wavelength than that of the exciting light. This is known as Anti-Stokes Fluorescence (ASF). ASF can be induced by multiphoton absorption processes as well.

1.7.2 Fluorescence Lifetime and Quantum Yield

The fluorescence lifetime (τ) of a substance usually represents the average amount of time the molecule remains in the excited state prior to its return to the ground state. Lifetime measurements are frequently necessary in fluorescence spectroscopy; for example they can reveal the frequency of collisional encounters with quenching agents, the rate of energy transfer and the rate of excited state reactions. Moreover, calculation of rotational correlation times from fluorescence anisotropies requires knowledge of the fluorescence lifetime.

The small magnitude of τ (nanoseconds for dyes) often requires careful instrumentation for its measurement. There are two methods being widely used for measuring fluorescence lifetimes. These are the pulse method and the harmonic or phase-modulation method. In the pulse method the sample is excited with a brief pulse of light and time-dependent decay of fluorescence intensity is measured. In the harmonic method the sample is excited with sinusoidally modulated light. The phase shift and demodulation of the emission relative to the incident light is used to calculate the lifetimes. Each method has its own unique advantages and disadvantages.

With reference to fig.1.7, the lifetime is given by

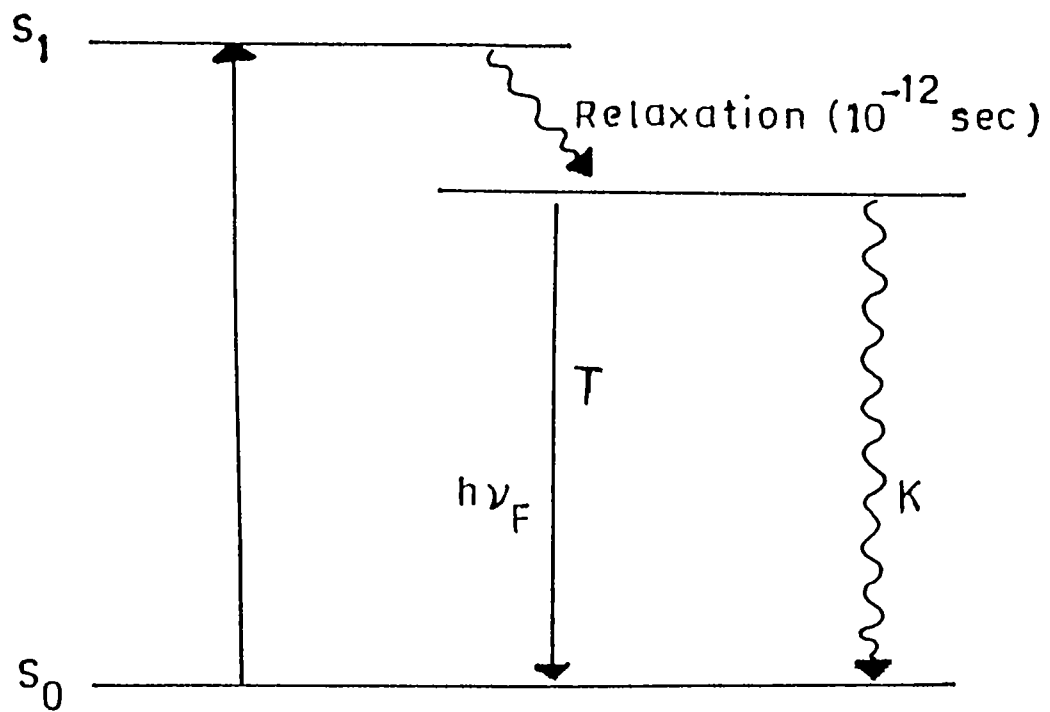


Fig.1.7. Radiative and nonradiative relaxations of an excited molecule (schematic)

$$\tau = \frac{1}{T + k} \quad (1.29)$$

where T is the emissive rate of the fluorophore and k is the rate of radiationless decay. In the absence of non radiative processes τ is called the intrinsic lifetime (τ_0) which is given by,

$$\tau_0 = \frac{1}{T} \quad (1.29a)$$

The fluorescence efficiency of a fluorophore is expressed in terms of the fluorescence quantum yield, which is defined as the ratio of the number of photons emitted to that absorbed. As we have seen the depopulation of the excited state is controlled by the radiative and non radiative rate constants T and k respectively; and the fraction of fluorophores which decay through emission (equal to the quantum yield) is given by,

$$Q = \frac{T}{T + k} \quad (1.30)$$

From the above equations we see that quantum yield (Q) and the lifetime (τ) are related through the equation

$$Q = \frac{\tau}{\tau_0} \quad (1.31)$$

and $Q = 1$ when $\tau = \tau_0$.

1.7.3 The Beer-Lambert law

Consider a parallel beam of light having an intensity I_0 falling on a flat specimen surface (fig.1.8). Part of the light (I_R and $I_{R'}$) is reflected at each interface, part (I_S) is scattered within the medium, part (I_A) is absorbed, and part (I_T) is transmitted. Then,

$$I_0 = I_R + I_{R'} + I_S + I_A + I_T \quad (1.32)$$

Compensating for ($I_R + I_{R'}$) and neglecting I_S for clear solutions, only the light absorbed and transmitted need be taken into consideration. If the incident beam of light is monochromatic and the specimen contains similar absorbing molecules, it is observed that (provided the rate of light absorption is small compared with the number of molecules present) the fraction of light absorbed is independent of the intensity of the incident beam.

The relation between I_T and I_0 is given by the Beer-Lambert law :

$$I_T / I_0 = e^{-Kcl} \text{ or } I_T / I_0 = e^{-\alpha l} \quad (1.33)$$

where I_T is the transmitted intensity, I_0 the incident intensity, K the effective absorption cross section, c is the no. of molecules/unit volume, α is the absorption coefficient and l is the path length of the beam through the sample.

Beer-Lambert law predicts that the optical density is

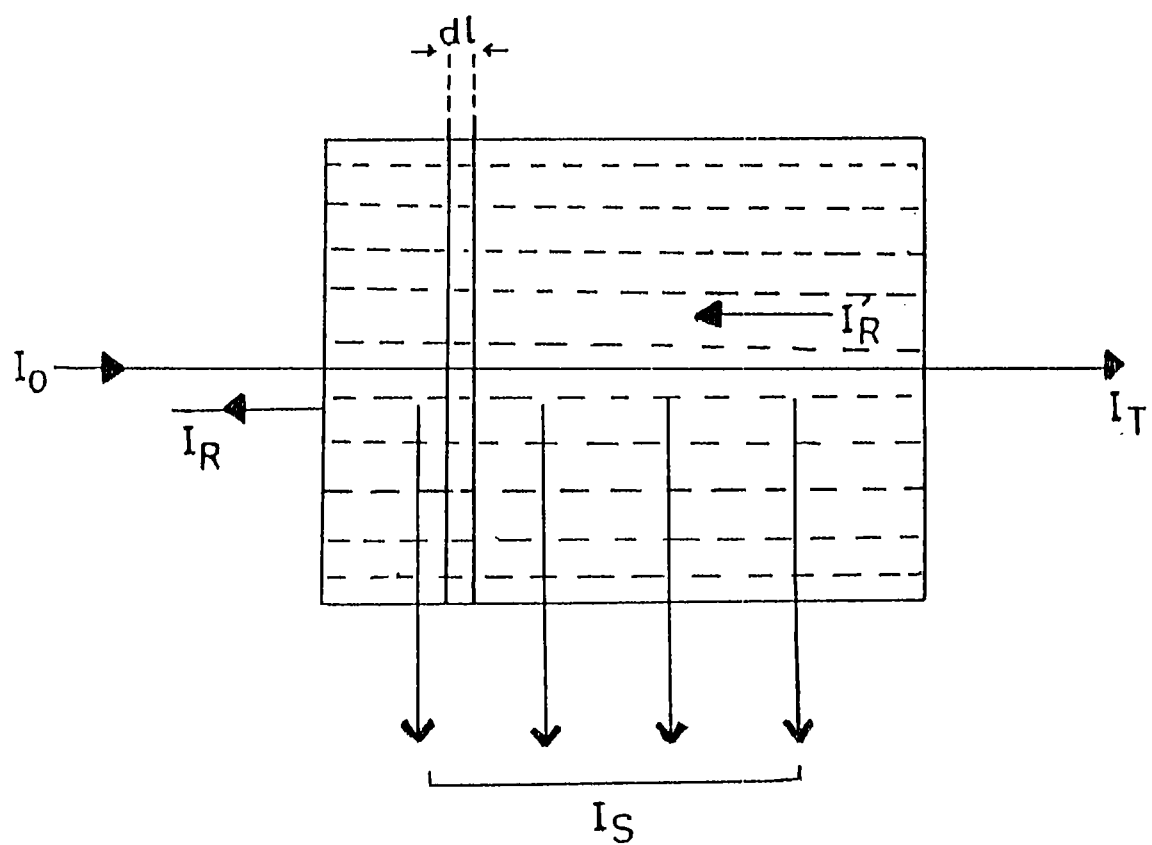


Fig.1.8. Derivation of Beer-Lambert Law

directly proportional to the concentration of the absorbing species. But if the light intensity is so high that an appreciable fraction of the molecules are raised to an excited state (so as to require a different effective cross section k), the above relation will not hold since nonlinear effects will set in.

1.7.4 Solvent dependence of fluorescence emission spectra

The emission spectra of many fluorophores, especially those containing polar substituents on the aromatic rings are known to be sensitive to the chemical and physical properties of the solvents. The absorption process occurs in about 10^{-15} sec, a time too short for significant displacement of nuclei (Franck-Condon principle), but evidently adequate for the redistribution of electrons. Generally the electronically excited states of aromatic compounds possess dipole moments (μ^*) which are larger than those in the ground states (μ). As a result the absorption of a photon by the fluorophore results in the essentially instantaneous creation of a dipole, which perturbs the environment surrounding the fluorophore. Subsequent to excitation, the solvent responds by a reorganisation of the solvent cage surrounding the fluorophore. This process is called solvent relaxation (solvation), the time scale of which is dependent upon the physical and chemical properties of the solvent. In a broad perspective, solvent effects can be divided into the *general* and *specific* categories.

Whereas the general solvent effects are expected to be always present, specific solvent effects will depend on the

precise chemical properties of the solvent and fluorophore [81,82]. Both interactions may, however, result in significant spectral shifts. The general solvent effects are mainly derived from the refractive index (η) and dielectric constant (ϵ). These physical constants reflect the freedom of motion of the electrons in solvent molecules, and the dipole moment of these molecules. It is seen that solute-solute interactions occur when the fluorophore is in solution, affecting the energy difference between the ground and excited states. In fact the energy difference (in cm^{-1}) depends on the refractive index (η) and dielectric constant (ϵ) of the solvent, as given by the Lippert equation [83,84,85];

$$\bar{\nu}_a - \bar{\nu}_f \cong \frac{2}{hc} \left(\frac{\epsilon - 1}{2\epsilon + 1} - \frac{\eta^2 - 1}{2\eta^2 + 1} \right) \left(\frac{\mu^* - \mu}{a} \right)^2 + \text{constant} \quad (1.34)$$

where h is the Planck's constant, c the speed of light, a is the radius of the cavity in which the fluorophore resides, and $\bar{\nu}_a$ and $\bar{\nu}_f$ are the wave numbers in cm^{-1} of the absorption and emission respectively.

An increase in η or a decrease in ϵ will thus decrease the Stoke's shift, $\bar{\nu}_a - \bar{\nu}_f$. Higher values of η allow both the ground and excited states to be instantaneously stabilized by the redistribution of electrons within the solvent molecule, that result in the decrease of $\bar{\nu}_a - \bar{\nu}_f$. This solvation of the ground and excited states occurs for solvents having large ϵ values too, but only after reorientation of the solvent dipoles. Here the

movement of the entire solvent molecule is required, not just its electrons. As a result, the stabilization of the ground and excited states of the fluorophore which depends on the dielectric constant (ϵ) is time dependent and the rate of stabilisation depends on the temperature and viscosity of the solvent.

Non polar solvents do not possess a dipole moment and hence no dipoles to reorient around the excited state of the fluorophore. So the Stoke's shift is very small. In polar solvents, substantially larger Stokes shifts are expected due to the larger orientational polarizability of the molecule, resulting from its dipole moment. This sensitivity of the Stoke's shift to solvent polarity is often utilized to estimate the polarity of the environment surrounding the fluorophore. On the other hand, specific solvent effects can be those due to specific chemical interactions between the solvent and fluorophore molecules. Hydrogen bonding, complexation, acid-base chemistry, charge transfer interactions etc. are a few of them.

Thus fluorescence emission is quite a complicated phenomenon in the sense that no single physical property of the solvent, such as polarity, orientation polarizability, viscosity, dielectric constant or refractive index can fully explain the emission characteristics.

1.7.5 Quenching of Fluorescence

Any process which reduces the *intrinsic* fluorescence quantum efficiency of a given substance is a fluorescence quenching process. (note that an *apparent* reduction in

fluorescence intensity that is often observed due to instrument artifacts does not come under this definition). A variety of phenomena such as collisional quenching, energy transfer, complex formation, self absorption, concentration quenching etc. can cause quenching and affect the quantum yield.

The process of impurity quenching is commonly due to an increase in the rate of intersystem crossing between the first excited singlet state and the triplet state in the presence of quencher. Such behaviour is typical of impurities such as oxygen, carbon tetrachloride and molecules containing heavy atoms. By the presence of a quenching impurity Q, the fluorescence quantum yield of a fluorescence solute M^* is reduced. The relation between the fluorescence quantum yield Φ_{QM} in the presence of a molar concentration [Q] of Q and the yield Φ_M in the absence of Q is given by

$$\frac{\Phi_M}{\Phi_{QM}} = 1 + K_{QM} [Q] \quad (1.35)$$

where $K_{QM} = k_{QM} \tau_M$ is the Stern-Volmer coefficient of impurity quenching rate parameter, and τ_M is the fluorescence lifetime of M^* in the absence of Q.

If the solution contains a molar concentration [Y] of an impurity Y, whose first excited singlet state lies below that of a singlet excited molecule M^* , then quenching can occur due to non-collisional radiationless energy transfer to Y. The fluorescence quantum yield Φ_{YM} of M^* in the presence of molar concentration [Y] of Y, and its yield Φ_M in the absence of Y are

related by

$$\frac{\Phi_M}{\Phi_{YM}} = 1 + K_{YM} [Y] \quad (1.36)$$

where $K_{YM} = k_{YM} \tau_M$ is the Stern-Volmer coefficient of energy transfer and k_{YM} is the energy transfer parameter.

The increase of molar concentration [M] of a fluorescent solute commonly causes a decrease in the molecular fluorescence quantum yield, often associated with the appearance of a new structureless fluorescence band at longer wavelengths. The molecular fluorescence quantum yield Φ_M decreases with increase in [M] according to the Stern-Volmer relation [86]

$$q/\Phi_M = 1 + K_{CM} [M] \quad (1.37)$$

where q_M is the value of Φ_M at infinite dilution, $K_{CM} = \left[\frac{[M]}{0.5} \right]^{-1}$ is the Stern-Volmer coefficient of concentration quenching and [M] is the half value concentration at which $\Phi_M = 0.5 q_M$.

There is generally an overlap of the 0-0 bands of the fluorescence and absorption spectra. Due to this spectral overlap, self-absorption of part of the fluorescence emission occurs except in very dilute solutions. This corresponds to a radiative migration of the M^* (molar concentration of excited molecules) excitation. In a fluorescence system with fluorescence quantum efficiency q_{FM} and lifetime τ_M in which "a" is the probability of self-absorption of an emitted photon, the quantum

yield of the escape of the fluorescence is given by [87]

$$\Phi_{FM} = \frac{q_{FM} (1-a)}{1 - a q_{FM}} \quad (1.38)$$

1.8 LASER ACTION IN FLUORESCENT DYES

From the discussion of the spectroscopic properties of dyes one might come to the conclusion that there are two possible ways, at least in principle, of using an organic solution as the active medium in a laser: One might utilize either the fluorescence or the phosphorescence emission. Eventhough the long lifetime of the triplet state makes phosphorescence more attractive, since the transition is strongly forbidden, a very high concentration of the active species is required to obtain an amplification factor large enough to overcome the inevitable cavity losses. Further, triplet-triplet absorptions would bring about large losses in the system. The triplet-triplet absorption bands are generally very broad and diffuse and the probability that they will overlap the phosphorescence band is high. Because of these difficulties no laser using the phosphorescence of a dye has yet been reported.

If the fluorescence band of a dye solution is utilized in a dye laser, the allowed transition from the lowest vibronic level of the first excited state will give a high amplification factor even at low dye concentrations. The main complication in these systems is the existence of the lower lying triplet states. The intersystem crossing rate to the lowest triplet state

is high enough in most molecules to reduce the quantum yield of fluorescence to values substantially below unity. This has a two-fold consequence: Firstly, it reduces the population of the excited singlet state, and hence the amplification factor; and secondly, it enhances the triplet-triplet absorption losses by increasing the population of the lowest triplet state. The population of the triplet level can be held arbitrarily small if the pumping light flux density rises fast enough, i.e. if it reaches threshold in a time t , which is small compared to the reciprocal of the intersystem crossing rate ($t \ll 1/k_{ST}$). Here t is the risetime of the pump light power, during which it rises from zero to the threshold level. For a typical value of $k_{ST} = 10^7 \text{ sec}^{-1}$, the risetime should be less than 100 ns. This is easily achieved, for example with a giant-pulse laser as pump light source, since giant pulses usually have risetimes of 5-20 nsec. In such laser-pumped dye laser systems one may neglect all triplet effects to a first approximation.

Restricting the discussion to the singlet states, molecules that take part in dye laser operation have to fulfill the following cycle (fig.1.9). Absorption of pump radiation at ν_p and with cross-section σ_p lifts the molecule from the ground state with population n_0 into a higher vibronic level of the first (or second) excited singlet state S_1 (or S_2) with a population n'_1 (or n'_2). Since the radiationless deactivation to the lowest level of S_1 is so fast, the steady-state population n'_1 is negligibly small, provided the temperature is not so high that this vibronic level is already thermally populated by the Boltzmann distribution of the molecules in S_1 . Fluorescence emission then occurs from the lowest vibronic level of S_1 to

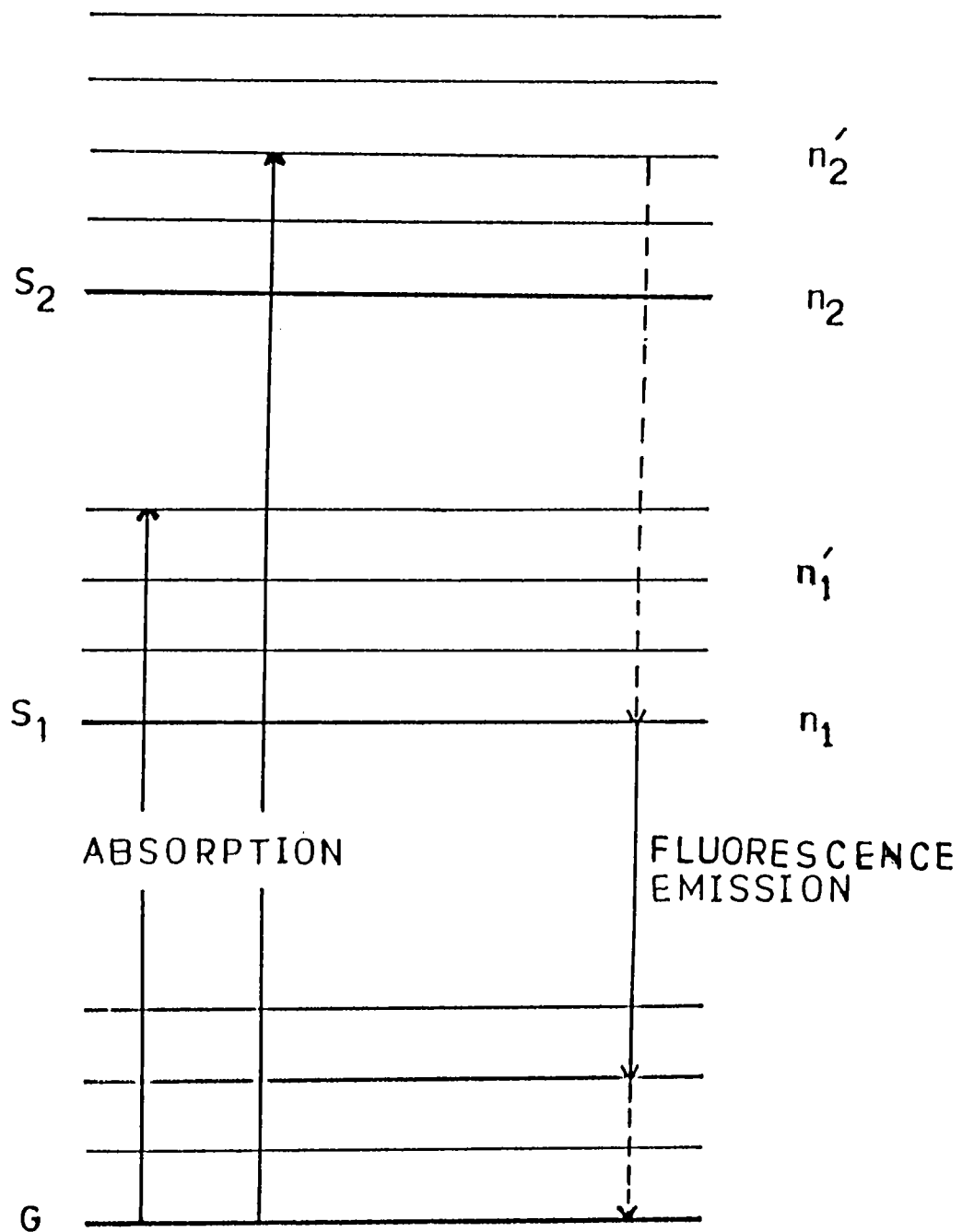


Fig.1.9. The typical optical pump cycle of dye molecules

higher levels of G. Again the population n_0' of this vibronic level is negligible since the molecules quickly relax to the lowest vibronic levels of G.

The solvent has a most significant influence on the wavelength and efficiency of the dye laser emission. The solvent shift is especially large for dyes whose dipole moments differ appreciably in the ground and excited states. The transition from ground to an excited state by light absorption is fast compared with the dipolar relaxation of the solvent molecules. As we have seen, the dye molecule finds itself in a nonequilibrium Franck-Condon state following light absorption, from which it relaxes to an excited equilibrium state. The return to the ground equilibrium state is also via a Franck-Condon level, followed by dipolar relaxation. The solvent relaxation times involved in these transitions depend on the solvent viscosity to a great extent. Another property of the solvent that can have an influence is the acidity of the solvent relative to that of the dye. The dye laser emission of molecules that are ionized usually changes with the pH of the solution as well, since generally the different ionization states of the molecule fluoresce at different wavelengths. In a broad perspective, the fluorescence yield and hence the lasing efficiency of a dye in solvent will depend also on the magnitudes of solute-solvent interaction, intersystem crossing, excited state absorption (ESA), and non radiative relaxation. Most of these phenomena in turn depend on the dye concentration and pump intensity.

A simple structure for dye solution laser was used in many of the early investigations, which is still useful for

exploratory studies of new dyes. It consists of a square spectrophotometer cuvette filled with the dye solution which is excited by the beam from a suitable laser. The resonator is formed by the two glass-air interfaces of the polished sides of the cuvette and the exciting and the dye laser beams are at right angles. Reflective coatings on the windows consisting of suitable metallic or multiple or dielectric layers enhance the Q of the resonator. However present day dye laser systems are more complicated in design several of which have been discussed by various authors [88 - 95].

1.9 SUMMARY

An outline of light - matter interaction relevant to the present studies has been presented in this chapter. The significance of two-photon and multiphoton absorption phenomena in spectroscopy is discussed. The physical and chemical properties of laser dyes are reviewed briefly, and an introduction to the techniques of photoacoustics and fluorescence is given.

REFERENCES

- [1] Yariv A, "Quantum electronics", Wiley, New York, 1967
- [2] Pantell R H and Puthoff H E, "Fundamentals of Quantum Electronics", Wiley, New York, 1969
- [3] Marcuse D, "Principles of Quantum Electronics", Academic Press, New York, 1980
- [4] Herzberg G "Molecular Spectra and molecular structure", vol.3, Spectra of diatomic molecules, (2nd ed.), Van Nostrand, 1950
- [5] Birks J B, "Photophysics of aromatic molecules", Wiley-Interscience, London, 1970, p.32
- [6] Bredikhin V I and Genkin V N, Sov. Phys. Solid-state, 11, 1871, 1970
- [7] Quantum Electronics : A Treatise vol.1, Nonlinear Optics, Part A, ed. Herbert Rabin and Tang C L, Academic press, New York
- [8] Goepfert Mayer M, Ann Physik, 9, 273, 1931
- [9] Evleth E and Peticolas W L, J. Chem. Phys., 41, 1400, 1964
- [10] Pao Y H and Rentzepis P M, J. Chem. Phys., 43, 1281, 1965
- [11] Bebb H B and Gold A, Phys. Rev., 143, 1, 1966
- [12] Hernandez J P and Gold A, Phys. Rev., 156, 26, 1967
- [13] Pantell R, Pradere F, Hanns J, Schott M and Puthoff H, J.Chem.Phys., 46, 3507, 1967
- [14] Giordamine J A, Rentzepis, Shapiro S L and Wecht K W, Appl. Phys. Lett, 11,216, 1967
- [15] Bey P P, Galbruith J F and Rabin H, IEEE J. Quantum. Electron. QE-7, 86, 1971
- [16] Diels J C and Schafer F P, Appl. Phys., 5, 197, 1974
- [17] Leupacher W, Penzkofer A , Runde B and Drexhage K H, Appl.

- Phys. B, 44, 1987
- [18] Cubeddu, Polloni R, Sacchi C A and Svelto O, IEEE J. Quant. Electron. QE -5, 470, 1969
 - [19] Ralston J M and Chang R K, Appl. Phys. Lett., 15, 164, 1969
 - [20] Van Stryland, Vanherzeele H, Woodall M A, Soilean M J, Smirl A L, Guha G and Boggess T F, Opt. Engg, 24, 613, 1985
 - [21] Rapp W and Gronav B, Chem. Phys. Lett., 8, 529, 1971
 - [22] Rubinov A N, Richardson M C, Sala K and Alcock A J, Appl. Phys. Lett., 27, 358, 1975
 - [23] John G Meadors, IEEE J. Quantum. Electron., QE-2, 638, 1966
 - [24] Shank C V, Rev. Mod. Phys., 47, 649, 1975
 - [25] Gregg D W and Thomas J, IEEE J. Quantum. Electron QE - 5, 302, 1969
 - [26] John Olmsted, III, J.Phys.Chem., 83, 2581, 1979
 - [27] Bell A G, Am. J. Sci., 20, 305, 1880
 - [28] Webb J D, Swift K M and Bernstein, J. Chem. Phys., 73, 4891, 1980
 - [29] Deutsch T F, J. Chem. Phys., 70, 1187, 1979
 - [30] Ambartzumian R V, Knyazev I N, Lobko V V, Makarov G N and Puretzky, Appl Phys., 19, 75, 1979
 - [31] Bagratashvili V N, Knyazev I N, Letokhov V S and Lobko V V, Opt. Comm., 18, 525, 1976
 - [32] Lussier F M, Steinfeld J I and Deutsch T F, Chem. Phys. Lett., 58, 277, 1978
 - [33] Black J G, Yablonovitch, Bloembergen N and Mukamel S, Phys. Rev. Lett., 38, 1131, 1977
 - [34] Deutsch T F, Opt. Lett., 1, 25, 1977
 - [35] Cox D M, Opt. Comm., 24, 336, 1978
 - [36] Barrett J J, in "Chemical Applications of nonlinear Raman

- Spectroscopy", edited by Harvey A B (Academic, New York 1981), 89-169
- [37] Barrett J J and Berry M J, Appl. Phys. Lett., 34, 144, 1979
- [38] West G A, Siebert D R and Barrett J J, J. Appl. Phys., 51, 2823, 1980
- [39] West G A and Barrett J J, Opt. Lett., 4, 395, 1979
- [40] Barrett J J and Heller D F, J. Opt. Soc. Am. 71, 1299, 1981
- [41] Patel C K N and Tam A C, Appl. Phys. Lett., 34, 760, 1979
- [42] Ready J F, "Effects of high-power laser radiation" , Academic, New York, 1971
- [43] Michelis C de, IEEE J. Quantum. Electron QE - 5, 188, 1969
- [44] Ostrovskaya G V and Zaidel A N, Sov. Phys. Usp., 16, 834, 1974
- [45] Grey Morgan C, Sc. Prog. (London), 65, 31, 1978
- [46] Brewer R G and Rieckhoff K, Phys. Rev. Lett., 13, 334, 1964
- [47] Lyamshev L M, Sov. Phys. Acoust., 24, 977, 1981
- [48] Emmony D C, Infrared Phys., 25, 133, 1985
- [49] Bloembergen N, IEEE J. Quantum. Electron QE - 10, 375, 1974
- [50] Lyamshev L M and Naugol'nykh K A, Sov. Phys. Acoust., 27, 357, 1981
- [51] Bunkin B V and Komissarov, Sov. Phys. Acoust., 19, 203, 1973
- [52] Tam A C, in "Ultrasensitive Laser spectroscopy" (Academic, New York, 1983)
- [53] Brueck S R J, Kildal H and Be'linger, Opt. Comm., 34, 199, 1983
- [54] Tam A C, Rev. Mod. Phys., 58, 381, 1986
- [55] Kasoev S G and Lyamshev L M, Sov. Phys. Acoust., 23, 510, 1977

- [56] Naugol'nykh K A, Sov. Phys. Acoust., 23, 98, 1977
- [57] Tam A C and Patel C K N, Appl. Opt., 18, 3348, 1979
- [58] White R M, J. Appl. Phys., 34, 3559, 1963
- [59] Carome C F, Clark N A, Moeller C E, Appl. Phys. Lett., 4, 95, 1964
- [60] Gournay L S, J. Acoust. Soc. Am., 40, 1322, 1966
- [61] Hu C L, J. Acoust. Soc. Am., 46, 728, 1969
- [62] Sigrist M W and Kneubuhl, J. Acoust. Soc. Am., 64, 1652, 1978
- [63] Lyamshev L M, Sedov L V, Sov. Phys. Acoust., 27, 4, 1981
- [64] Bozhkov A I, Bunkin F V, Kolomeskii A I A, Mikhalevich, Sov. Sci. Rev. A, Physical review, vol.3, ed. by Khalatnikov I M (Harwood Academic, New York, 1981) p. 459-551
- [65] Terzic M, Sigrist M W, J. Appl. Phys., 56, 93, 1984
- [66] Patel C K N and Tam A C, Rev. Mod. Phys., 53, 517, 1981
- [67] Nelson E T and Patel C K N, Opt. Lett., 6, 354, 1981
- [68] Sigrist M W and Chen Z H, Appl. Phys. B, 43, 1, 1987
- [69] Carome E F, Moller C E and Clark N A, J. Acoust. Soc. Am., 40, 1462, 1966
- [70] Busshanam G S and Barnes F S, J. Appl. Phys., 46, 2074, 1975
- [71] Sullivan B and Tam A C, J. Acoust. Soc. Am., 75, 437, 1984
- [72] Hutchins D A, Proceedings of the Conference on New Techniques in Sonar Transducers, Proceedings of the Institute of Acoustics, vol.6, Birmingham, U.K., 1984, pp.24-30
- [73] Fukumi T, Opt. Comm., 30, 351, 1979
- [74] Brenner D M, Brezinsky K and Curtis P M, Chem. Phys. Lett., 72, 202, 1980
- [75] Weulersse J M and Genier R, Appl Phys., 24, 363, 1981

- [76] Chin S L, Evans D K, McAlpine and Selander W N, Appl. Opt., 21,65,1982
- [77] Bass M, Van Stryland E W and Steward A F, Appl. Phys. Lett.,34, 142, 1979
- [78] Bae Y J, Song J and Kim Y B, Appl. Opt. 21,35, 1982
- [79] Tam A C and Patel C K N, Nature (London), 280, 304, 1979
- [80] Rosencwaig A, "Photoacoustics and Photoacoustic Spectroscopy", Wiley, New York, 1980
- [81] Perov A N, Opt. Spectrosc., 49, 371, 1980
- [82] Neporent B S and Bakhshiev N G, Opt. Spectrosc.,8,408,1960
- [83] Lippert Von E, Z.Electrochem 61, 962, 1951
- [84] Kawski A, Acta Phys. Pol., 29, 507, 1966
- [85] Mataga N, Kaifu Y and Koizumi M, Bull. Chem. Soc. Jpn., 29, 465, 1956
- [86] Th. Forster and Kasper K, Z. Electrochim., 59, 976, 1955
- [87] Birks J B, Phys. Rev., 94, 1567, 1954
- [88] Sorokin P P, Culver W H, Hammond E C, Lankard J R, IBM J. Res. Develop., 10, 428, 1966
- [89] Hansch T W, Appl. Opt., 11, 895, 1972
- [90] Runge P K, Opt.Comm., 4, 195, 1971
- [91] Michael G Litmann and Harold J Metcalf, Appl.Opt., 17, 2224, 1978
- [92] Nair L G and Dasgupta K, IEEE J. Quantum. Electron., QE - 16, 111, 1980
- [93] Eesley G L, Levenson M D, Nitz and Smith A V, IEEE J. Quantum. Electron., QE - 16, 113, 1980
- [94] Jethwa J, St. Anufrik S, and Docchio F, Appl. Opt., 17, 2224, 1978
- [95] Sperber P, Weidner M and Penzkofer, Appl. Phys. B, 42, 185, 1987

CHAPTER-II

INSTRUMENTATION

2.1 INTRODUCTION

Light absorbed by a sample will excite a fraction of the ground state molecular population into higher energy levels. These excited states will subsequently relax through a combination of radiative and non radiative pathways. The non radiative component will generate heat in the localized region of the excitation light beam and generate a pressure wave that propagates away from the source. The pressure wave is then detected with a suitable sensor such as a microphone or a transducer. The photoacoustic detection technique is unique in that it is a direct monitor of the non radiative relaxation channel. The radiative component (generally the transitions from the lowest vibrational level of the first excited singlet state) is detected using the fluorescence spectroscopic technique. This chapter gives a broad outline of the experimental techniques employed in the present investigations of the pulsed photoacoustic (PPA) and fluorescence phenomena. Finer details of the respective experimental arrangements will be given in the following chapters.

2.2 PHOTOACOUSTICS

The essential components of a PA spectrometer are (i).a source of periodic radiation (ie. modulated continuous wave or pulsed) in the spectral region of interest (ii).a PA cell (iii).a

means of detecting the acoustic signal (iv).signal processing equipment. The block diagram of a basic PA spectrometer is shown in fig 2.1.

2.2.1 Source

The lamp/monochromator and the laser are two types of light sources currently in use in photoacoustic as well as fluorescence spectroscopy. Lasers, with their nearly monochromatic beam of high spectral brightness, enjoy significant advantages over lamp/monochromator combination which account for their wider acceptance as PA light sources. As compared to cw modulated sources, the pulsed source is capable of delivering radiation of very high peak powers. Also, pulsed excitation sources seem to enhance the detection sensitivity when dealing with condensed phases [1].

In the present scheme of experiments, a pulsed Q-switched Nd:YAG laser (Spectra Physics, DCR-11) has been used as the optical source. The emission wavelength is $1.06 \mu\text{m}$ having a pulse width of 8-9 ns and a maximum pulse energy of 275 mJ. The linewidth is $< 1 \text{ cm}^{-1}$ and beam divergence $< 0.5 \text{ mrad}$. The pulse repetition frequency can be varied from 1-14 Hz. The laser cavity is diffraction coupled and the beam is nearly diffraction limited. The beam diameter is 6.4 mm, and has a linear polarization $> 98 \%$ at $1.06 \mu\text{m}$.

The Nd:YAG laser is equipped with a KD^*P crystal that generates second harmonic radiation at 532 nm with a maximum pulse energy of 135 mJ. The planes of polarization of 1060 nm and

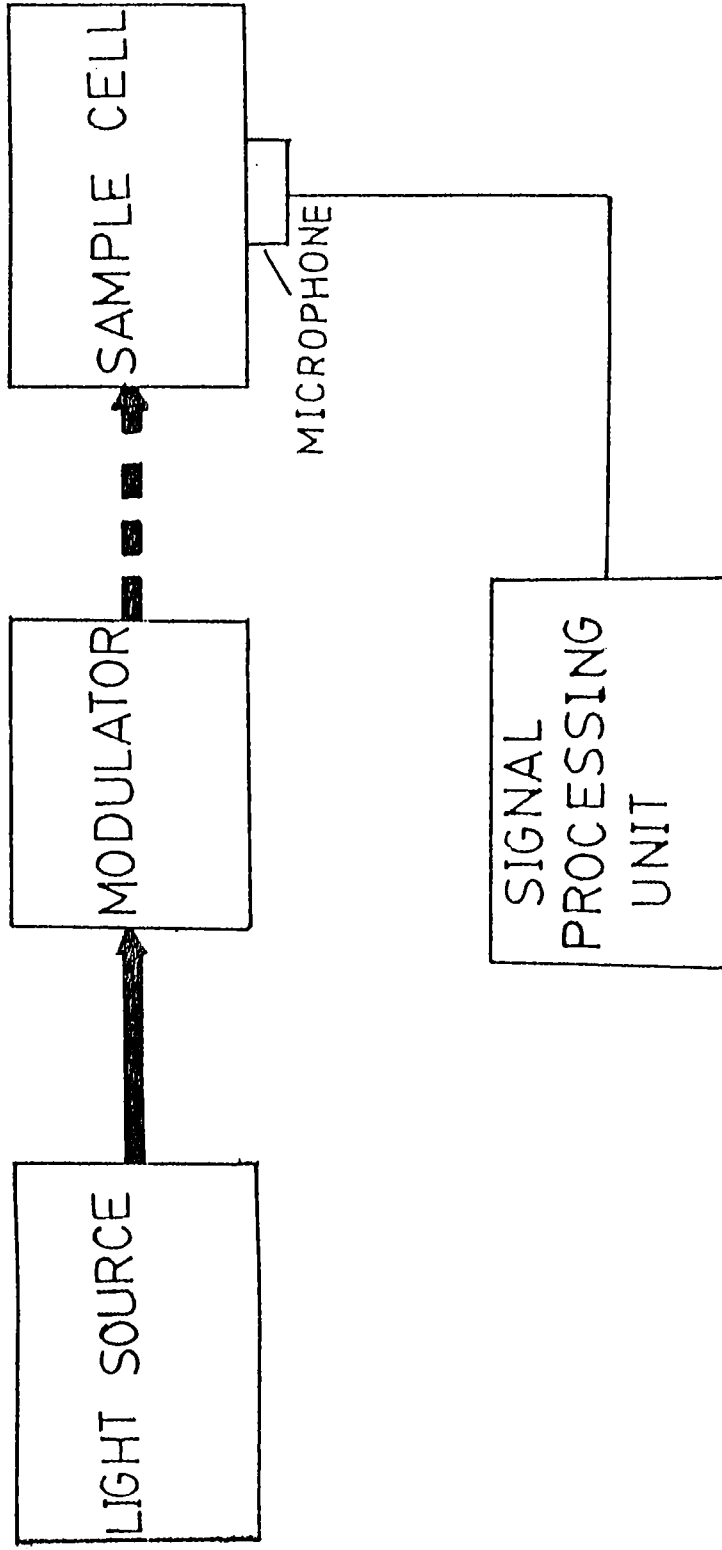


Fig.2.1. Block diagram of a basic PA spectrometer.

532 nm beams are mutually orthogonal.

2.2.2 PA Cell

In our experimental set up, the liquid sample cell is made of stainless steel having an inner diameter of 2 cm and length 5 cm. Fig.2.2 shows the schematic of the PA cell. The cell is equipped with two glass windows, which are seated in stainless steel flanges. Teflon O-rings are used between the window and the end surface of the cell. The transducer is screwed into the sample cell perpendicular to the direction of the laser beam so that the diaphragm makes good acoustic contact with the liquid taken in the same.

Since stray light absorbed at cell walls constitutes a possible source of large spurious signals, the choice of cell material needs to be examined carefully. The stray light absorbed is distributed over a diffusion depth δ as given in the equation;

$$\Delta T = \text{Constant} / (\delta \rho C_p) \quad (2.1)$$

where ρ and C_p are the density and specific heat of the metal. The constant contains surface optical absorption and reflection factors. The material for constructing the PA cell should have small surface optical absorption, large thermal diffusion length, high density and specific heat. Eventhough for silver or aluminium the factor $1/(\delta \rho C_p)$ is smaller than in stainless steel, the high degree of chemical reactivity of silver or aluminium makes the choice of stainless steel a reasonable compromise.

2.2.3 Transducer

In recent years, several authors have realised that the photoacoustic spectroscopy scheme first used by Harshbarger and Robin [2] and by Rosencwaig [3] utilizing gas phase microphones, is quite insensitive for photoacoustic (OA) studies of condensed matter. Thus the technique of piezoelectric detection of the OA signal has been used by Kohanzadeh et al [4], Bonch-Bruevich et al [5, 6], Emmony et al [7], Callis [8], Sladky et al [9], Lahmann et al [10], Lahmann and Ludewig [11], Hordvik and Schlossberg [12], Farrow et al [13], Sigrist and Kneubühl [14], Burt [15], Sam et al [16], Edward Voigtman et al [17], Masahide Itoh et al [18], Hutchins [19], Pak-Kon Choi et al [20], Hangyo et al [21], Peralta et al [22] and others. The reason is that acoustic impedance matching is very good for piezoelectric detectors directly coupled to solids, and acoustic transmission exceeding 50% from solid to the detector is generally possible. For liquids, the transmission generally exceeds 10%. This is in sharp contrast to the transmission across an interface between condensed matter and gas, where the transmission is typically of the order of 10^{-5} only. Detection using the piezoelectric sensor has other advantages over the microphone cell, like the piezoelectric transducer responds faster than the microphone as well, for eg. and can be used at low temperature without any special precautions.

Piezoelectricity is the phenomenon related to changes in the physical dimensions of a material with changes in an externally applied electric field. Piezoelectric crystals and

ceramics are among the principal detectors and generators of acoustic power. Although piezoelectric crystals such as quartz and Rochelle salt are still widely used for certain applications, most piezoelectric transducers are currently made from polycrystalline ceramics that have been poled or polarized. A common piezoelectric ceramic which is widely in use is a solution of lead zirconium titanate (PZT), usually modified with other additives.

Piezoelectric transducers of various geometries are in use for acoustic detection. In our experiments, we followed the design described by Patel and Tam [23]. Fig.2.3 shows the schematic of the transducer. The transducer consists of a lead zirconium titanate (PZT) cylinder, 4 mm thick and 15 mm in diameter. The PZT cylinder is firmly mounted on a stainless steel casing with a front diaphragm of the same material having a thickness of 1 mm. The purpose of mounting the PZT cylinder inside the stainless steel casing is to minimize external electrical pick up and prevent sample contamination by PZT. The PZT cylinder is spring loaded against the diaphragm, with a thin layer of silicone grease applied between them to ensure good acoustic coupling. The backing plate of the PZT cylinder is a lead disc soldered to a copper disc. The use of lead is for reducing acoustic reflection back into the transducer, thus minimizing ringing effects. The signal from the PZT is taken out through a BNC connector.

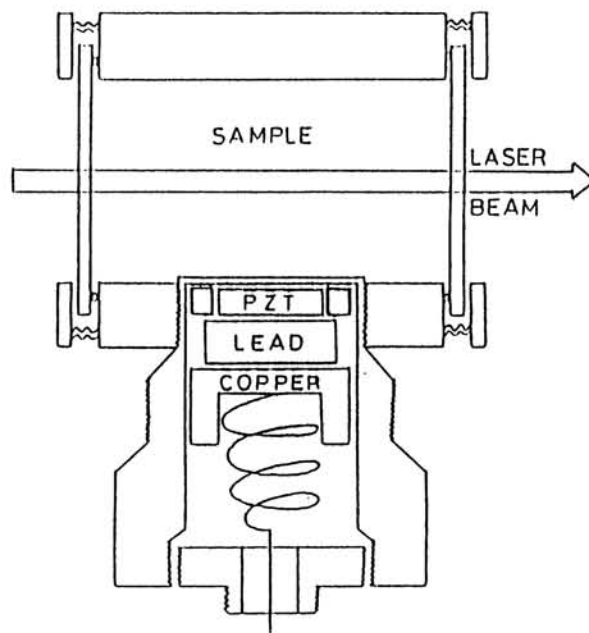


Fig.2.2. The present photoacoustic cell for liquid samples.

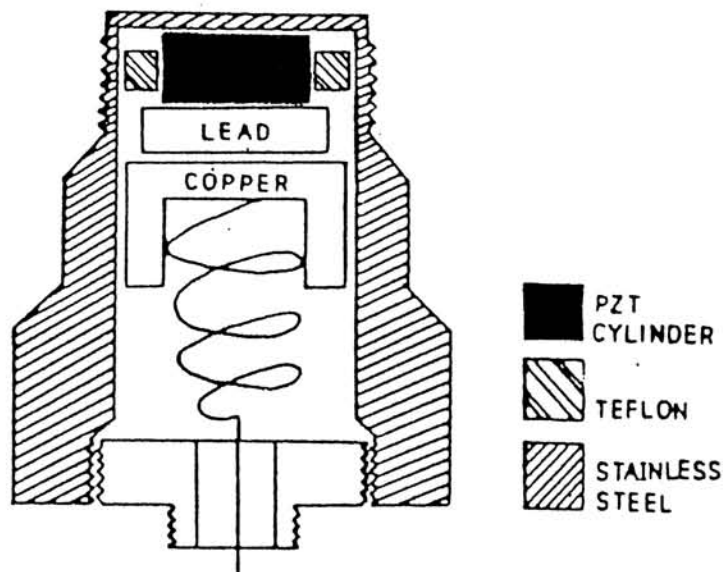


Fig.2.3. The transducer chamber

2.2.4 Detection of PA signals

2.2.4a Cathode Ray Oscilloscope

The PA signal is observed on oscilloscopes whenever possible to make the experimental set up simple. The oscilloscopes used are :

- (1). Iwatsu, DS - 8621, digital storage type (200 MHz)
- (2). Tektronix 466, Analogue Storage type (100 MHz)

Various signal processing options like pulse averaging, smoothing etc are available on this oscilloscope. RS-232 and GPIB interface facility is also present.

- (3). SS - 5321 (250 MHz), Iwatsu, non storage type

2.2.4b Gated Integrator and Boxcar averager

The lock-in detection is used for periodically modulated low frequency signals (typically less than 5 kHz) for isolating the required signal, but for pulsed excitation, gating and averaging technique is appropriate. The boxcar averager is uniquely adept at handling the noisy, short lived, repetitive signals characteristic of experiments using pulsed lasers.

In the pulsed photoacoustic signal profile, measurements have been taken on the first peak. The peak is gated and the voltage averaged by employing a gated integrator and boxcar

averager system. The improvement in S/N ratio is proportional to the square root of the number of samples being averaged.

The following models have been used :

- (1). (EG & G) Model 162 (Boxcar averager), with models 163 and 164 (Gated integrators)
- (2). SRS Model SR 250

2.2.5 Power Meters

For measuring the laser energy/power during various experiments, the following power meters were used.

(a). Laser power energy meter : (Scientech model 362)

This is a disc calorimeter that employs a calibrated thermopile which generates a voltage proportional to the heat that is liberated from the absorption of the input laser flux. Many thermoelectric junctions are arranged in series and sandwiched between an absorption surface producing heat which flows through the thermopile. The heat flow is accurately proportional to the laser beam power and substantially independent of the laser beam spatial distribution of power. The thermopile output is a linear low impedance, dc signal of approximately 0.09 volts/W.

The following are the major specifications of Scientech 362 : a flat spectral response in the region of 400 nm to 1200 nm, a continuous power range (for cw lasers and average power

measurement of pulsed lasers) from 0 to 10 watts, a maximum power density of 47 W/cm^2 and a maximum pulse energy density of 3.3 J/cm^2 .

(b). Pulsed energy monitor (Delta developments)

This on line laser power meter uses a polarization compensated beam splitter to sample the beam, 85 % of which is transmitted through the exit face. The sampled beam strikes a retroreflecting diffuser and reaches a photo-diode via a 'Range plate' which attenuates the light appropriately for the range of energies being measured. All positions on the diffuser give equal signals. Different plates can be used for different energies or laser wavelengths. The spectral range extends from 200 nm to 1100nm. A maximum energy of 300 mJ/pulse can be measured with Delta developments meter.

(c). Labmaster(Coherent)

Labmaster is a microprocessor based laser energy/power measurement instrument. The LM - P5 detector head can be used for pulsed energy measurement in the spectral range 0.19 to $20 \mu\text{m}$, energy upto 5 joules, with a maximum average power of 5 watts. A crystalline pyroelectric sensor is used in this power meter.

2.2.6 Optical Components

The hard coated optical components including mirrors, beam splitters, dichroic mirrors etc., suitable for laser based experiments have been procured from Melles Griot and CVI

orporation.

2.7 Experimental Set-up to study pulsed PA Signals

A simple schematic set up for pulsed photoacoustic experiments is shown in fig.2.4. The IR output (1060 nm) or the delimitated second harmonic output (532 nm) of the Nd:YAG laser is focussed by a convex lens of 5 cm focal length into the PA cell containing the sample. The laser is run at either 10 Hz or 5 Hz and the energy meter monitors the pump energy. Signals, if strong are observed on a storage oscilloscope. When the signal level is low, a pulse pre-amplifier is used before the oscilloscope. In still adverse conditions, boxcar detection and averaging is employed. The boxcar gate is usually set on the first peak of the PA signal trace. For most of our experiments we used a typical gate width of 1 μ s. A typical CRO trace of the PA signal is shown in fig.2.5.

For evaluating the performance of the constructed PA cell an experiment to measure the velocity of laser induced acoustic waves in certain materials has been performed (fig.2.6). The details are as follows.

532 nm radiation from the Nd:YAG laser is used as the exciting light source for producing the acoustic signal in liquids taken in the PA cell described earlier. The laser beam is focussed into the medium in the sample cell so that the beam waist is formed exactly in front of the transducer. When the pump beam is so aligned as to enter the cell along the centre of the front window, the separation between the beam focus and transducer surface is nearly 1.5 cm. The PA signal is strong enough to be displayed on the oscilloscope without a pre-amplifier, for laser energies > 15 mJ.

The PA signal amplitude is measured for various values of

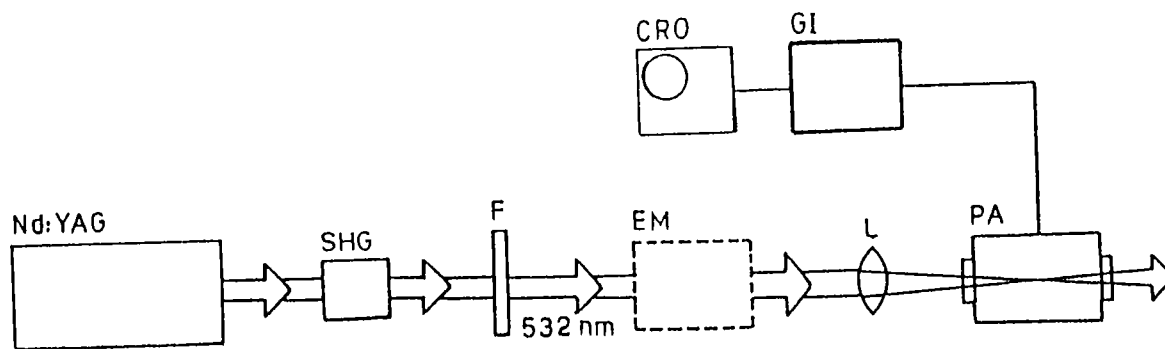


Fig.2.4. Schematic experimental set up for pulsed photoacoustic experiments.

SHG - Second harmonic generator, F- harmonic separator, EM - energy meter, L -lens, PA - photoacoustic cell, GI - gated integrator and boxcar averager, CRO - cathode ray oscilloscope

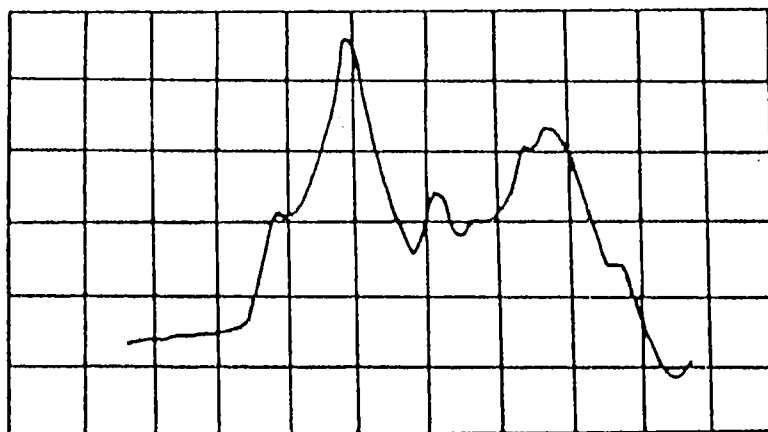


Fig.2.5. A typical pulsed PA transient trace, amplified and observed on the oscilloscope. Horizontal scale - 5 μ s/div., Vertical scale - 50 mV/div.

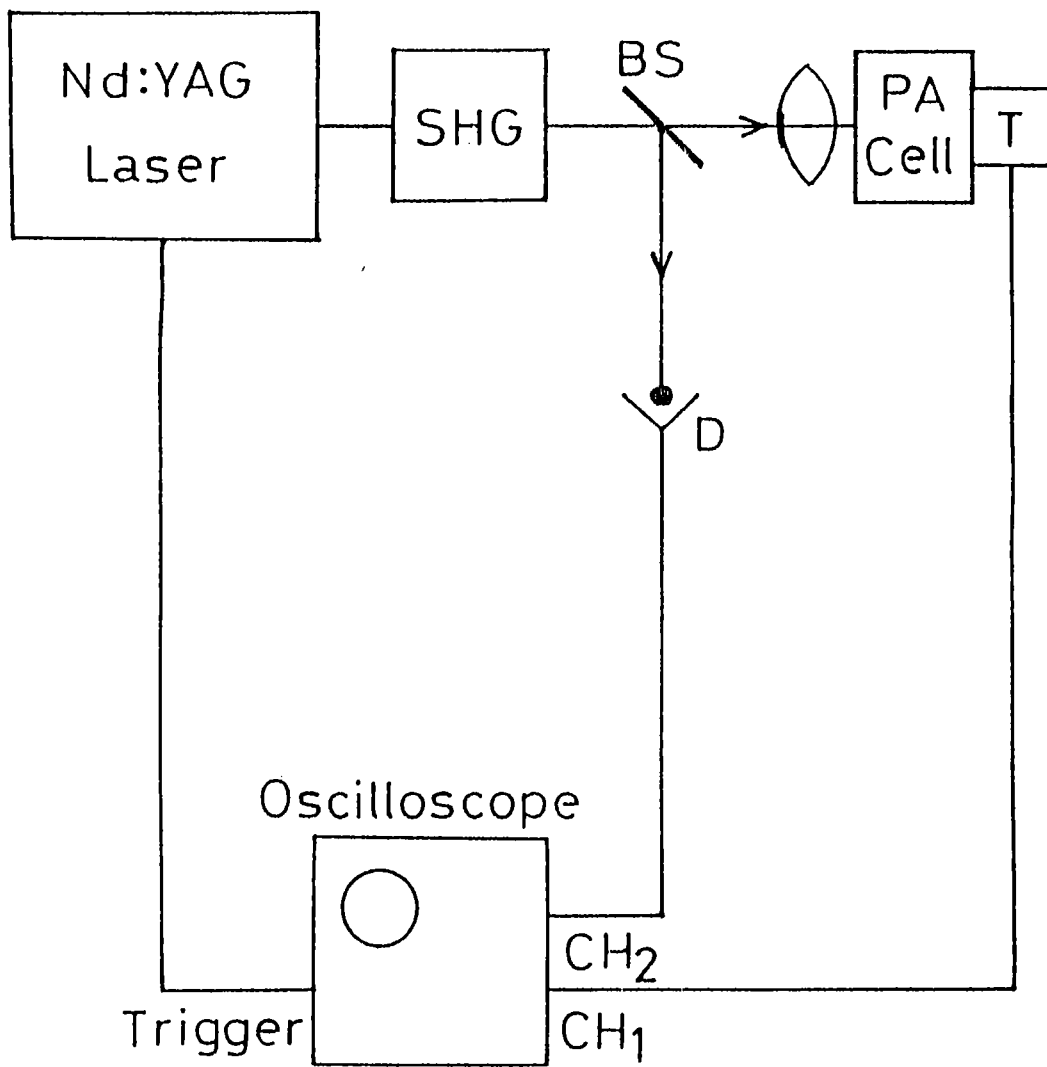


Fig.2.6. Schematic experimental set up for measuring acoustic velocities.

laser power level and is found to vary linearly (fig.2.7) in accordance with the expression,

$$P = \text{constant} \cdot \frac{\alpha \beta V E}{C_p} \quad (2.2)$$

where P is the PA signal amplitude, E is the laser pulse energy, β is the thermal expansion coefficient, C_p is the specific heat at constant pressure, V is the acoustic velocity and α is the optical absorption coefficient. The PA signal appears after a well defined delay time t with respect to the laser pulse. Knowing the separation between the beam waist and transducer surface 'd' and delay time t, the velocity of the acoustic waves generated (d/t) can be calculated. Results obtained have been in good agreement with previous reports.

Laser induced acoustic pulses in solid objects also have been detected using a similar experimental set up, where the transducer is firmly attached to the solid object in the form of plates or cylinder. Fig.2.8 shows the dependence of delay time with respect to the beam-transducer separation 'd' measured in the case of an aluminium plate 0.5 mm thick and 15 cm long.

Table 2.1 shows the values of calculated acoustic velocities in certain media.

2.3 FLUORESCENCE

The successful application of fluorescence methods

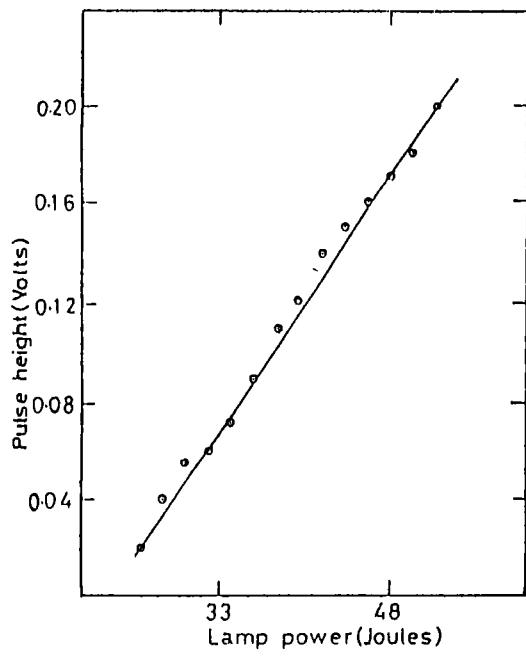


Fig.2.7.
 Variation of the photoacoustic pulse amplitude with laser power

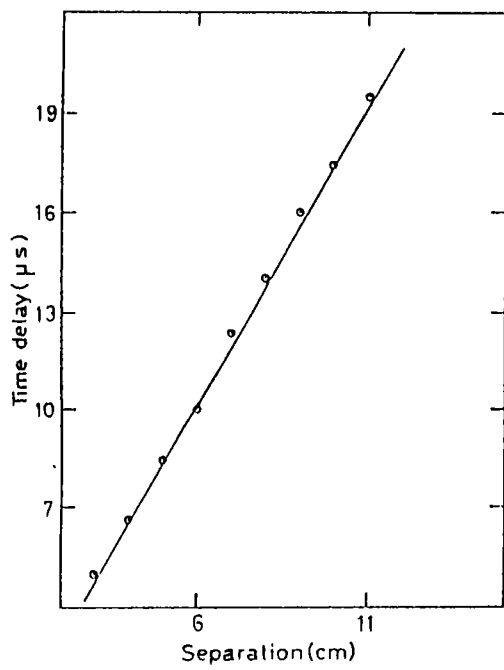


Fig.2.8.
 Variation of the delay time with beam-transducer separation

TABLE : 2.1 Sound velocity in certain materials measured using pulsed laser induced photoacoustic technique

Sample	Sound velocity	
	Present result (m / sec)	Reported result (m / sec) [24]
Distilled water	1449.7	1440
Toulene	1298.1	1300
Acetic acid	1140.1	1150
Nitrobenzene	1497.3	1490
Chlorobenzene	1333.3	1333
Aluminium cylinder	6133.3	6156
Aluminium plate	5714.2	--

requires a good understanding of the instrumentation involved. Considerable attention to the experimental details is necessary owing to the following reasons: Fluorescence is a highly sensitive method, in the sense that the gain or amplification of the instruments can invariably be increased to obtain observable signals. However, these signals may not originate with the fluorophore of interest. Instead one may observe interference due to background fluorescence from the solvents, light leaks in the instrumentation, stray light scattered by turbid solutions, Rayleigh and Raman scatter etc. to name a few. In a spectrofluorometer the non uniform spectral output of the light sources and the wavelength dependent efficiency of the monochromator and of the photomultiplier tubes may also affect the fluorescence spectrum. The polarization or anisotropy of the emitted light can also affect the measurement of fluorescence intensities. To obtain reliable spectral data one should be aware of, and control these numerous factors, for example, the apparent fluorescence intensity and spectral distribution can be dependent upon the optical density and the precise geometry of the sample. The most common geometry used for fluorescence is right angle observation of the center of a centrally illuminated cuvette. Other geometric arrangements include front-face and off-center illumination. In the case of front face illumination, the intensities become independent of sample concentration whereas for right angle observation the apparent fluorescence intensity will be distorted at high optical densities.

In the following sections a brief discussion of the important aspects of fluorescence instrumentation is given. For a discussion of optical sources for fluorescence spectroscopy,

please see section 2.21.

2.3.1 Monochromators

In selecting a monochromator for fluorescence spectroscopy, one looks for low stray light levels, high efficiency, and sufficient resolution. In fact it is rather impossible to find a monochromator with all the good qualities : for example a monochromator of high efficiency need not have a high resolution. So the experimenter usually settles down for the best compromise possible on his conflicting requirements. A typical monochromator will have entrance and exit slits, the widths and heights of which are generally variable. Larger slit widths yield increased signal levels, and therefore high signal to noise ratios. Smaller slit widths yield higher resolution, but at the expense of light intensity. The light intensity which passes through a monochromator is approximately proportional to the square of the slit width.

Grating monochromators generally use may have planar or concave gratings. Planar gratings are usually produced mechanically and may contain imperfections in some of the grooves. Concave gratings are produced by holographic and photoresist methods, and imperfections are rare. Imperfection of the grating is the major source of stray light transmission and formation of ghost images in the monochromator. For this reason the holographic gratings are preferred in fluorescence spectroscopy. The transmission efficiency of grating monochromators is a function of wavelength and with mechanically produced gratings the efficiency at any given wavelength can be

maximized by choosing an appropriate "blaze angle". Holographic gratings are not blazed, but the shape of the grooves can be varied. In general, their peak transmission efficiency is less than that for a planar grating, but the efficiency is more widely distributed on the wavelength scale than that of the planar grating.

The following two grating monochromators have been employed in the fluorescence studies :

(a). Jarrell-Ash : Model 82-000

This is a 0.5 meter Ebert scanning spectrometer. This instrument provides a smooth scanning motion in eight speeds ranging from 1 A°/minute to 500 A°/min and has a maximum resolution of 0.2 A°. The entrance and exit slit widths can be varied independently from 0 to 2000 microns. The monochromator covers a spectral range of 200 nm to 1600 nm with three interchangeable gratings blazed at 180 nm, 500 nm and 750 nm respectively. The spectral limit of this scanning spectrometer can be extended from 200 nm to 178 nm by flushing the instrument with nitrogen. The reciprocal linear dispersion at the exit slit is 16 A°/mm.

(b). Mc Pherson : Model 275

Mc Pherson, Model 275 is a 0.2 meter concave holographic grating monochromator. It has two flat folding mirrors. The monochromator covers a spectral range of 185 nm to 4000 nm using different gratings. The entrance and exit slit widths can be varied independently from 0 to 500 microns. The scanner of the monochromator has nine digitally controlled speeds : 5, 10, 50, 100, 200, 1000 and 2000 Å / minute. The wavelength accuracy is ± 0.5 nm and wavelength

reproducibility is ± 0.1 nm. Due to its high light gathering power, this monochromator is suitable for high sensitivity fluorescence work.

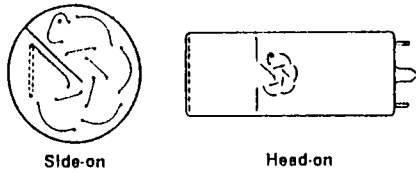
2.3.2 Photomultiplier tubes (PMT)

PMT s are almost exclusively used as detectors in fluorescence spectroscopy. A PMT is best regarded as a source of current, which is proportional to the light intensity. Although a PMT responds to individual photons, these individual pulses are generally detected as an average signal.

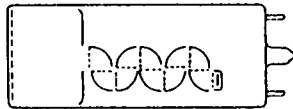
A PMT consists of a photocathode and a series of dynodes which form the successive amplification stages (see fig.2.9). The photocathode is a thin film of metal, on the inside of the window. Incident photons cause electrons to be ejected from this surface, with an efficiency dependent upon the incident wavelength. The photocathode is held at a high negative potential, typically 1000 to 2000 volts. The dynodes are also held at negative potentials, that decrease towards zero along the dynode chain. Each dynode in the chain is at a relatively positive potential with respect to the one before it, as a result of which a photoelectron emitted by the cathode will follow a path along the dynode chain, liberating more electrons from the dynodes in its travel. Thus an optical pulse detected by the PMT will invariably result in a current pulse at the anode, the amplitude of which will be proportional to the optical intensity detected by the cathode and the voltage applied to the PMT. Higher voltages result in an increased number of electrons ejected from each dynode, and hence higher amplification within

Types of Electron Multipliers

(a) Circular-Cage Type



(b) Box-and-Grid Type



(c) Linear Focused Type



(d) Venetian Blind Type

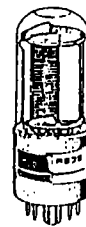


Fig.2.9a.

Types of photoelectron multipliers.

External Appearance

a) Side-On Type



b) Head-On Type

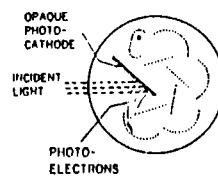


Fig.2.9b.

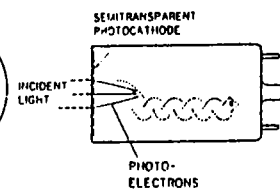
External appearance of photomultiplier tubes and types of photocathode

Types of Photocathode

a) Reflection Mode



b) Transmission Mode



the working voltage range of the PMT.

We have used the following PMT s in our fluorescence experiments:

(a). Thorn EMI

In our experimental set up the output from the Jarrell-Ash monochromator is detected by an EMI PMT (Model No.9683 KQB) with S- 20 cathode. This PMT has a fairly good quantum efficiency in the 300 - 800 nm spectral range. The PMT is operated at 1350 V DC derived from an EMI model PM28B high voltage power supply. The tube has an air cooled, RF shielded housing and it can be directly mounted in a line with the exit slit of the monochromator.

(b). Hamamatsu R 446 (Side-on)

R 446 has a diameter of 28 mm. It has a 9 stage circular cage structure with a multialkali photocathode. The tube has high quantum efficiency, high current amplification and good S/N ratio. It has a spectral response in the region of 185 nm to 870 nm. R446 has been in conjunction with the Mc Pherson monochromator in our experiments.

2.3.3 Fluorescence signal processing

In a practical set up to observe weak fluorescence emission with moderate spectral resolution, the actual signal is usually immersed in various types of noises. Generally noise is

generated due to the following reasons : (a) External light that may come through the collection optics, (b) Scattered laser light from the sample, (c) Dark current of the PMT which is a dc level of a few nA, (d) Shot noise from the PMT whose periodicity is very low, (e) Johnson noise, (f) Amplifier noise etc..Of these (a) and (b) can be minimized by proper positioning of the sample holder and optical components. Nowadays PMT s with minimal dark current ratings also are available. Boxcar detection is particularly useful in eliminating noise in pulsed fluorescence experiments.

2.3.4 Experimental set up for Fluorescence studies

Fig.2.10 shows the schematic experimental set up employed in our fluorescence studies. 1060 nm, 532 nm or (1060 + 532) nm beam selected from the pulsed Nd:YAG laser is used as the source of excitation for producing fluorescence emission from various samples. The laser beam excites fluorescence in the sample solution taken in a quartz cuvette, which is collected and focussed by a convex lens of 5 cm focal length onto the entrance slit of the monochromator. Slit widths less than 25 microns each are sufficient for recording the strong Stokes fluorescence from the samples. However, recording of the weak antistokes fluorescence (to be discussed later) is possible only using larger slitwidths, typically between 50 and 100 microns. Proper optical filters have been used in some of the experiments to avoid the entry of the scattered laser radiation into the monochromator. These are, a coloured glass filter (Glendale Optical Co.) that filters wavelengths less than 540 nm, and a distilled water cell of 3 cm pathlength that cuts off the 1060 nm

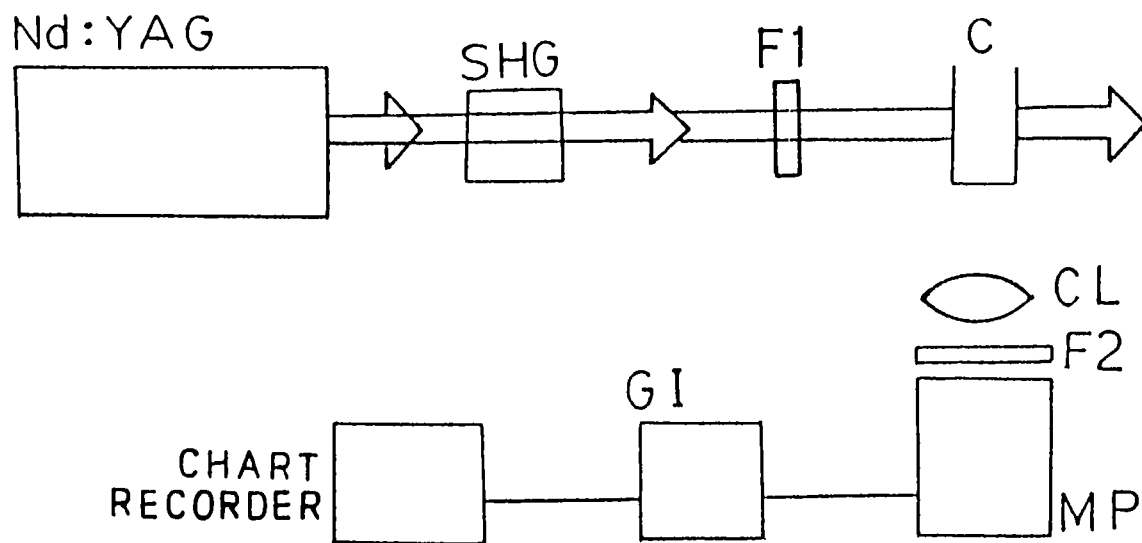


Fig.2.10. Schematic experimental set up for fluorescence studies
 SHG - Second harmonic generator, C -cuvette, CL -
 collection lens, F2- filter, MP - monochromator and PMT,
 GI- gated integrator and boxcar averager,
 F1- Harmonic separator

radiation. The emission is then wavelength scanned in the desired region and the optical intensity is detected by the photomultiplier tube which is terminated by a 100 k ohm dc return resistor. The signal from the PMT is gated (typical gate delay is $1 \mu s$ and gate width $10 \mu s$) and averaged using the gated integrator and boxcar averager system whose output is read on a digital multimeter or fed to a chart recorder.

For normalization, the spectral response of the two monochromator-PMT combinations used in our experiments have been calculated (fig.2.11) in the following way : The emission of a xenon arc lamp (Mueller) is recorded over a broad wavelength region using these detectors and the obtained output is then compared with the true emission spectrum of the lamp supplied by the manufacturer. The spectral response curves are hence drawn. For correcting a spectrum obtained from experiment, the values are divided by the spectral response of the detector at every wavelength. The new values give the actual spectrum corrected for the spectral response of the detector.

2.4 SUMMARY

The general aspects of Photoacoustic and Fluorescence instrumentation are briefly discussed in this chapter. The design and fabrication details of the photoacoustic cell are outlined and the description of an experiment performed to calculate the laser induced acoustic velocities in liquid and solid media are presented. The actual experimental arrangements which were employed for the studies to be discussed in this thesis are given.

REFERENCES

- [1] Harshbarger W R and Robin M B, *Acc. Chem. Res.*, 6, 329, 1973
- [2] Rosencwaig A, *Opt.Comm.*, 7, 305, 1973
- [3] Kohanzadeh Y, Whinnery J R and Carroll M M, *J.Acoust.Soc.Am.*, 57, 67, 1977
- [4] Bonch-Bruevich A M, Razumova T K and Starobogatov I O, *Sov. Phys. Tech. Phys. Lett.*, 1, 26, 1975
- [5] Bonch-Bruevich A M, Razumova T K and Starobogatov I O, *Opt. Spectrosc.*, 42, 45, 1977
- [6] Emmony D C, Sigrist M W and Kneubühl, *Appl.Phys.Lett.*, 29, 547, 1976
- [7] Callis J B, *J. Res. Nat. Bur. Stand.*, 80 A, 413, 1976
- [8] Sladky P, Danielius R, Sirutkaitis V and Boudys M, *Czech. J. Phys.*, B27, 1075, 1977
- [9] Lahmann W and Ludewig H J, *Chem.Phys.Lett.*, 45, 177, 1977
- [10] Lahmann W, Ludewig H J and Welling H, *Anal.Chem.*, 49, 549, 1977
- [11] Hordvik A and Scholssberg, *Appl.Opt.*, 16, 101, 1977
- [12] Farrow M M, Burnham R K, Auzanneau M, Olsen S L, Purdie N and Eyring E M, *Appl. Opt.*, 17, 1093, 1978
- [13] Sigrist M W and Kneubühl F K, *J.Acoust.Soc.Am.*, 64, 1652, 1978
- [14] Burt J A, *J.Acost.Soc.Am.*, 65, 1164, 1979
- [15] Sam C L and Shand M L, *Opt.Commun.*, 31, 174, 1979
- [16] Edward Voigtman, Arthur Jurgensen and James Winefordner, *Anal.Chem*, 53, 156, 1981
- [17] Masahide Itoh and Hiroyoshi Saito, *Opt.Commun.*, 44, 229, 1983
- [18] Hutchins D A, *Proceedings of the conference on New Techniques in Sonar Transducers, Proceedings of the Institute of Acoustics, Birmingham, U.K*, 6, 24, 1984

- [19] Pak-Kon Choi and Kenshiro Takagi, Jpn.J.Appl.Phys., 26, L1388, 1987
- [20] Hangyo M, Nakashima S, Oohara Y and Kumira, J.Appl.Phys., 63, 295, 1988
- [21] Peralta S B , Al-Khafagi H H and Williams A W, J.Phys.E : Sci.Instrum, 21, 195, 1988
- [22] Patel C K N and Tam A C, Chem.Phys.Lett., 62, 511, 1979
- [23] Patel C K N and Tam A C, Appl.Phys.Lett., 34,467,1979
- [24] Robert C Weast (ed.), Handbook of Chemistry and Physics, (CRC ; USA), 1974

CHAPTER - 3

TWO PHOTON ABSORPTION IN RHODAMINE 6G - INVESTIGATIONS BY PULSED PHOTOACOUSTIC EFFECT

3.0 INTRODUCTION

Almost simultaneously with the invention of the laser the question of output tunability over a broad range of wavelengths was raised, which was realized for the first time in a solution of an organic dye by Sorokin et al [1]. The tunability of the dye laser is a consequence of the broadened electronic levels characteristic of organic dyes which form the active medium. Various lasing compounds have been discovered over years, which are divided into classes according to their chemical structures. Some of the important classes of organic dyes include scintillators, coumarins, xanthenes, oxazines, polymethines etc., each having specific wavelength tunability ranges. Most dye lasers today operate with materials that belong to the class of xanthene dyes. They have a xanthene ring as a chromophore. Xanthenes emit in the wavelength region of 500-700 nm and give excellent lasing results. These dyes are also widely utilized in color cloths, papers, cosmetics, food stuffs etc.

The Rhodamines form a group in the xanthene dye family in which the 2- and 7- positions of the xanthene ring are substituted by amino (NH_2) radicals. Rhodamine dyes exhibit a large number of conjugated double bonds and delocalized p - electron orbitals. The broad electron delocalization results in large polarizabilities and strong absorption in the visible region of

the spectrum. The lasing efficiency of rhodamine dyes is very high and the chemical stability fairly good. An energy conversion efficiency of over 50% is available for green pumping sources such as the second harmonic of Nd:YAG laser, Cu vapor laser etc.

Probably Rhodamine 6G (R6G) is the most popular member of the Rhodamine group, the structure of which is shown in fig.3.1. R6G dissolved in liquid solvents is one of the important laser dyes utilized for cw operation [2] and short-pulse (~ 1.5 ps) generation [3]. This dye has been considered as a laser material in a PMMA (poly methyl methacrylate) matrix [4] and in glasses. R6G has been a standard for evaluating other dyes ever since various ways of laser operation were first tried.

3.1 ABSORPTION AND FLUORESCENCE PROPERTIES OF R6G

The π -electron distribution in the chromophore of the xanthene dyes can be described approximately by the two identical mesomeric structures A and B (fig.3.2). Since the forms A and B have the same weight in xanthene dyes there is no static dipole moment parallel to the long axis of the molecule in either the ground or excited state. The transition moment of the main absorption band, which occurs between 450 nm and 600 nm is oriented parallel to the long axis of the molecule. The position of the long wavelength band depends markedly on the substituents in 3 - and 6 - positions of the xanthene nucleus. The methyl substituents found in R6G have no influence on either absorption or fluorescence of this dye. The absorption maximum of the rhodamines is dependent on the solvent, in particular with those dyes whose amino groups are not fully alkylated (eg. R110 and

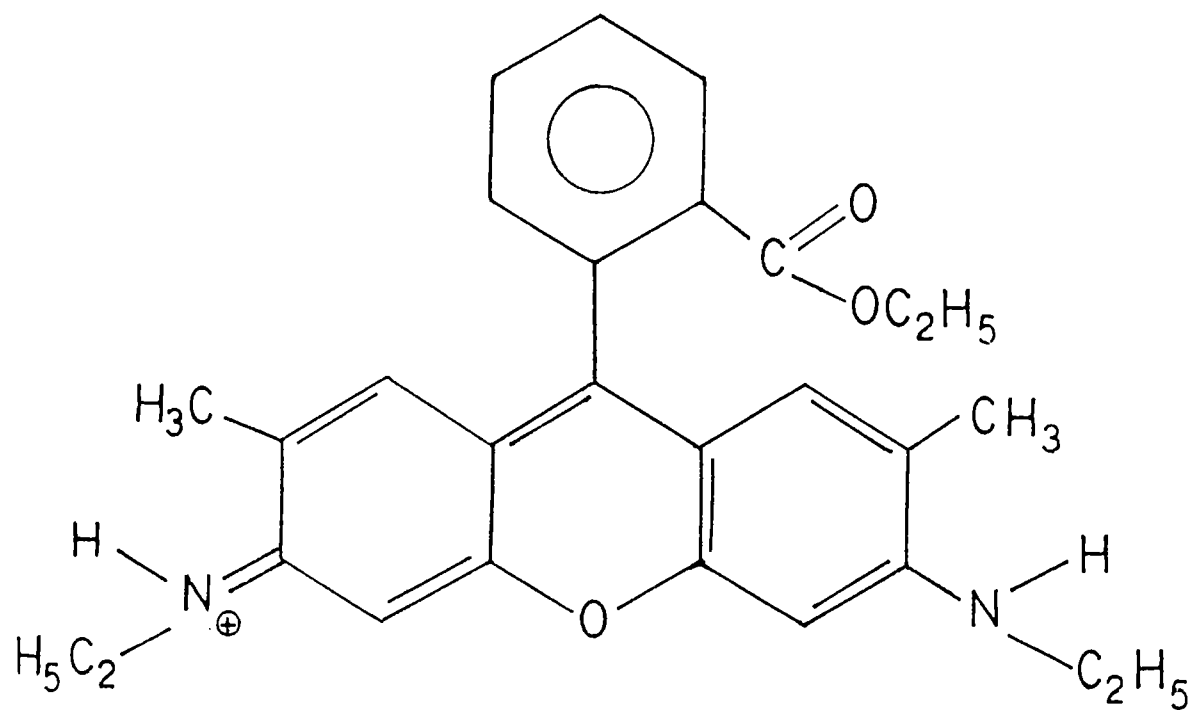


Fig.3.1. Structure of Rhodamine 6G

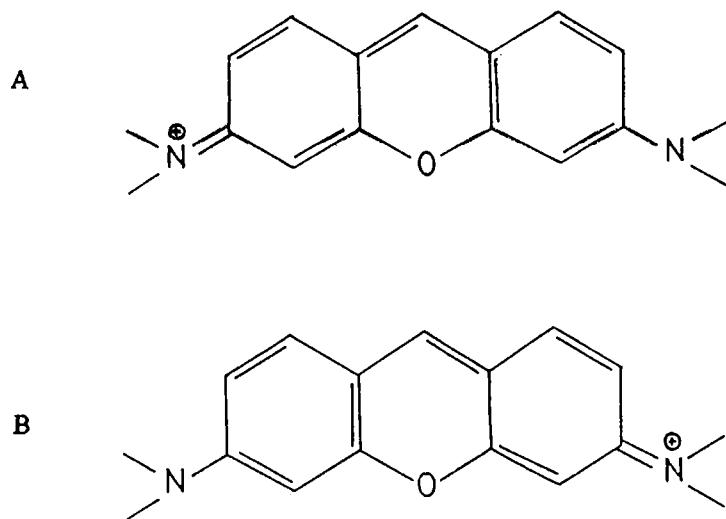


Fig.3.2. The mesomeric structures

R6G). The fluorescence spectrum closely resembles the mirror image of the long-wavelength absorption band, and for R6G the emission maximum is shifted by about 20 nm with respect to the absorption maximum.

3.1.1 Effects of solvent and concentration

In general, the absorption and emission spectra of the dyes in various solvents differ from each other. The spectra for different concentrations in the same solvent also show variations. The absorption spectra of R6G in water, methanol and ethylene glycol at different concentrations (ranging from 10^{-3} moles/lit to 10^{-6} moles/lit) recorded in a UV - VIS - NIR spectrophotometer (Hitachi, model U- 3410), are shown in the figures 3.3a, 3.3b, 3.3c respectively. The samples were taken in a 1 cm square quartz cuvette.

For observing the Stokes fluorescence from these samples, the experimental set up given in chapter 2 was employed. The laser beam (532 nm) falls on a cuvette that contains the sample solution. The fluorescence emission normal to the pump beam is collected by a convex lens ($f = 5$ cm) and analyzed by a 0.2 m grating monochromator. The emission is wavelength scanned and detected by a photomultiplier tube, the output of which is fed to a gated integrator and boxcar averager system. The gated and averaged signal is then recorded by means of a chart recorder. The charts obtained are shown in figs.3.4a and 3.4b. Concentration dependent spectral shifts are observed, arising from reabsorption of fluorescence and possible molecular aggregate formation at high concentrations.

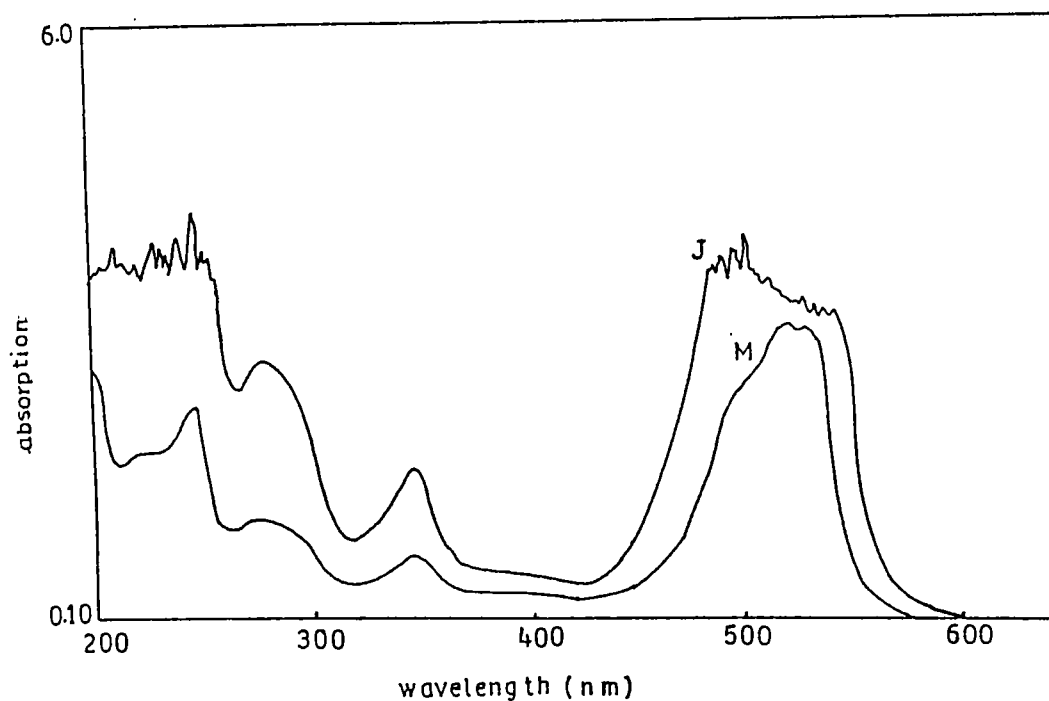


Fig.3.3a. Absorption spectra of Rhodamine 6G in water
M - 0.008 milli moles/lt, J - 0.178 milli moles/lt

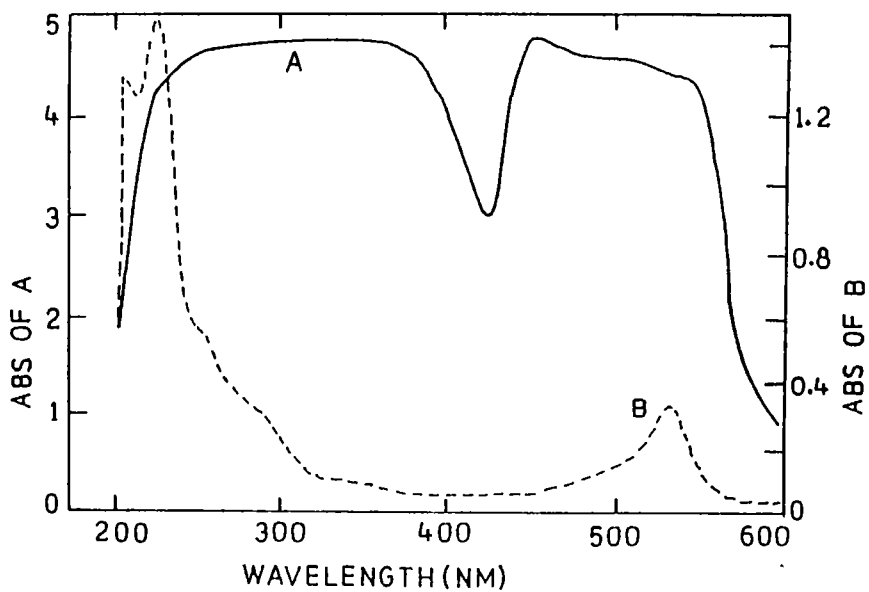


Fig.3.3b. Absorption spectra of Rhodamine 6G in methanol
A - 2.08 milli moles/lt, B - 0.069 milli moles/lt

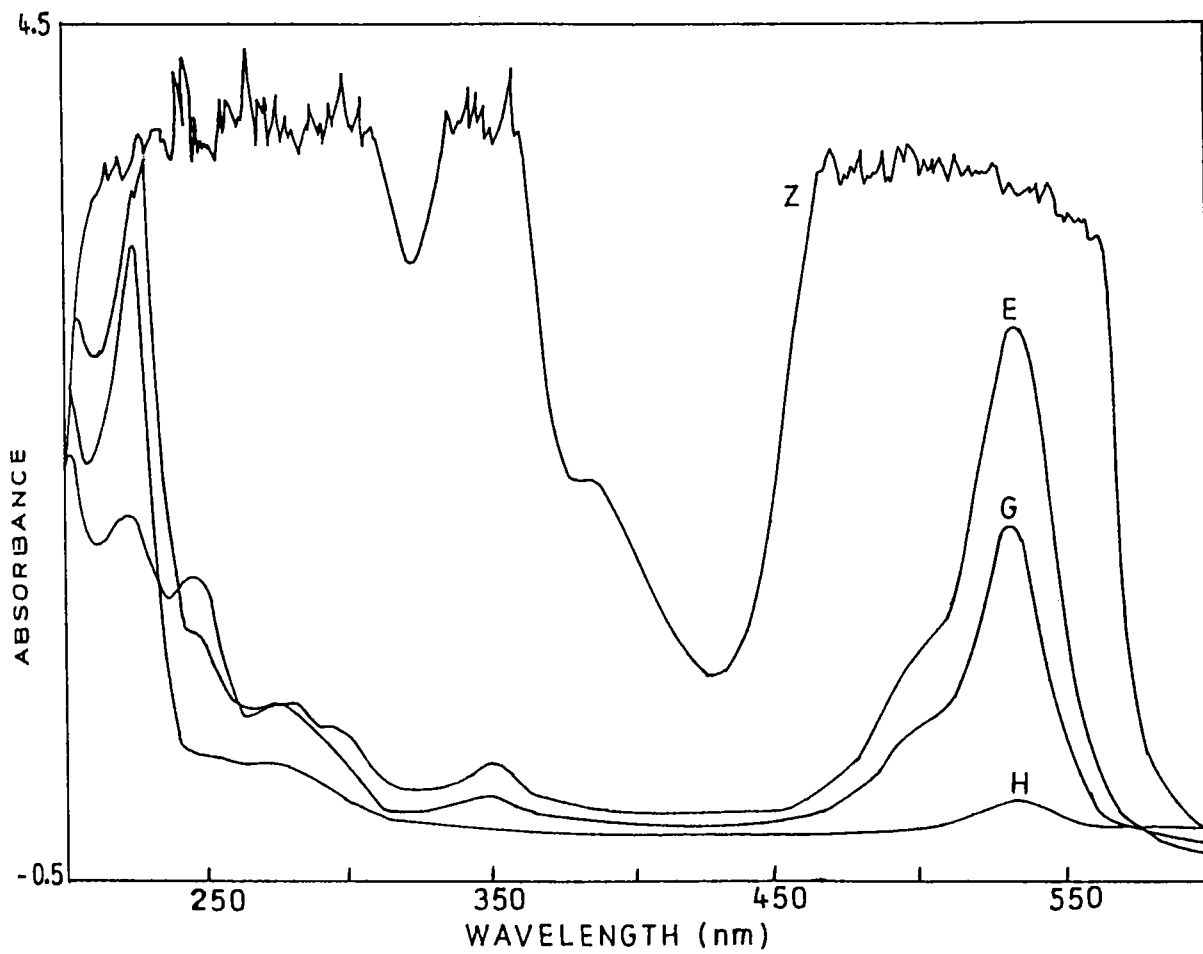


Fig.3.3c. Absorption spectra of Rhodamine 6G in ethylene glycol
Z - 1.06 milli moles/lt, E - 0.028 milli moles/lt,
G - 0.0045 milli moles/lt, H - 0.0018 milli moles/lt

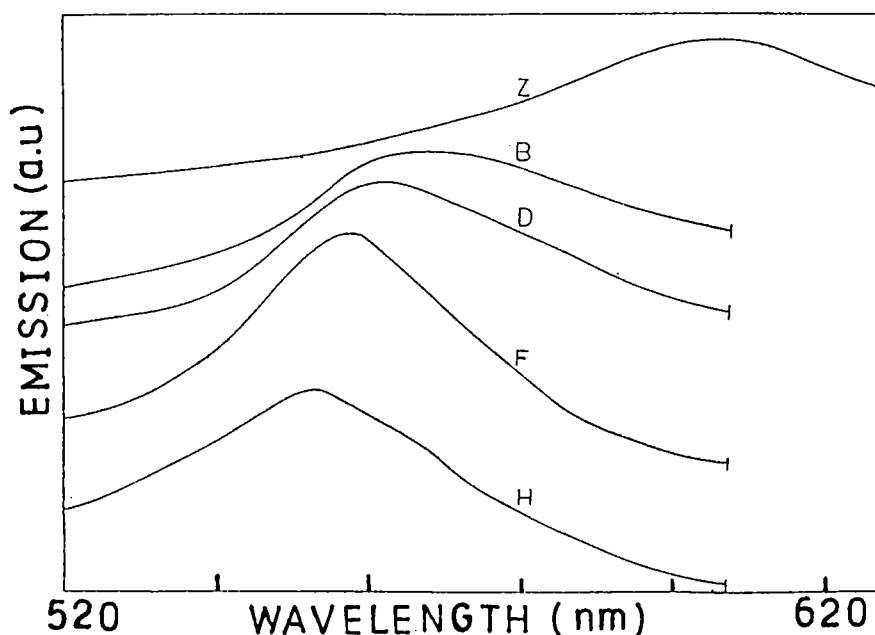


Fig.3.4a. Fluorescence emission spectra of Rhodamine 6G in water.

The emission peaks are shown in brackets for each concentration.

Z - 1.29 milli moles/lt, (605 nm), B - 0.899 milli moles/lt, (568 nm), D - 0.532 milli moles/lt, (562 nm), F - 0.37 milli moles/lt, (556 nm), H - 0.25 milli moles/lt, (551 nm)

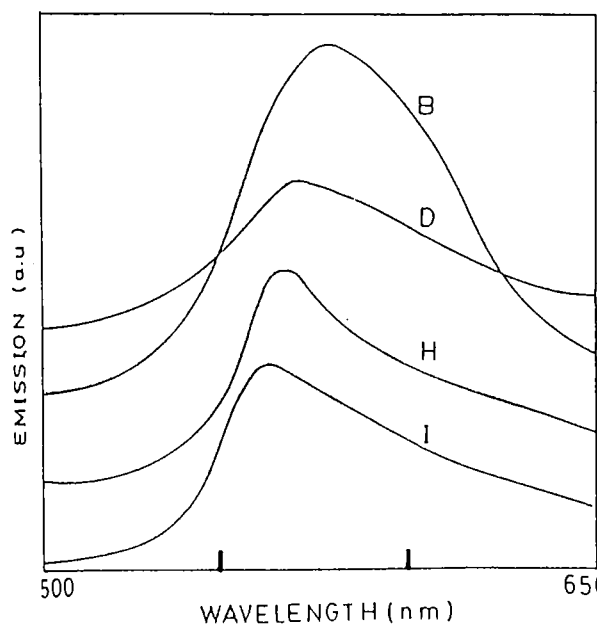


Fig.3.4b.

Fluorescence emission spectra of Rhodamine 6G in methanol.

The emission peaks are shown in brackets for each concentration.

B - 1 milli mole/lt, (580 nm)
 D - 0.69 milli moles/lt, (570 nm)
 H - 0.34 milli moles/lt, (565 nm)
 I - 0.173 milli moles/lt, (560 nm)

In solutions of low concentration dyes dissolve practically completely into monomers. The absorption spectra are determined by the intrinsic absorption of the dye molecules and the dye-solvent interaction. Dye-dye (solute-solute) interaction is negligible because of the large average distance between dye molecules. The absorption characteristics obey the Beer-Lambert law, i.e., the absorption cross-sections are independent of concentration. With increasing dye concentration dimers or higher aggregates of the dye molecules are formed [5-14] and the absorption spectrum is modified, with contributions from the aggregates. For example, a dimer molecule will have an absorption towards the shorter wavelength side of the monomer band. The strength of dimer (and higher aggregate) formation and the solubility are strongly dependent on the solute-solvent combination and on the temperature. For highly soluble dye solutions the dye-dye interaction gains importance at high concentrations since the mean distance between the dye molecules becomes sufficiently small. This dye-dye interaction of neighbouring dye molecules will also contribute to deviations of the absorption spectra from Beer's law at high concentration [5, 15, 16]. Since the upper level from which the fluorescence starts is always the lowest-lying excited electronic level, and since a small transition moment is coupled to a long-lifetime of the excited state, the dimers would show a very slow decay of their fluorescence [2]. In most cases the fluorescence of the dimers is completely quenched and cannot be observed. This is the reason why dimers constitute an absorptive loss of pump power in dye lasers and must be avoided by all means.

For R6G, the dimer formation in the solvent water seems

to be due to the linking of two dye molecules by two hydrogen bridges of water of the form *dye-H-O-H-dye*. In non-polar solvents the separation of R6G cation and chloride anion is inefficient, the molecule is uncharged and the electrostatic repulsion between the molecules is negligible. The energetics of such a situation favour the formation of dimers; however the nature of the bonding orbitals is different from those in water. In the case of R6G in methanol, the solvent shell around the dye molecules seems to hinder or lower the probability of dye-dye linkage (in methanol only one H-atom is capable of hydrogen bonding). However several reports have appeared confirming aggregate formation in R6G : methanol systems at very high concentrations [5-14].

For large molecules, reabsorption of luminescence by the ground state molecules is a familiar fact. Reabsorption occurs due to the overlap of absorption and emission bands, which becomes significant at high concentrations. This effect has often been pointed out as an explanation to account for the tendency of certain laser dyes to lase at longer wavelengths than is expected. With increased pump intensity, however, it has been noted that the ground state absorption is reduced and the fluorescence emission shifts to shorter wavelengths [17]. In another report on R6G in methanol system, [18] the variation of peak gain spectrum showed that the peak gain increases superlinearly in the lower concentration region ($<10^{-3}$ moles/l) and sublinearly in the high concentration region ($>10^{-3}$ moles/l). Also the peak wavelength becomes longer in the higher concentration region. This behaviour has been attributed to the concentration dependence of the fluorescence lifetime [19,20], radiation trapping and concentration quenching effects.

3.2 NONLINEAR ABSORPTION IN DYES

The study of TPA and higher order multiphoton excitations in various compounds has been mostly based on the observation of radiative transitions induced by the same from a higher excited electronic state, usually at a shorter wavelength than the pump wavelength (ASF). However, in organic dyes the fluorescence quantum yield of ASF is negligible since higher excited states are depopulated through strong non radiative coupling to the S_1 state, thus making the observation of ASF very difficult. This non radiative relaxation $S_n \rightarrow S_1$ ($n>1$) should give rise to photoacoustic signals of high amplitudes as compared to the ASF signal. Since the non-radiative coupling between S_n ($n>1$) and S_1 states is very strong in dyes TPA can be better studied by analysing these non-radiative processes rather than ASF. If we measure the pulsed photoacoustic signals generated in an absorbing dye using the experimental set up described in chapter 2, and if the absorption is by single-photon processes only, then the amplitude of the piezoelectric signal per laser pulse is given by, [21]

$$q(\nu) = A I(\nu) \tau \eta (\nu) (1 - e^{-\beta(\nu)l}) \quad (3.1)$$

where A is a constant determined by calibrations, $I(\nu)$ is the intensity of the laser pulse, τ is the pulse length, ν is the quantum yield of non-radiative transitions, β is the optical absorption coefficient, and l is the optical path length in the cell. The constant A is a function of the cell geometry, piezoelectric transducer properties and the ultrasonic attenuation of the solution.

If the laser intensity is sufficiently high, multiphoton absorption can occur, and the piezoelectric signal is then given by

$$q(\nu) = \sum_{m=1}^n A [I(\nu)]^m \eta(\nu_m) \rho(\nu) N l \quad (3.2)$$

where $\eta(\nu_m)$ represents the quantum efficiency for nonradiative transitions of the ν_m level, $\rho(\nu)$ is the absorption cross-section, and N is the density of absorbing molecules. Here we have assumed that the solution is optically thin, and $(1 - e^{-\beta l}) \sim \beta l = \rho(\nu) N l$. Thus if PA signals are generated in a sample due to two photon absorption and subsequent nonradiative relaxation, then these signals will have a quadratic dependence on the pump intensity. Hence by monitoring the dependence of PA signals on pump laser power one can identify the occurrence of nonlinear absorptions taking place, if any, in the sample.

3.3 GENERATION OF PHOTOACOUSTIC SIGNAL IN R6G - PUMPING BY 532 NM

It is possible to populate the higher excited states of R6G molecule by using uv pumping or certain broadband sources like flashlamps. However this happens with strong monochromatic pump sources operating in the visible as well, by multiphoton excitation. The usual one photon excitation with the typical 532 nm beam from the second harmonic output of an Nd:YAG laser raises the R6G molecule to a vibronic level of the S_1 state ($\approx 18000 \text{ cm}^{-1}$). Excitation to level S_3 ($\approx 37000 \text{ cm}^{-1}$) can simultaneously take place by two photon absorption. In general under intense pumping, along with direct TPA and possible multiphoton

absorption, excited singlet state absorption (ESA) can also occur in dyes populating higher singlets. Excited singlet state absorption in R6G was studied earlier by various groups. Magde et al. [22] investigated the region, 3000 - 6500 Å and reported an absorption maximum at 4400 Å and submaxima at 4000 Å and 5300 Å. Sahar and Treves [23] investigated the region 4600 - 6150 Å and reported two maxima at 5300 Å and 5650 Å, which were confirmed by Benstein et al [24].

Subsequent to a two photon excitation in the dye, PA signals are generated due to the strong $S_n (n>1) \rightarrow S_1$ non-radiative coupling. These signals should have a quadratic dependence on laser energy. On the other hand, molecules populating the various vibronic levels of S_1 due to OPA will rapidly de-excite non radiatively to the lowest vibrational level of the S_1 manifold in accordance with the Franck-Condon principle as to produce PA signals of much lesser intensity and with a linear dependence on laser energy. Generation of PA signals from $S_1 \rightarrow S_0$ internal conversion can be neglected in R6G due to its high quantum yield and the comparatively large energy separation about 18000 cm^{-1} . On a first approximation all triplet effects leading to PA generation also can be ruled out, since the pulse width (t) of the pump laser pulse is only 10 ns in our case, such that $t \ll 1/k_{st}$ where k_{st} is the $S_1 \rightarrow T$ intersystem crossing rate which is approximately $4.2 \times 10^5 \text{ s}^{-1}$ in R6G [35].

4 EXPERIMENTAL SET UP

The schematic experimental set up is as shown in chapter

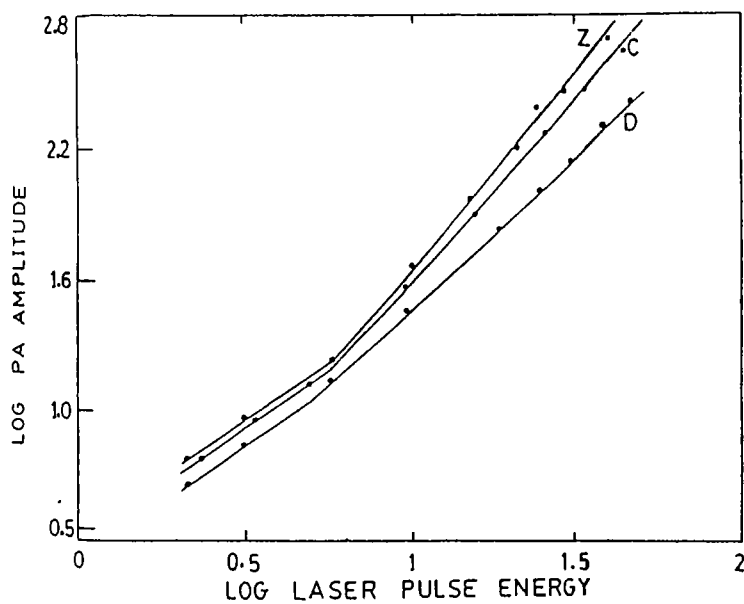
2. The IR eliminated second harmonic output (532 nm) of a Q-switched pulsed Nd:YAG laser (Quanta-Ray, DCR-11) is focussed by a convex lens (focal length = 5cm) into the PA cell containing the sample. The laser pulse duration is ≈ 10 ns and the pulse repetition frequency is 14 Hz. The pump energy is monitored by a laser power/energy meter. The transducer output is observed on a digital storage oscilloscope. The amplitude of the first pulse in the PA signal trace is monitored as a function of the pump pulse energy, with dye concentration as the changing parameter.

3.5 RESULTS

3.5.1 Rhodamine 6G : Water system

The physical and thermal properties of water makes it an ideal solvent for most laser dyes. However care should be taken while preparing aqueous dye solutions, to prevent aggregation of dye molecules. Tuccio and Strome [24] have described the operation of a three element cw dye laser using a water solution of R6G. They obtained an output which is tunable from 550-640 nm.

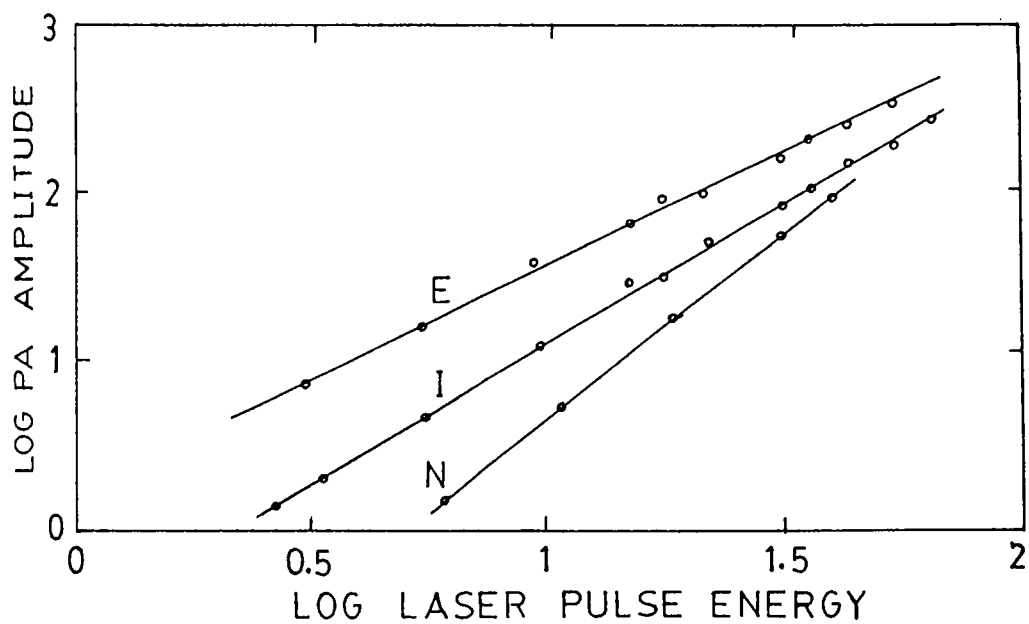
Using the experimental set up described above the PA signals from solutions of R6G:Water samples of different concentrations (10^{-3} moles/lt to 10^{-5} moles/lt) have been detected at various input laser energies (2mJ to 30mJ). The log of PA signal is plotted against the log of laser pulse energy for each sample. We have classified the samples taken into a set of lower concentrations and a set of higher concentrations based on these log-log plots. In the group of lower concentrations, the plots are found to be straight lines with slopes changing from



(a) High concentration samples

Z - 1.295 milli moles/lt, C - 0.691 milli moles/lt,

D - 0.532 milli moles/lt



(b) Low concentration samples

E - 0.44 milli moles/lt, I - 0.213 milli moles/lt,

N - 0.055 milli moles/lt

Fig.3.5. Log photoacoustic signal amplitude vs log laser pulse energy for Rhodamine 6G :water system

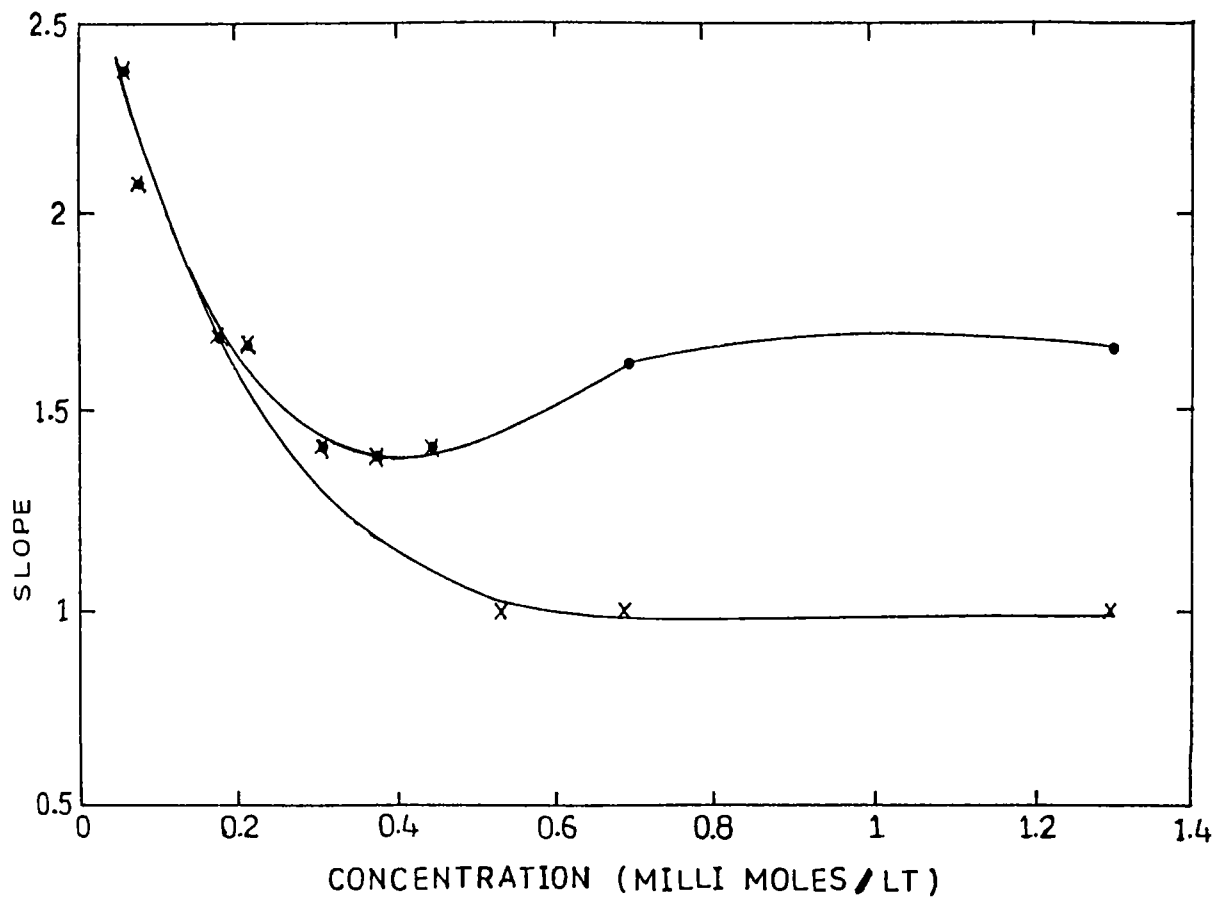


Fig.3.6. Variation of the slope of log-log plots with concentration in aqueous solutions of Rhodamine 6G,

x - laser pulse energy < 7 mJ, • - laser pulse energy > 7 mJ

1.4 to 1.3 as the concentration is increased (fig.3.5b). For higher concentrations, while lower slope (corresponding to the energy range 2 - 7 mJ) is almost one, the higher slope (energy > 7 mJ) is found to be greater than one, and the threshold of this change in slope varies inversely with concentration (fig.3.5a). The estimated error in the slope calculations is approximately ± 0.1 .

From earlier investigations, the R6G molecule in the ground state has been assigned practically C_{2v} symmetry [25]. The ground state of the π electrons belong to the totally symmetric representation A_1 whereas the excited states belong to either A_1 or B_2 . Considering the R6G molecule as quasi symmetric (C_{2v} group), $A_1 \rightarrow B_2$ transition moments are weak for two photon transitions [25]. However due to the lack of perfect symmetry of the R6G molecule both the one photon and two photon transitions seems to be allowed between all states [26]. Even though previous studies conducted in ethanol solutions [25, 27] report that R6G molecule has B_2 symmetry in the S_1 state, our results explained with the help of the absorption spectra indicate that variations may be occurring with change in concentration.

Fig.3.3a shows the absorption spectra of R6G in water at two concentrations of which one is high and the other is low. From the spectra it can be seen that absorption $S_0 \rightarrow S_1$ (visible region) is more favoured as compared to uv absorption in the low concentration regime. Assuming from the absorption spectra that S_1 has B_2 symmetry and S_3 has A_1 symmetry, it is obvious that in one photon process $S_0 (A_1) \rightarrow S_1 (B_2)$ is strongly allowed while the absorption $S_0 (A_1) \rightarrow S_3 (A_1)$ is weaker. The converse is true for TPA process. Hence at low concentrations TPA process should be favoured to OPA. Further,

earlier studies on light quenching of dye fluorescence have shown that excited state absorption (ESA) is stronger in low concentration solutions [38]. Thus the slopes should be high for the low concentration samples; this is confirmed from the obtained log-log plot (fig.3.5b) where an increase in slope from 1.3 to 2.4 is observed as the concentration is decreased. Slopes > 2 can be indicative of the probability of higher order absorption processes in the samples of very low concentrations. With the increase of concentration the OPA process in uv region gets enhanced in comparison to that in the visible (probably due to various kinds of complex formation, solute-solute and solute-solvent interactions) as revealed by the absorption spectra. Our conjecture is that S_3 at higher concentrations takes up more of B_2 character so that $S_0 \rightarrow S_3$ OPA becomes strongly allowed whereas TPA is not favoured [36]. This means that S_1 and S_3 now have nearly B_2 symmetry thereby reducing the $S_1 \rightarrow S_3$ OP excitation, so that contribution due to ESA ($S_0 \rightarrow S_1 \rightarrow S_3$) is lowered along with the TPA process $S_0 \rightarrow S_3$. In addition at concentrations above 10^{-4} moles/lt, absorbing but nonfluorescent dimers will be formed in aqueous solutions of R6G [39] leading to strong $S_0 \rightarrow S_1$ OPA resulting in almost complete nonradiative relaxation. These effects are collectively manifest by the decrease in the slope reaching unity with increase in sample concentration (fig.3.5a). However at higher pump energies, slopes ≈ 1.5 are observed even for higher concentrations due to the following reasons : (i) TPA is quadratically proportional to the pump energy and linearly proportional to the population of level S_0 and (ii) ESA is proportional to population of level S_1 as well as the pump energy. The contribution from these two effects will hence effectively compete with the $S_0 \rightarrow S_1$ OPA process.

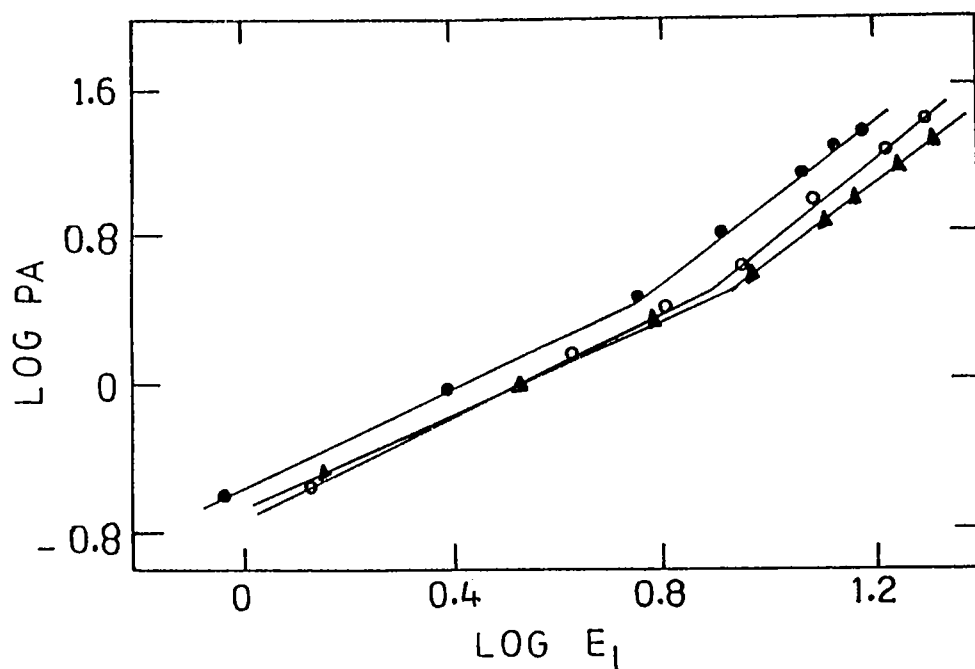
Fig.3.6 shows the variation of the slope of the log laser pulse energy vs log PA plots with concentration.

3.5.2 Rhodamine 6G : Methanol system

R6G in water forms stable ground state dimers whereas R6G in methanol has a low tendency to form stable ground state dimers [28]. The fluorescence quantum efficiency and the fluorescence lifetime for R6G:methanol system has been extensively studied earlier [29].

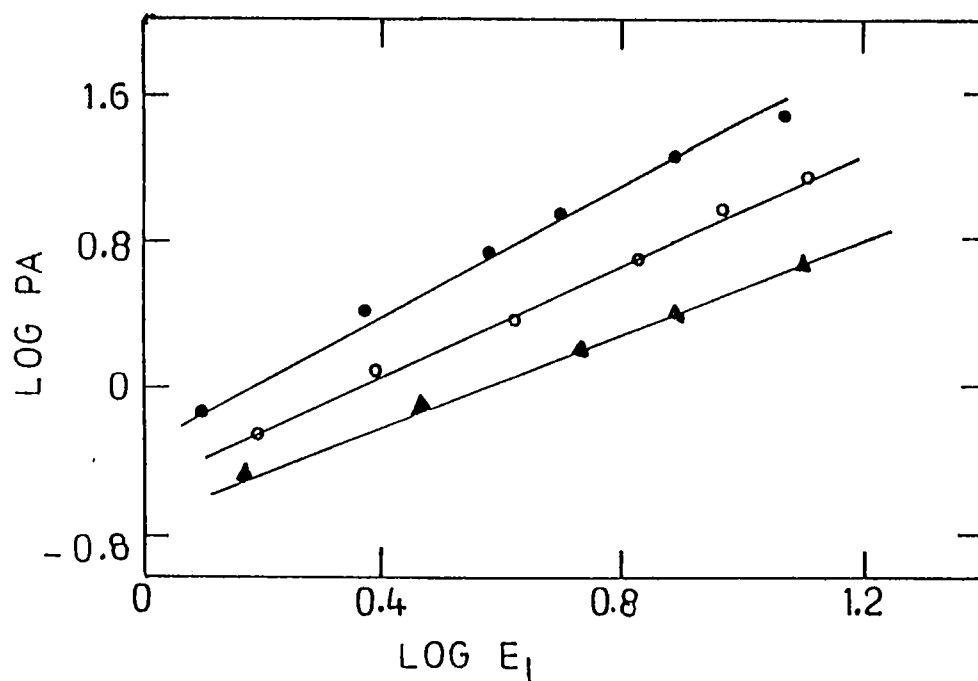
At various laser energies (2 mJ to 30 mJ), the PA signals from solutions of R6G:Methanol of different concentrations (10^{-3} moles/lit to 10^{-5} moles/lit) have been detected. Figs.3.7a and 3.7b show the log of laser pulse energy plotted against log of PA amplitude for different sample concentrations. As before, the samples have been divided into two groups: one of high concentrations (≥ 0.69 m mol/lit) and the other of low concentrations (< 0.69 m mol/lit). At higher concentration the log-log plot has two distinct slopes, one with an average value of 1.1 ± 0.1 at lower energies and another which is significantly greater than 1, with an average value of 1.9 ± 0.1 at higher energies (> 6 mJ) (fig.3.7a). The threshold for changeover from OPA to TPA is found to decrease as concentration increases. In the low concentration group it is observed that as concentration increases, the slope changes from 1.6 ± 0.1 to 1.1 ± 0.1 (fig.3.7b).

The absorption spectrum of R6G in methanol shows maxima at 19230, 28571, 36363 and 41666 cm^{-1} , corresponding to the excited singlets S_1 , S_2 , S_3 and S_4 respectively. From the spectra (fig.3.3b) we see that at relatively low concentrations (0.069 milli moles/lit) absorption in the visible region is much lower as



(a) High concentration samples

● - 2.08 milli moles/lt, ○ - 1.04 milli moles/lt,
▲ - 0.69 milli moles/lt



(b) Low concentration samples

● - 0.034 milli moles/lt, ○ - 0.069 milli moles/lt,
▲ - 0.155 milli moles/lt

Fig.3.7. Log photoacoustic signal amplitude vs log laser pulse energy for Rhodamine 6G : methanol system

compared to that in ultraviolet. Note that this is not the case in aqueous solutions. This indicates that in methanol solution, at low concentrations S_1 state of R6G has nearly of the same symmetry (A_1) as that of S_0 (A_1) while S_3 state will be nearly B_2 symmetry. This results in a reduced role for OPA, and actually we observe a competition between OPA and TPA at low concentrations as indicated by slopes < 1.6 . However TPA is not much favoured either, otherwise the slopes should have been still higher. On the other hand, both uv and visible absorptions are enhanced, and greater increase is seen for the $S_0 \rightarrow S_1$ absorption in comparison to the $S_0 \rightarrow S_3$ transition (fig.3.3b). It is probable that with an increase in concentration the excited state symmetries are modified by solute-solute and solute-solvent interactions.^[37] This implies that level S_1 will take up more of B_2 symmetry character at high concentrations making $S_0 \rightarrow S_1$ OPA transition symmetry allowed. Hence as concentration is increased more and more OPA takes place reducing TPA (fig.3.7a), and the slope comes down to nearly one. However at high laser energies a strong enhancement in TPA is observed owing to the strengthening of TPA and ESA, as discussed before.

Fig.(3.8) shows the variation of the slope of the log laser pulse energy vs log PA plots with concentration.

3.5.3 Rhodamine 6G : ethylene glycol system

Eventhough the most favourable dye solvents are water and alcohols, they do not seem to form stable streams from simple nozzles, which are used as "dye jets" in certain lasers. Experiments have been performed with ethylene glycol and glycerol

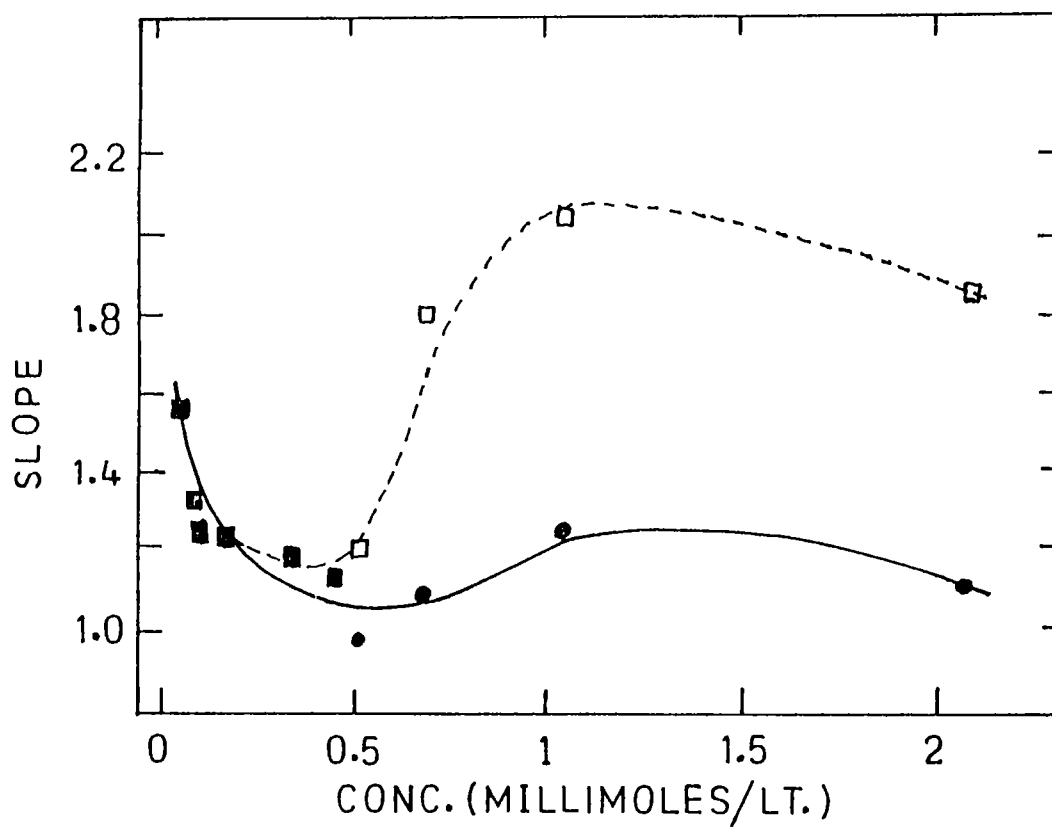


Fig.3.8. Variation of the slope of log-log plots with concentration in methanol solutions of Rhodamine 6G

● - laser pulse energy < 10 mJ, □ - laser pulse energy > 10 mJ

based dye solutions in such cases. Although the thermal properties of these solvents are undesirable, good performance is claimed for cw dye lasers using the free stream. Another application of these highly viscous solvents is in the investigation of the intermediate unequilibrated excited states of dyes [30].

The PA signals produced from sample solutions of R6G:Ethylene glycol at different concentrations (10^{-3} moles/lt to 10^{-6} moles/lt) are measured at various input laser energies (6mJ to 50 mJ). Compared to the R6G solutions prepared in water and methanol the irradiation laser energy is in the higher power region. The log-log plots of PA signal against laser energy are plotted for each sample (fig.3.9). The slope at the lowest concentration studied (1.8×10^{-6} moles/lt) has a value of 1.5. As the concentration increases (7×10^{-5} moles/lt) the slope is found to increase to a value of 2. (Note that in R6G :water and R6G : methanol solutions the samples studied were at higher concentrations than 7×10^{-5} moles/lt). At still higher concentration the slope is found to decrease, but shows an increase to a value of 1.8 at the highest concentration (1×10^{-3} moles/lt). The estimated error in the slope values is ± 0.1 .

From the absorption spectra (fig.3.3c), it is seen that for the lowest sample concentration (1.8×10^{-6} moles/lt), the OPA in the visible is weak, whereas that at uv is strong. This indicates that for very low concentrations S_1 state of R6G has nearly the same symmetry (A_1) as that of S_0 (A_1) while S_3 state will be nearly of B_2 symmetry. The situation is equivalent to the case of low concentration R6G:methanol samples. Step-wise excitation $S_0 \rightarrow S_1 \rightarrow S_3$ will be limited here due to the low S_1 state population. Thus the chances for TPA and OPA are more or

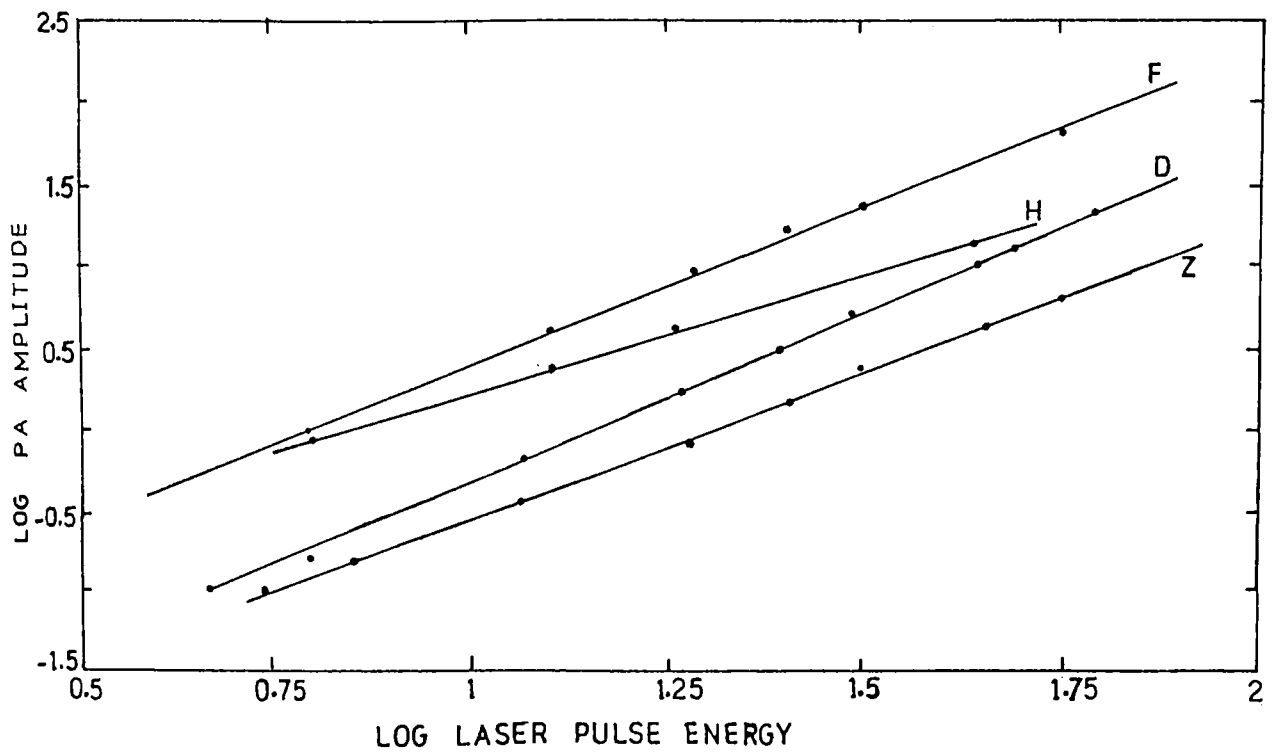


Fig.3.9. Log photoacoustic signal amplitude vs log laser pulse energy for Rhodamine 6G : ethylene glycol system

Z - 1 milli mole/lt, D - 0.07 milli moles/lt,

F - 0.01 milli moles/lt, H - 0.0018 milli moles/lt

less the same in the very low concentration region, which is confirmed by our observation of a slope of 1.5 in the log-log plot. But at higher concentrations $S_0 \rightarrow S_1$ OPA gets considerably enhanced as compared to $S_0 \rightarrow S_3$ OPA as revealed from the absorption spectra. S_1 appears to take up more of B_2 character here, thereby increasing the level population. The slope also increases towards 2 indicating a favoured step-wise absorption. (One may be interested to note here that the orientational relaxation times of typical dye molecules in excited singlet states are ≈ 100 ps in methanol and ≈ 2 ns in ethylene glycol [31]. Also the directions of the $S_0 \rightarrow S_1$ and $S_1 \rightarrow S_3$ transition moments are not oriented parallel to each other, they have an angle ϕ between them [32,35]). As concentration is further increased more and more OPA takes place from the higher vibrational levels of S_0 overcoming TPA and the slope comes down to nearly 1.3. However for the highest concentration a strong enhancement in TPA (a slope of 1.8) is observed resulting from the causes mentioned before. A special feature of R6G:Ethylene glycol system is that pump power dependence of TPA is not as obvious as that observed for R6G :water and R6G:methanol systems.

Fig.3.10 shows the variation of the slope of the log laser pulse energy vs log PA plots of PA signal against laser energy with concentration.

3.5.4 Variation of PA signal with concentration

A direct comparison of the PA signals detected by the PZT transducer at various concentrations is not, strictly speaking, feasible with the experimental set up used in the above experiments. This is primarily because of the variations in the

acoustic source geometry, as observed by the transducer. In the above samples the absorption coefficients (at 532 nm) vary in a large range with concentration, resulting in various penetration depths of the beam into the solutions. This will in turn generate different acoustic source geometries, radiating spherical, cylindrical or plane acoustic waves depending on the sample concentration [33,34]. Further, properties like acoustic attenuation may vary in a large range with concentration. Hence a genuine comparison of the kind mentioned above is not an easy task in the present context. Still, it is not impossible to reach certain general conclusions from this data, shown in figs.3.11 and 3.12.

One may note that there is a certain order in these curves. The tendency is for a higher value of PA signal at higher concentrations (in agreement with theory) in R6G : methanol sample. The obvious increase of PA amplitude in high concentration samples at high laser energies is due to the enhanced TPA which has been discussed before. However a sharp decrease is observed for the detected PA amplitude at higher concentrations in R6G : Ethylene glycol. This might be due to a higher value of ultrasonic attenuation in the viscous solvent ethylene glycol.

3.6 PA GENERATION IN R6G : PUMPING BY 1060 NM

The log-log plots corresponding to the PA signals produced in various concentrations of the R6G solutions on irradiation with 1060 nm laser radiation are given in figs.3.13, 3.14 and 3.15. Eventhough TPA at 1060 nm has been identified in R6G earlier from the subsequent $S_1 \rightarrow S_0$ fluorescence [25], our

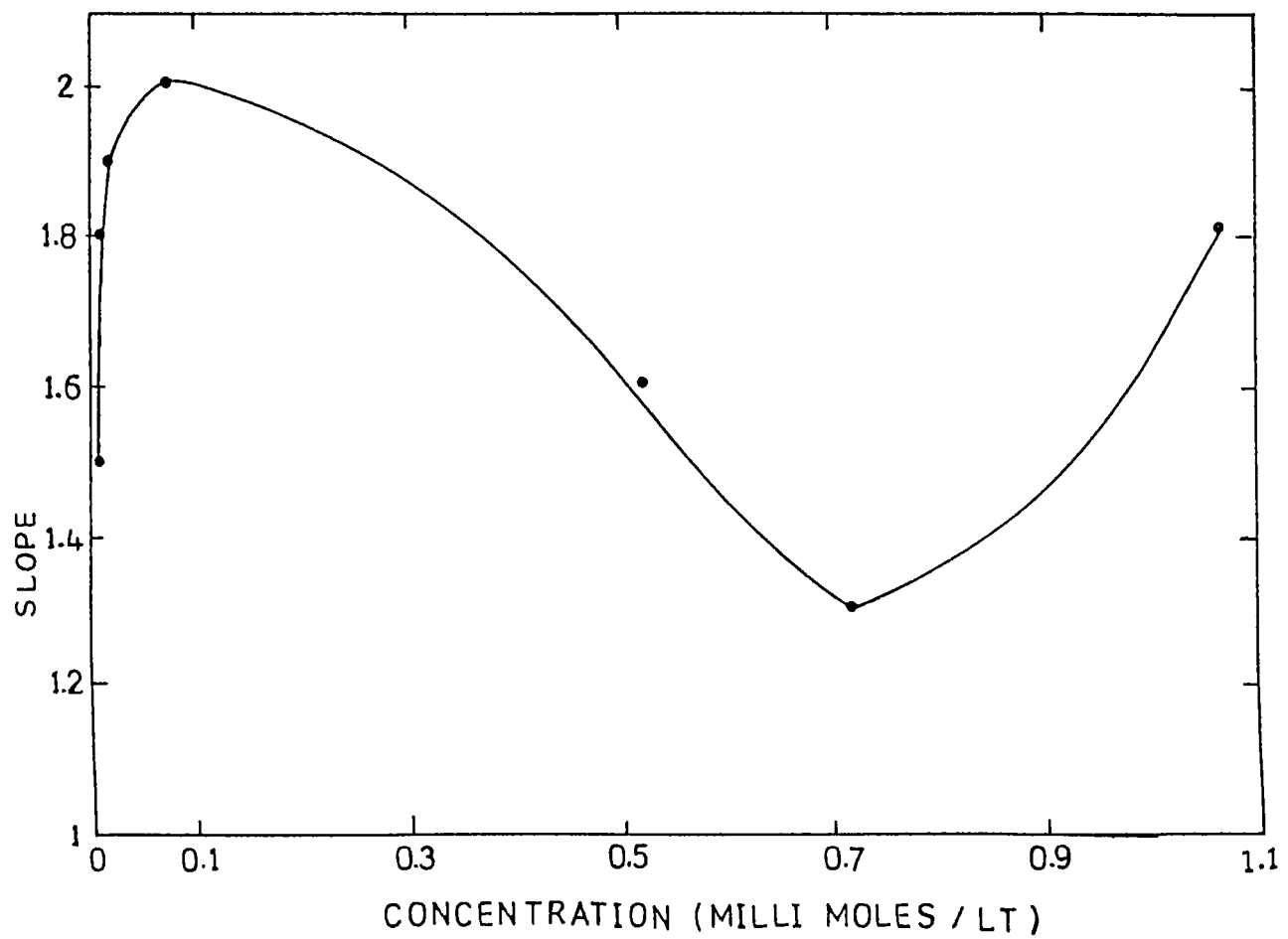


Fig.3.10. Variation of the slope of log-log plots with concentration in Rhodamine 6G : ethylene glycol system

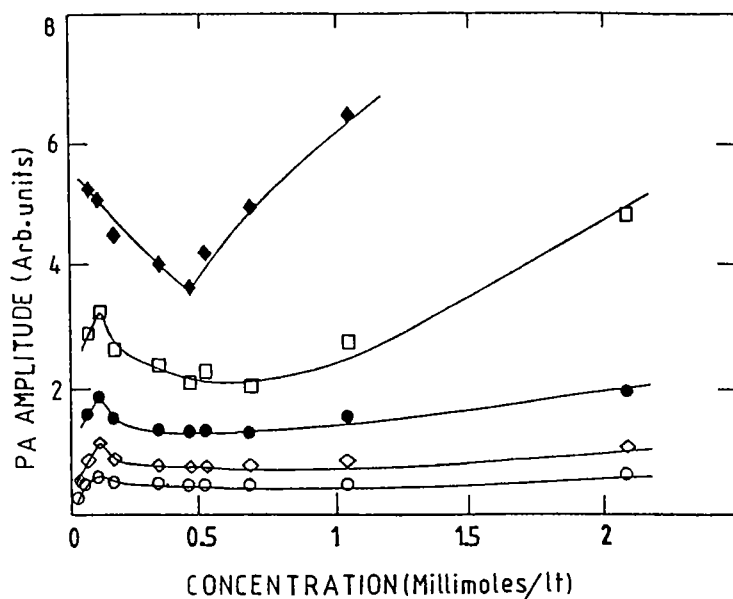


Fig.3.11. Concentration dependence of photoacoustic signal, in methanol solutions of Rhodamine 6G, shown at various laser pulse energies

○ - 2.5 mJ, ◇ - 4 mJ, ● - 6.3 mJ, □ - 10 mJ, ◆ - 16 mJ

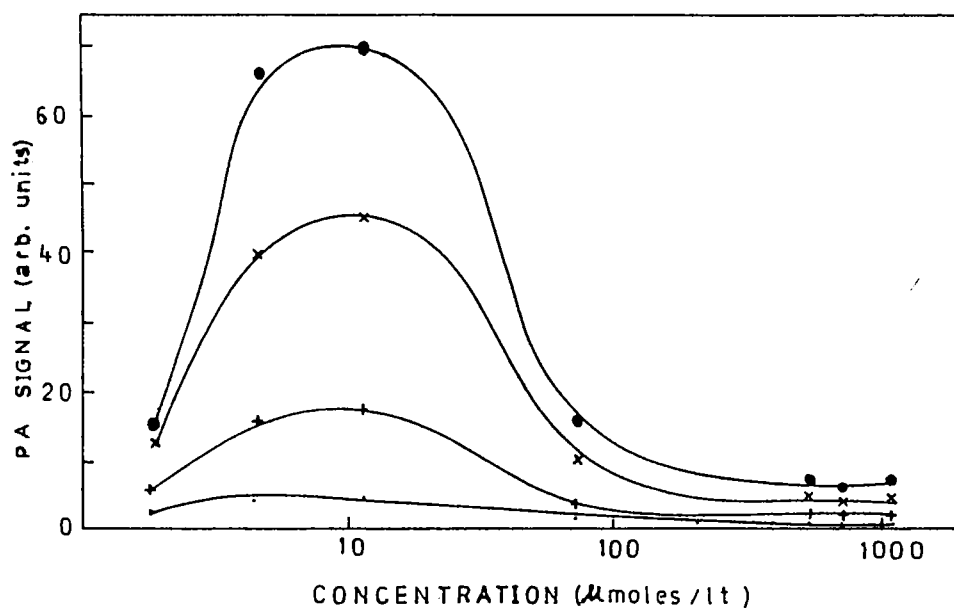


Fig.3.12. Concentration dependence of photoacoustic signal, in ethylene glycol solutions of Rhodamine 6G, shown at various laser pulse energies

● - 6.25 mJ, + - 12.5 mJ, × - 43.75 mJ, ● - 62.5 mJ

PA measurements consistently gave a slope of 1 ± 0.1 in all samples. This indicates that the observed PA signal has a large contribution from a strong OPA process, which is undoubtedly the overtone absorption and subsequent vibrational relaxation taking place in the solvent molecules. $S_1 \rightarrow S_0$ internal conversion and possible $S_2 \rightarrow S_1$ nonradiative relaxation are the weak additional pathways for PA generation here, but these channels are found to be "masked" due to the presence of the much stronger overtone excitation at the pump wavelength. This example clearly illustrates the need for a careful choice of the pump wavelength in similar experiments where the spurious background has to be considerably limited, if not eliminated.

3.7 CONCLUSIONS

The nature of two photon absorption at the typical dye pump wavelength of 532 nm is investigated in solutions of Rhodamine 6G prepared in the solvents water, methanol and ethylene glycol using pulsed photoacoustic technique. TPA is found to be prominent at low dye concentrations in all samples; at high concentrations the TPA probability has a marked dependence on the pump energy. Absorption spectra of the samples indicate the possibility of symmetry variations with change in concentration, and attempts have been made to correlate the same with the results of PA studies. The role played by dimers in aqueous solutions of R6G at high concentrations is discussed.

Using the experimental set up described in chapter 2, Stokes fluorescence from the dye samples at 532 nm pumping has been recorded, and emission peak shifting due to reabsorption

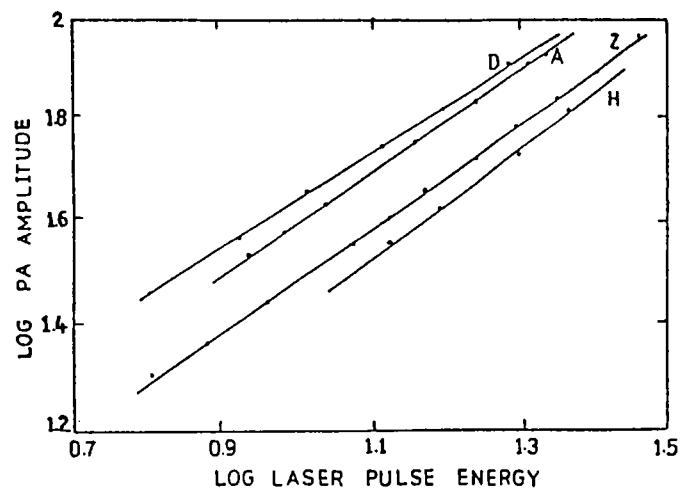


Fig.3.13. Log photoacoustic signal amplitude vs log laser pulse energy for Rhodamine 6G : water system; 1060 nm irradiation
 Z - 1.29 milli moles/lt, A - 1.07 milli moles/lt,
 D - 0.53 milli moles/lt, H - 0.256 milli moles/lt

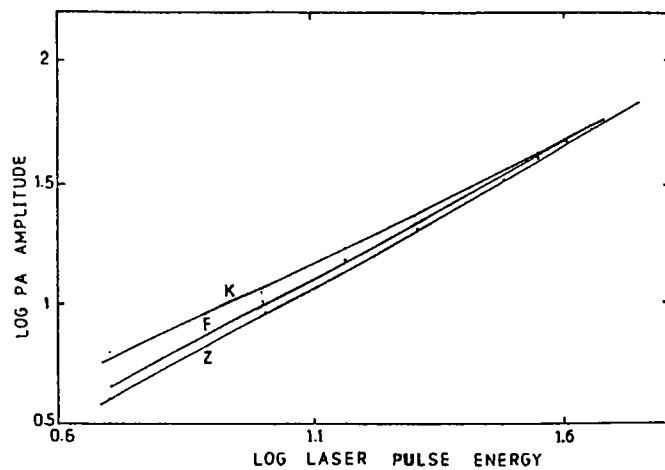


Fig.3.14. Log photoacoustic signal amplitude vs log laser pulse energy for Rhodamine 6G : methanol system; 1060 nm irradiation
 Z - 2 milli moles/lt, F - 0.5 milli moles/lt,
 K - 0.069 milli moles/lt

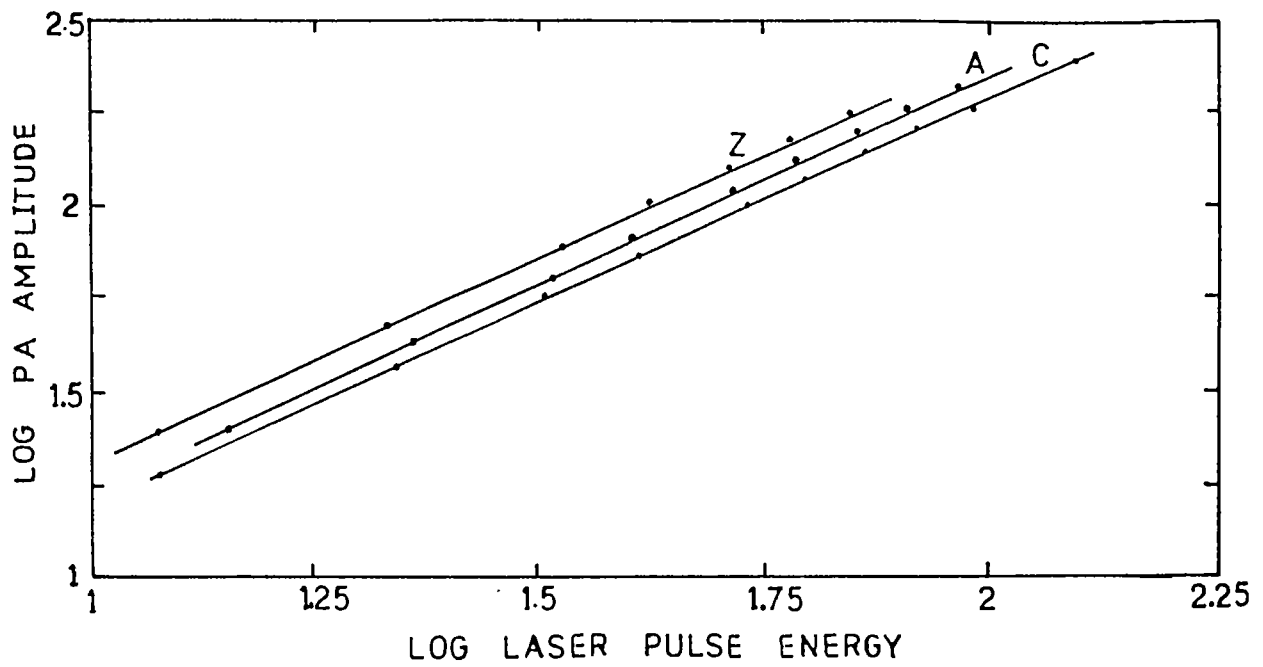


Fig.3.15. Log photoacoustic signal amplitude vs log laser pulse energy for Rhodamine 6G:ethylene glycol system; 1060 nm irradiation

Z - 1 milli mole/lt, A - 0.071 milli moles/lt,
 C - 0.178 milli moles/lt

effects at high concentrations is observed and measured. In addition the dye samples have been pumped by 1060 nm and the corresponding PA signals are recorded. Information on TPA is not revealed from these signals due to the prominence of strong overtone absorptions at this wavelength.

REFERENCES

- [1] Sorokin P P and Lankard J R, IBM J.Res.Develop., 10, 162, 1966
- [2] Schafer F P, Topics in Applied Physics, vol 1, Dye lasers (Springer, Berlin), 1977
- [3] Singh S, Appl.Opt., 26, 66, 1987
- [4] Rodchenkova V V, Tsogoeva S A, Muraveva T M, Demisov L K and Uzhinov B M, Opt. i. Spectroskopiya, 60, 35, 1986
- [5] Th.Forster, Fluoreszenz organischer Verbindungen (Vandenhoeck and Ruprecht, Gottingen, 1951)
- [6] Parker C A, Photoluminescence of solutions (Elsevier, Amsterdam, 1968)
- [7] Drexhage K H, in Dye lasers, Topics in applied physics, vol.1, ed. F.P.Schafer (Springer, Berlin), p.144, 1977
- [8] Rabinowitch E and Epstein L F, J.Am.Chem.Soc. 63, 69, 1941
- [9] Th Forster and Konig E, Z.Electrochem., 61, 345, 1957
- [10] Ignat'eva, Levshin L V, Osipova T D and Polukhin Yu M, Opt.Spectr., 13, 219, 1962
- [11] Baranova E G, Opt.Spectr., 13, 452, 1962
- [12] Selwyn J E and Steinfeld, J.Phys.Chem. 76,1962
- [13] Arbeoa I L and Ojeada P R, Chem.Phys.Lett., 87, 556, 1982
- [14] Kopainsky B and Kaiser W, Chem.Phys.Lett., 88, 357, 1982
- [15] Perrin M F, C R Hebd Seances. Acad. Sci., 178, 1978, 1924
- [16] Penzkofer A, Glas H and Schmailzl J, Chem.Phys., 70, 47, 1982
- [17] Falkenstein W, Penzkofer A and Kaiser W, Opt. Commun., 27, 151, 1978
- [18] Tsueno Urisu and Kenji Kajiyama, J.Appl.Phys., 47, 3559, 1976

- [19] Lin C and Dienes A, J.Appl.Phys, 44, 5050, 1973
- [20] Alfano R R, Shapiro S L and Yu W, Opt.Comm., 7, 191, 1973
- [21] Rosencwaig A, 'Photoacoustics and Photoacoustic spectroscopy' Wiley, New York, 1980
- [22] Magde D, Gaffney S T and Campbell B F, IEEE J.Quantum Electron. QE - 17, 48, 1981
- [23] Sahar E and Treves D, IEEE J.Quantum Electron. QE - 13, 962, 1977
- [24] Tuccio S A and Strome Jr. F C, Appl.Opt., 11, 64, 1972
- [25] Hermann J P and Ducuing J, Opt.Comm., 6, 101, 1972
- [26] McClain W M, J.Chem.Phys., 55, 2789, 1971
- [27] Rulleire C and Kottis P, Chem.Phys.Lett., 75, 478, 1980
- [28] Lu Y and Penzkofer A, Chem. Phys., 107, 175, 1986
- [29] Penzkofer A and Lu Y, Chem. Phys., 103, 399, 1986
- [30] Malley M M and Mourou G, Opt. Commun., 10, 323, 1974
- [31] Chuang T J and Eisenthal K B, Chem.Phys.Lett., 11, 64, 1972
- [32] Aristov A V and Shevandin V S, Opt.Spectrosc.,44,276,1978
- [33] Hutchins D A, Can. J. Phys., 64, 1247, 1986
- [34] Patel C K N and Tam A C, Rev.Mod.Phys., 533, 517, 1981
- [35] Penzkofer A and Wiedmann J, Opt. Commun., 35, 81, 1980
- [36] Sathy P, Reji Philip, Nampoori V P N and Girijavallabhan C P G, Opt. Commun., 74, 313, 1990
- [37] Reji Philip, Sathy P, Nampoori V P N, Jacob Philip and Girijavallabhan C P G, J.Phys.B, 25, 155, 1992
- [38] Wieder I, Appl.Phys.Lett., 21, 318, 1972
- [39] Renata Reisfeld, Rivka Zusman, Yoram Cohen and Marek Eyal, Chem.Phys.Lett., 147, 142, 1988

CHAPTER -4

TWO PHOTON ABSORPTION IN FLUORESCIEN : INVESTIGATION BY PULSED PHOTOACOUSTICS

In the preceding chapter, we have outlined various aspects of the general solvent and concentration dependence of the optical properties of dyes. Studies on nonlinear absorptions in the dye Rhodamine 6G employing pulsed PA technique has also been discussed. In this chapter we present the results obtained from similar studies carried out in another laser dye viz. Fluorescien.

4.0 INTRODUCTION

Fluorescien dyes, belonging to the xanthene family, are widely used in dye lasers [1]. The usual solvents are water, methanol, ethylene glycol etc., with some NaOH added for reducing the triplet yields [1]. Their absorption bands are located in the uv and blue-green regions of the spectrum and effective pumping can be accomplished using the second harmonic of ruby or neodymium lasers, N_2 lasers and flashlamps. Laser action in fluorescien dye has been obtained in the 520 - 600 nm region [2]. Other major applications of these dyes are in solar energy conversion [3,4] and photosensitized reactions [4-7]. In fluorescien, the 2- and 7- positions of the xanthene ring are substituted by hydroxyl radicals and the structure is as shown in fig.4.1a. The acidic and basic forms of the dye are given in fig.4.1b. The spectral properties of these dyes which have a dissociable carboxyl group at the 2- and an aryl hydroxy at the

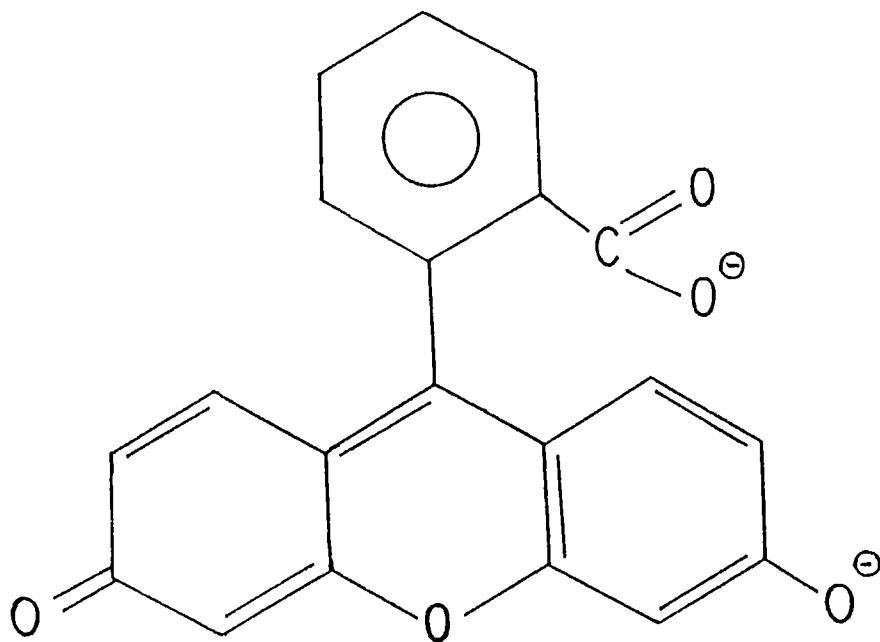


Fig.4.1a. The Fluorescein molecule

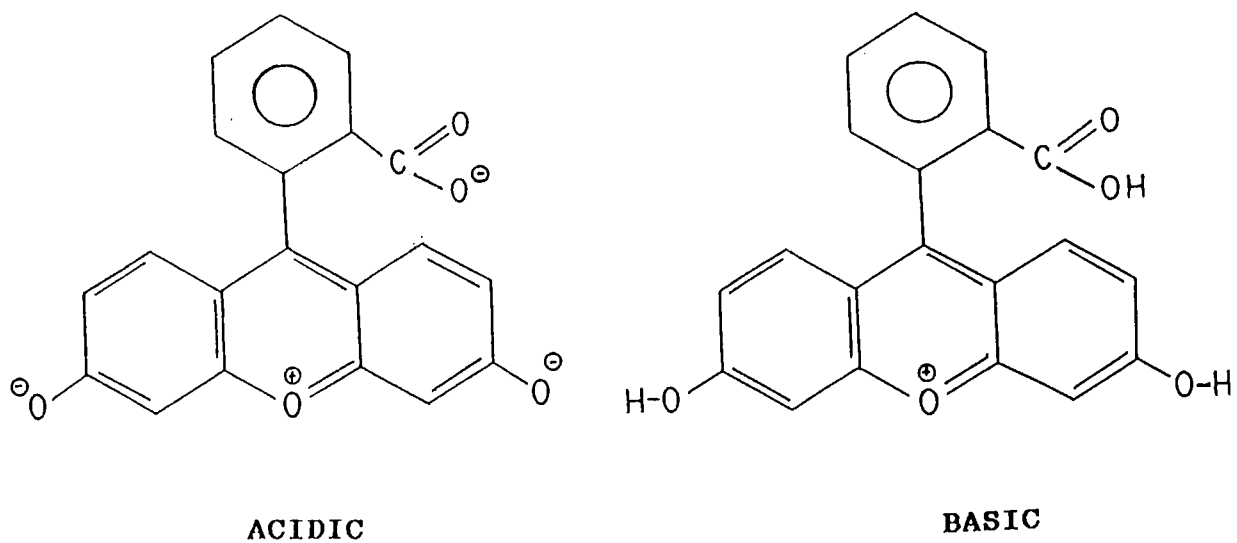


Fig.4.1b. Acidic and basic forms of fluorescein

6- positions are very susceptible to the pH value of solutions and the polarity of solvents, to the extent that on some occasions they have no colour at all. Depending on the pH of the solution, fluorescein can exist in the cationic, anionic and neutral forms. The poor solubility of fluorescein dyes in many non-polar solvents limits their applications in certain cases.

It is well known that dyes of the fluorescein family have high fluorescence quantum efficiencies, thus making them likely candidates for effective laser media. The rigid, planar structure of the fluorescein molecule limits the structural mobility of the chromophore resulting in a reduced internal conversion rate and hence a high quantum efficiency. The quantum yield of fluorescein in alkaline alcoholic solutions is 10% below and that of R6G in alcohol is 5% below the maximum value of 100%. This can be ascribed mostly to hydrogen vibrations in the end groups of the chromophores, involving solvent molecules in the case of fluorescein. According to Drexhage's loop rule [1], in the case of a dye where the π -electrons of the chromophore can make a loop when oscillating between the end groups, the triplet yield will be higher than that in a related compound where this loop is blocked. Hence fluorescein should have a low triplet yield in alkaline solution and a high triplet yield in acidic solution. This prediction has been confirmed by experiments [1,8].

The fluorescence quantum yield of fluorescein has been determined carefully with several independent methods, and is generally assumed to have the value $90 \pm 5 \%$. Whereas the quantum yield of this dye seems to be most reliable, its use as a standard solution to measure the unknown quantum yields of other

samples is hampered by poor chemical stability. Rhodamine 6G perchlorate seems to be superior to all the compounds proposed so far for such measurements in the wavelength region between 500 and 600 nm.

If the dye is substituted with heavier elements which increase the spin-orbit coupling, the intersystem crossing rate which is intrinsic to the chromophore can be greatly enhanced. This undesirable effect for a laser dye has been demonstrated on the fluorescein derivatives eosin and erythrosine [1]. The triplet yield of eosin in an alkaline solution is found to be 76%, as compared to the corresponding value of 3% for fluorescein. Another example is the dye dithiofluorescein, which is obtained by the replacement of the oxygen atoms in the 3- and 6- positions of fluorescein by sulphur. Eventhough dithiofluorescein has an absorption maximum at 635 nm in alkaline ethanol, it is absolutely non-fluorescent.

4.1 ABSORPTION AND FLUORESCENCE PROPERTIES

Earlier reports [9] show that the peak absorption in aqueous medium of fluorescein sodium used in our experiments is at ≈ 490 nm and peak emission at ≈ 520 nm. We have recorded the absorption spectra for different concentrations of fluorescein (ranging from 10^{-3} to 10^{-6} moles/lit) in water:NaOH and in methanol:NaOH on a UV-VIS-NIR spectrophotometer. The spectra obtained for samples taken in a 1 cm cuvette are shown in figs.4.2a and 4.2b.

Using the set up Similar to that described in chapter 3,

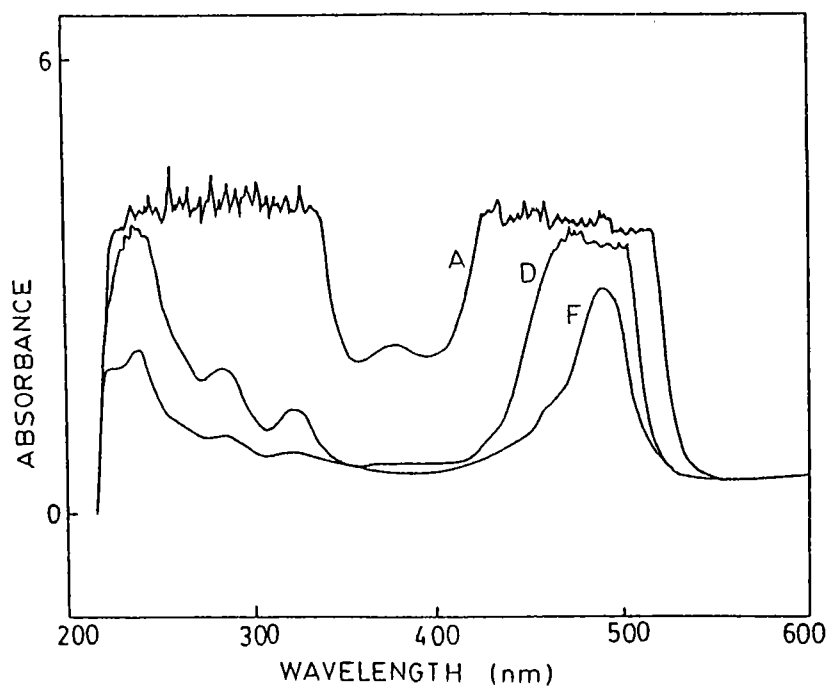


Fig.4.2a. Absorption spectra of Fluorescein in alkaline water, at different concentrations

A - 2.5 milli moles/lt, D - 0.137 milli moles/lt,

F - 0.034 milli moles/lt,

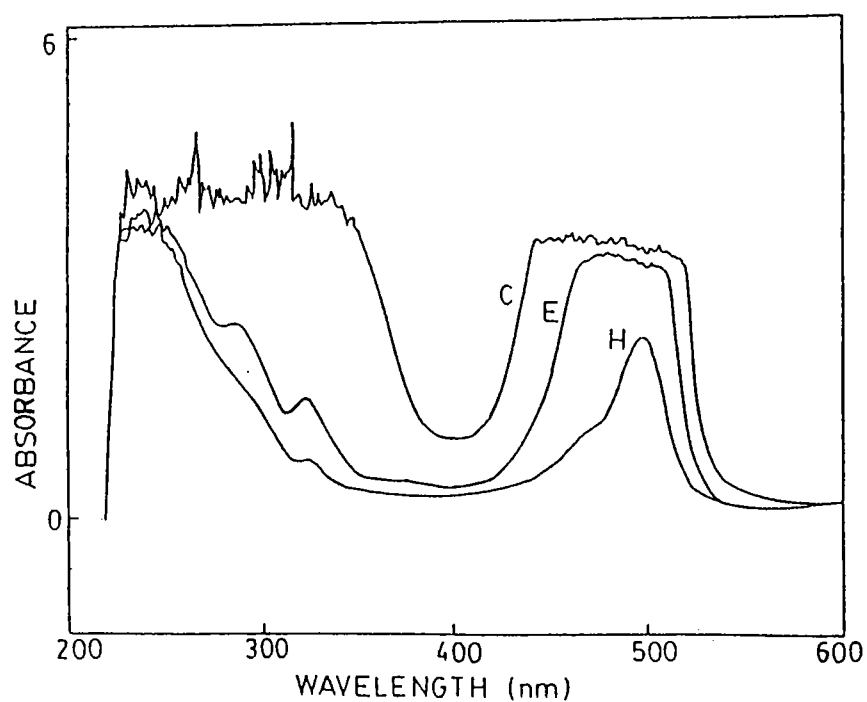


Fig.4.2b. Absorption spectra of Fluorescein in alkaline methanol at different concentrations

C - 0.414 milli moles/lt, E - 0.069 milli moles/lt,

H - 0.043 milli moles/lt

(only changing the source of excitation) the Stokes fluorescence emission from the samples have been recorded. Since the 532 nm wavelength available from the present laser is at the falling edge of the dye's absorption band, we preferred instead the weak, broadband flashlamp emission coming from the laser for excitation. (When the Nd:YAG laser is operated in the "single shot mode" without triggering one obtains a part of the light emitted by the flashlamp alone. Details are given as a footnote to fig.4.3) The fluorescence spectrum so obtained shows a maximum at ≈ 517 nm (fig.4.3). However for a comparison we recorded the emission spectra using 532 nm laser excitation also (fig.4.4). At low concentrations (3.4×10^{-5} moles/l) the spectra obtained from flashlamp excitation and 532 nm excitation are identical. In the 532 nm excitation case, the absorption occurs from thermally excited higher vibrational levels of the ground state to the first excited state and the resulting fluorescence peak is at a higher energy than the pump radiation. The emission peak is found to shift towards 545 nm as the concentration is increased which is due to the usual reabsorption of fluorescence by the ground state molecules. Reabsorption effects occurring due to the overlap of absorption and emission bands become significant at high concentrations.

4.2 GENERATION OF PA SIGNAL IN FLUORESCIEN - PUMPING BY 532 nm

Details of the generation of PA signal in R6G upon 532 nm irradiation have been discussed in the preceding chapter. The role of the state symmetries in determining the relative cross sections of OPA, TPA and ESA also were outlined. These discussions are applicable in the case of fluorescien also to a considerable degree. However one may note that there is a

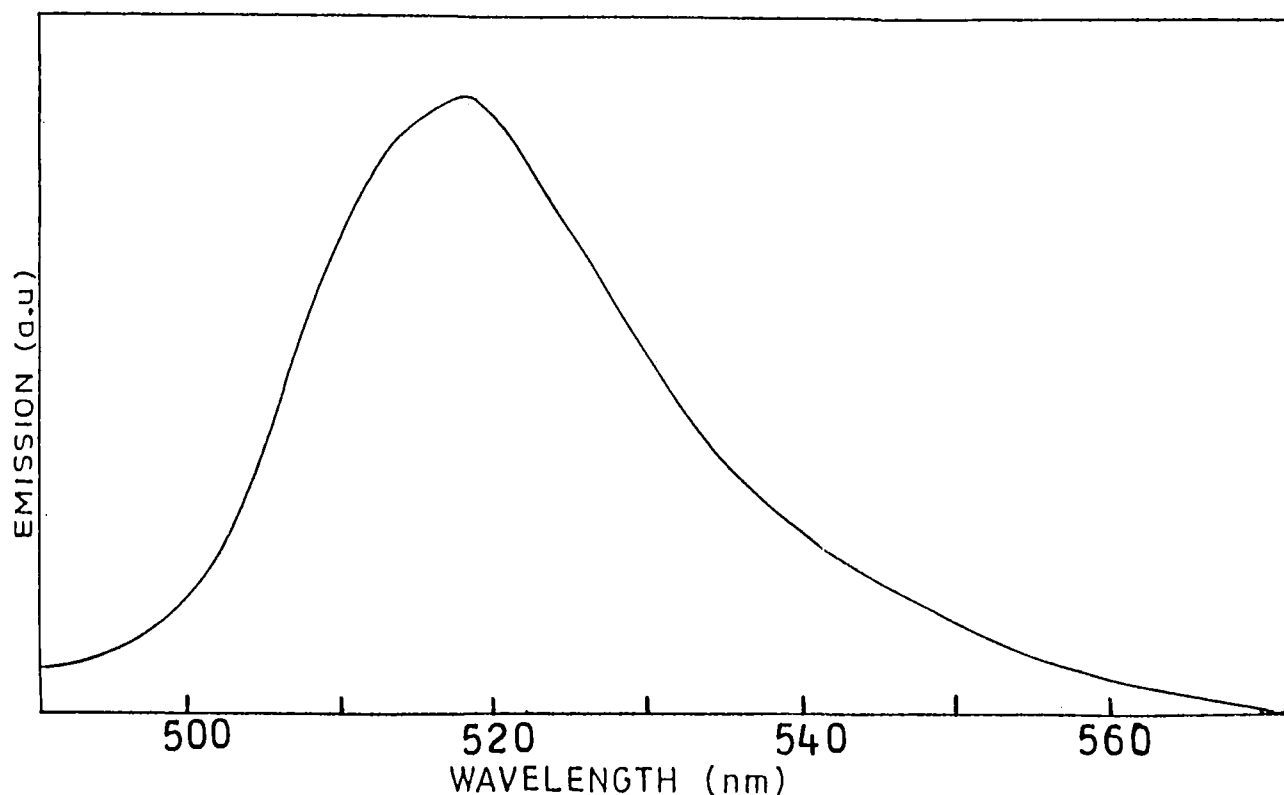


Fig.4.3. Fluorescence emission spectra of Fluorescein in water obtained on flashlamp excitation. Concentration - 0.034 milli moles/lt, Peak at 517 nm.

Note : When our pulsed Nd:YAG laser is operated in the normal 'repetitive' mode, along with the laser pulse a weak, diverging part of flashlamp emission also appears as a low level noise background. In the 'single shot' mode the flash lamp will be running but laser action will be inhibited because the system waits for a trigger pulse (to be given by pressing the 'Fire' button) to initiate Q-switching. Hence in the single shot mode if we do not press the 'fire' button we get only this weak fraction of the flashlamp emission from the laser cavity. We used this emission as source radiation for recording the above spectrum.

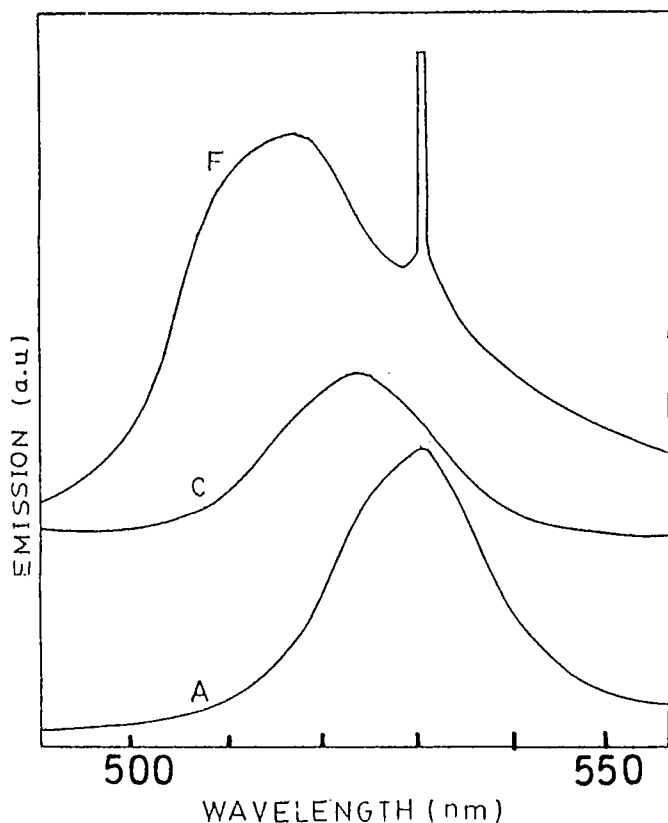


Fig.4.4a.

Fluorescence emission spectra of Fluorescein in alkaline water obtained on 532 nm excitation. Emission peaks are shown in brackets.

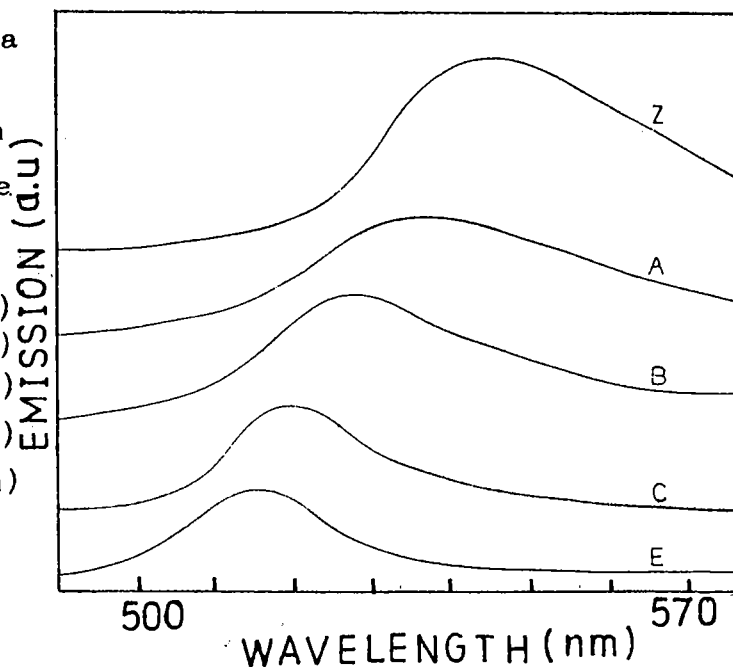
The excitation line can be seen superposed on the spectrum of sample F.

- A - 2.5 milli moles/lt (531 nm)
- C - 0.413 milli moles/lt (523 nm)
- F - 0.034 milli moles/lt (516 nm)

Fig.4.4b.

Fluorescence emission spectra of Fluorescein in alkaline ethanol obtained on 532 nm radiation. Emission peaks are shown in brackets.

- 4.43 milli moles/lt (545 nm)
- 2.59 milli moles/lt (537 nm)
- 0.86 milli moles/lt (527 nm)
- 0.41 milli moles/lt (520 nm)
- 0.069 milli moles/lt (537 nm)



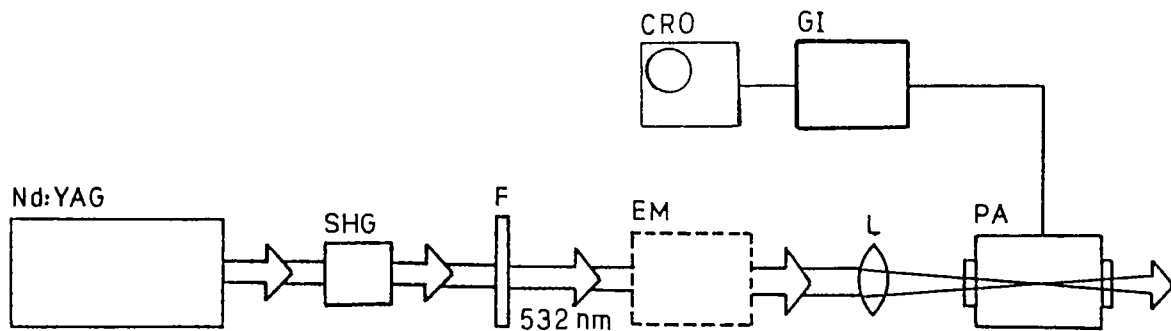
significant enhancement of TPA and ESA in R6G since the $S_0 \rightarrow S_1$ transition exactly matches with the pump wavelength. For fluorescien this is not the case since the absorption maximum is at ≈ 490 nm as seen from the absorption spectra (fig.4.2a,4.2b). Hence the higher order absorption process will be strongly dependent on the number of thermally excited molecules in the ground state which is given by the Boltzmann distribution.

The preparation of dye samples is similar to that described before. The solutions have been made alkaline by adding a few pellets of NaOH to the stock solution. Part of the experimental set up used in the following experiments is identical to that described in chapter three (fig.4.5a). In addition we have carried out the same experiments in a different configuration also, which is shown in fig.4.5b. Here the samples are taken in a cuvette bonded to the PZT transducer chamber, and using two lenses the beam diameter has been reduced to approximately 4 mm. The reduced beam diameter ensures a high intensity in the interaction region which is, however, less than that obtained at the focal point of the focussed beam. This setup was employed in order to observe possible variations in the measured PA signals due to changes in the pumping geometry and intensity. For convenience, we will refer to the above two configurations as *focussed* and *unfocussed* respectively.

4.2.1 Fluorescien :water system

The log laser pulse energy vs log PA amplitude plots obtained for fluorescien in the concentration range of 4.3×10^{-3} moles/lt to 4.13×10^{-4} moles/lt, in both focussed and unfocussed

(a) Focussed



(b) Unfocussed

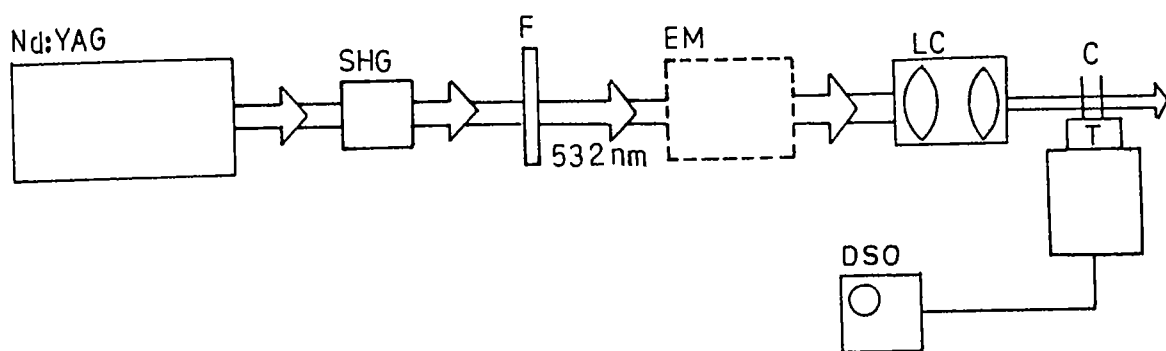
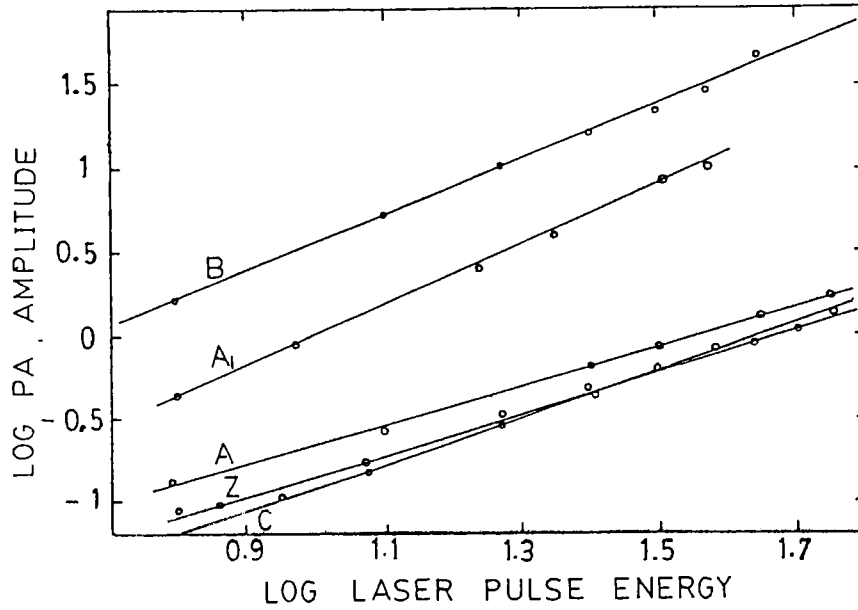


Fig.4.5. The two configurations of the experimental set up.

configurations, are shown in figs.4.6a and 4.6b respectively. Due to the low absorptivity of the samples at still lower concentrations, in the focussed configuration the energy density at the focal point exceeds the threshold for dielectric breakdown resulting in large PA signals which do not correspond to true non-radiative relaxations in the sample. Hence measurements could not be taken below the concentration of 4.13×10^{-4} moles/lt. The slope of the log-log plots for PA as a function of concentration (fig.4.7a,4.7b) shows a similar behaviour in both the focussed and unfocussed configurations. In the concentration range studied, the slope shows a variation from ≈ 1.2 to 1.8 (fig.4.7a) for the focussed case, and from ≈ 1.1 to 1.36 for the unfocussed case (fig.4.7b) with an accuracy of ± 0.1 . Let us consider the focussed case first. The slope increases for concentrations upto 1.5×10^{-3} moles/lt, reaching a maximum of 1.8. At higher concentrations the slope is found to come down to one. The unfocussed configuration yields comparable results, which can be seen from the corresponding figure. Here the maximum value of slope obtained is only 1.36, clearly indicating the strong dependence of nonlinear absorption processes on the pump intensity. These curves also reveal that nonlinear absorptions are occurring not only at the beam focus, but also in a region near the focal point along the beam axis where the pump intensity can exceed a certain threshold value. In fact, the obtained PA signal has contributions from all points along the beam path in both cases, and the nonlinear contribution will be primarily from a region surrounding the focal point in the focussed case.

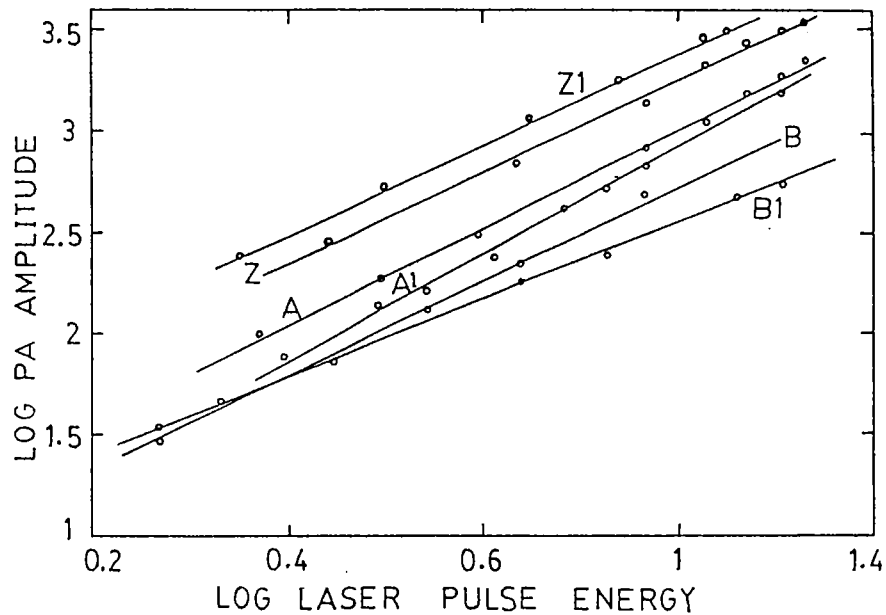
To construct an energy level scheme for fluorescien we adopted the method followed by earlier workers in the case of

Fig.4.6. Log photoacoustic signal amplitude vs log laser pulse energy plot for Fluorescien in water.



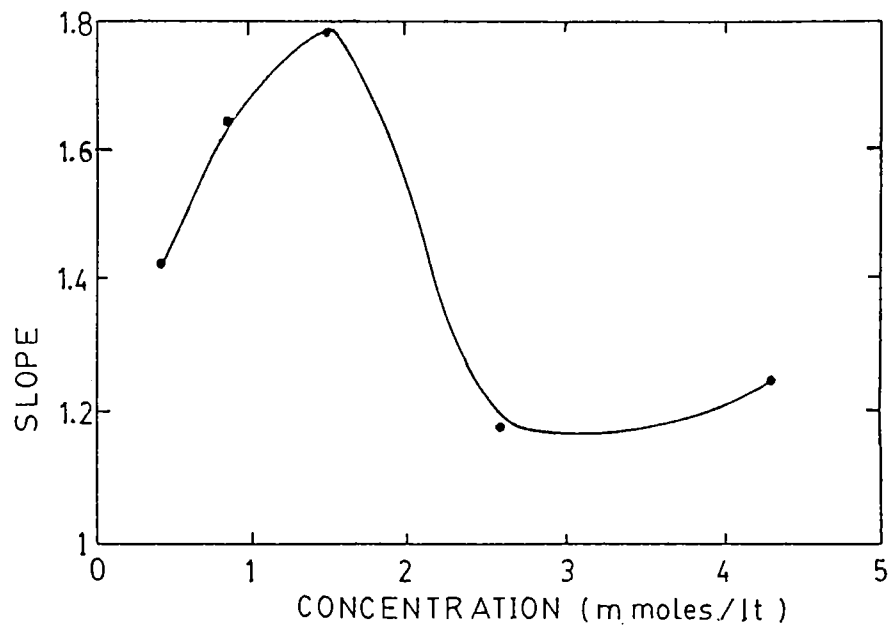
(a) Focussed

Z - 4.3 milli moles/lt, A - 2.58 milli moles/lt, A₁ - 1.5 milli moles/lt, B - 0.86 milli moles/lt, C - 0.413 milli moles/lt

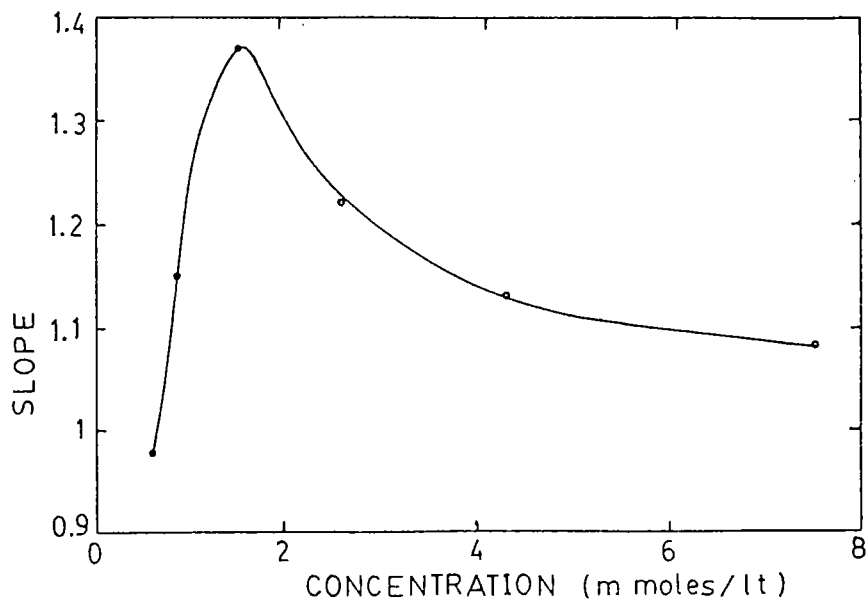


(b) Unfocussed

Z₁ - 7.5 milli moles/lt, Z - 4.3 milli moles/lt, A - 2.58 milli moles/lt, A₁ - 1.5 milli moles/lt, B - 0.86 milli moles/lt, B₁ - 0.6 milli moles/lt



(a) Focussed



(b) Unfocussed

Fig.4.7. Variation of the slope of log-log plots with concentration of aqueous solutions of Fluorescien.

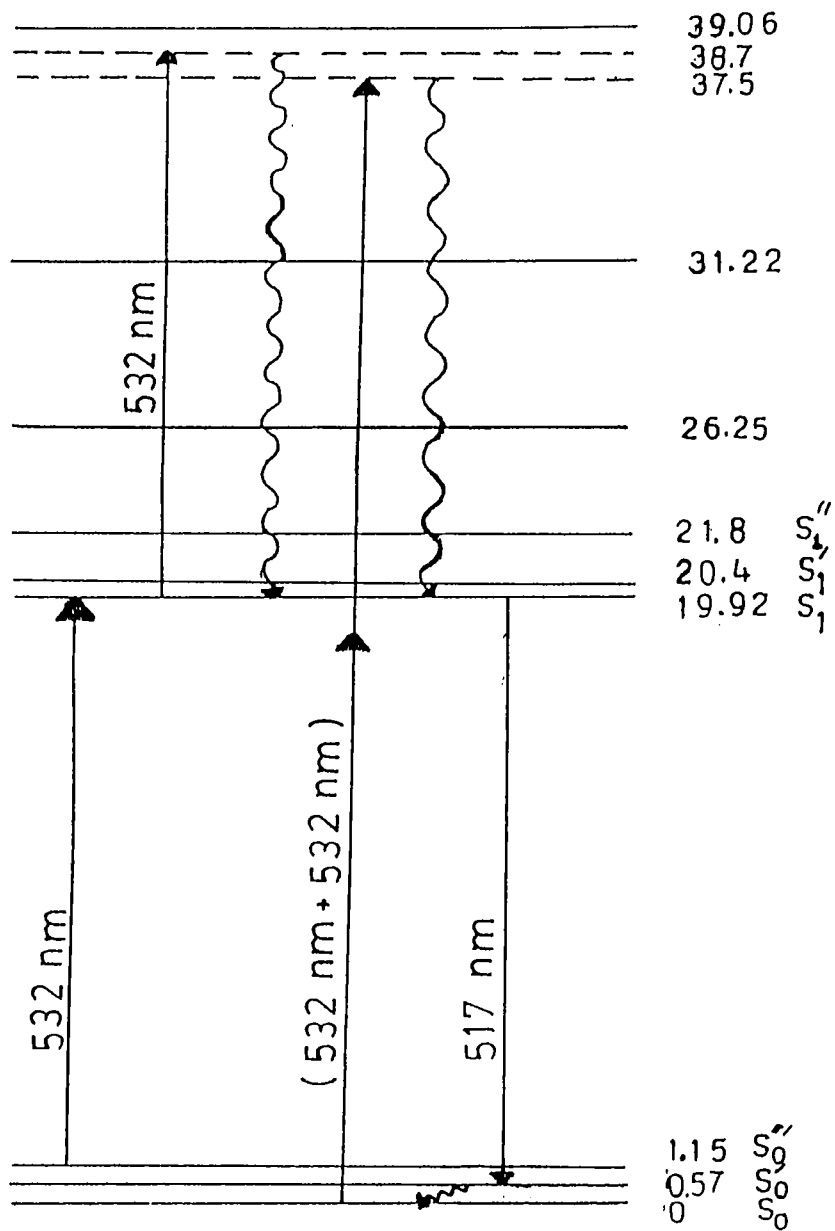
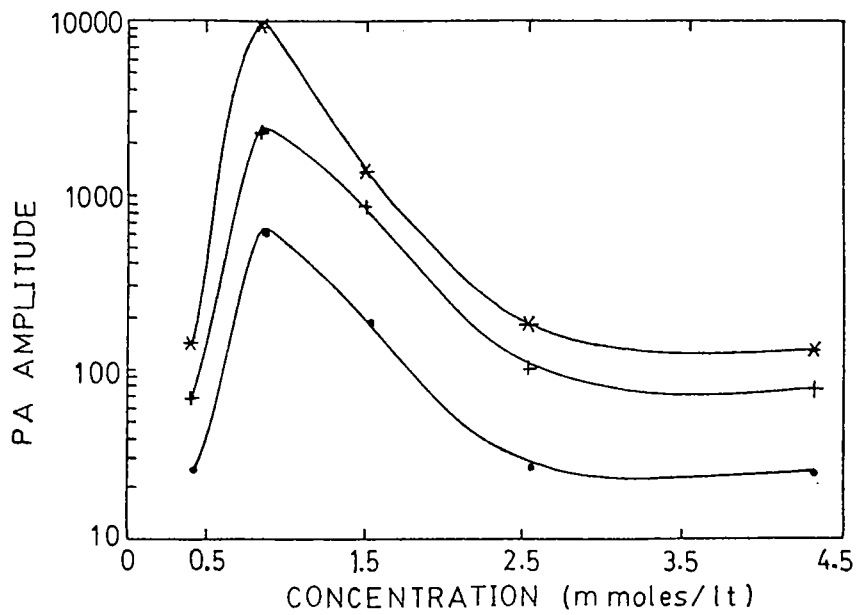


Fig.4.8. Schematic energy level diagram of the Fluorescein molecule.

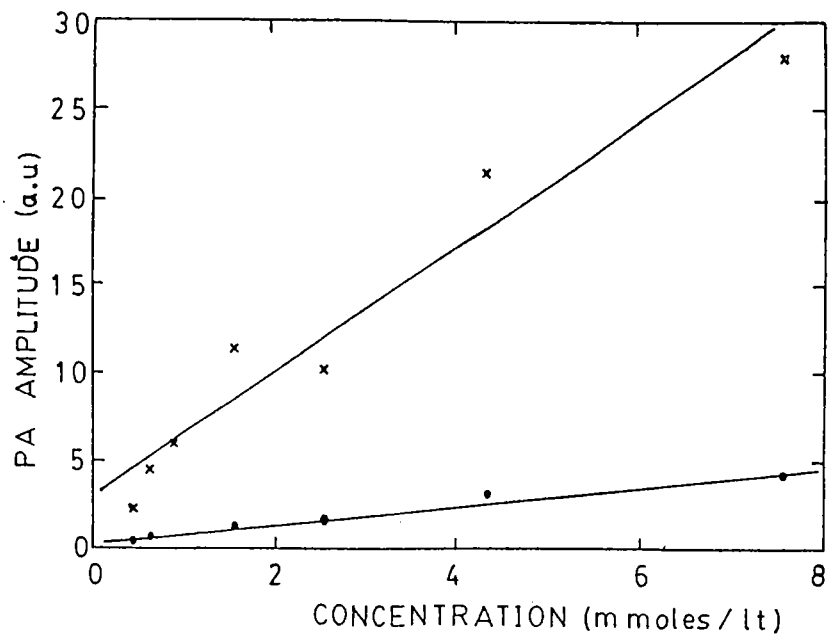
Energies are given in 10^3 cm^{-1}

Rhodamine 6G [10,11]. Initially we measure the point of intersection of the normalized absorption and fluorescence spectra of the sample, which gives the energy of the lowest vibrational level of S_1 . The calculated value is 19920 cm^{-1} . An energy difference corresponding to 532 nm shows the lower absorbing vibronic level to be at 1152 cm^{-1} in S_0 . Similarly, fluorescence peak at 517 nm corresponds to a terminal vibronic level at 570 cm^{-1} in S_0 . Higher excited singlets also can be positioned from the absorption spectra. It should be noted that the energy levels constructed are purely from experimental data. Normal mode vibrational analysis of complex molecules like dyes are practically impossible and is outside the scope of the present work. The possible transitions at 532 nm pumping according to this scheme are shown in fig.4.8. There can be a two-photon channel $S_0 \rightarrow S_n$, which results in the generation of PA and fluorescence emission. Here, the two photon excited state is one of the vibronic levels of S_n . It may be noted that PA will now have components which will depend linearly as well as quadratically on the incident pump flux. Hence the slope of the log-log plot will take values between 1 and 2, and the actual value at a given concentration will depend on the strength of either process. From the absorption spectra we see that as the concentration increases, relative absorption in the uv region is considerably enhanced as compared to that at 532 nm. Taking the ground state of fluorescien to be of A_1 symmetry, this means that for low concentrations the S_n state has more of A_1 symmetry, and as the concentration increases there is a shift towards B_2 symmetry. The strong absorption around 490 nm for all concentrations indicates that S_1 state has B_2 symmetry which is more or less unaffected by concentration. Following the arguments adopted in the case of R6G in the previous chapter we see that at



(a) Focussed

● - 12.5 mJ, + - 31.25 mJ, * - 50 mJ



(b) Unfocussed

● - 5 mJ, * - 28.12 mJ

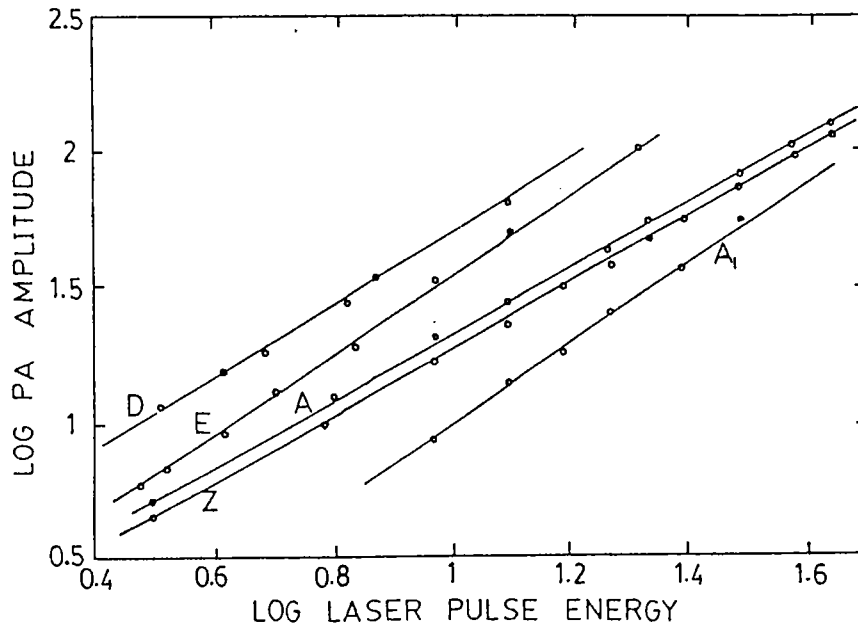
Fig.4.9. Concentration dependence of the photoacoustic signal, in aqueous solutions of Fluorescien. Measured at various laser pulse energies.

low concentrations there will be an enhanced TPA and ESA in fluorescien + water:NaOH system. Hence we get a slope of around 1.4 for the lowest concentration studied (4×10^{-4} moles/lit) in the focussed case. (The classification into low and high concentrations is based more on the absorbance at 532 nm, than on the actual molar concentrations). However, the slope shows a tendency to increase upto 1.5×10^{-3} moles/lit before it starts to decrease. This is probably due to an enhancement of ESA around this region. At higher concentrations increased OPA and the presence of nonfluorescing dimers play the major role in bringing down the slope. In the unfocussed case also, the dependence of slope on concentration is comparable, except that the maximum value obtained is < 1.4 . This clearly illustrates the role of pump intensity in inducing TPA and ESA in these samples.

4.2.2 Fluorescien : methanol system

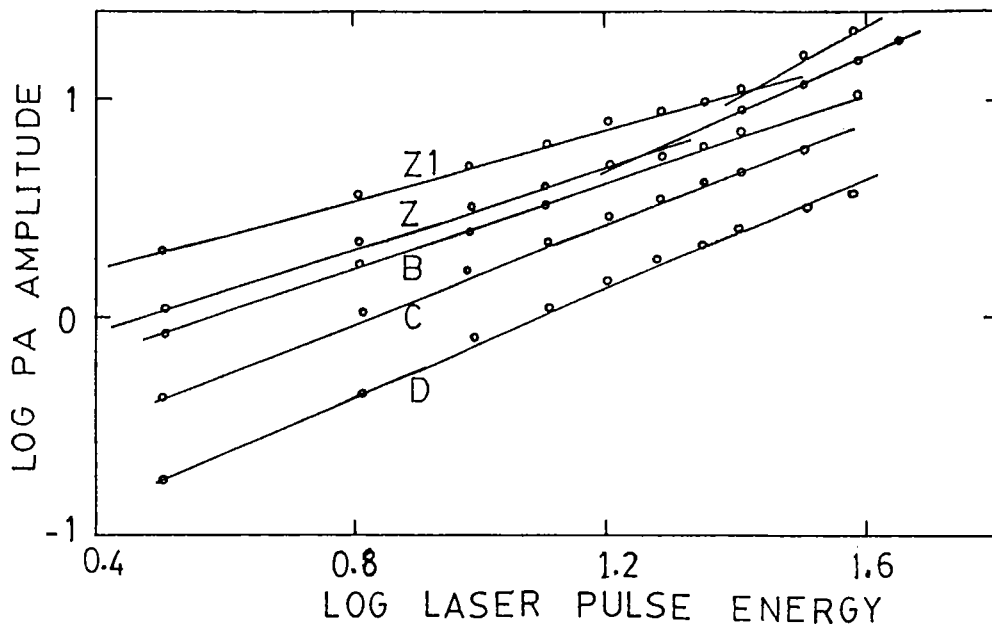
For observing solvent effects on nonlinear absorptions, the above studies have been repeated in a Fluorescien:methanol system. Except for the solvent, all other parameters have been kept the same. The absorption spectra given earlier show that the absorbance is generally higher for a given concentration when the dye is dissolved in methanol. Hence PA signals could be measured at still lower concentrations, than that was possible in Fluorescien:water system. The general behaviour of the log laser pulse energy vs log PA signal plots (figs.4.10a,4.10b) and the dependence of the slope on concentration (figs.4.11a,4.11b) for the focussed and unfocussed cases is similar to that of the Fluorescien:water system. One may note that the slope shows a maximum for concentrations near 1.5×10^{-3} moles/lit here, similar to the observation made in aqueous solution. However a notable

ig.4.10. Log photoacoustic signal amplitude vs log laser pulse energy plot for Fluorescien in methanol.



(a) Focussed

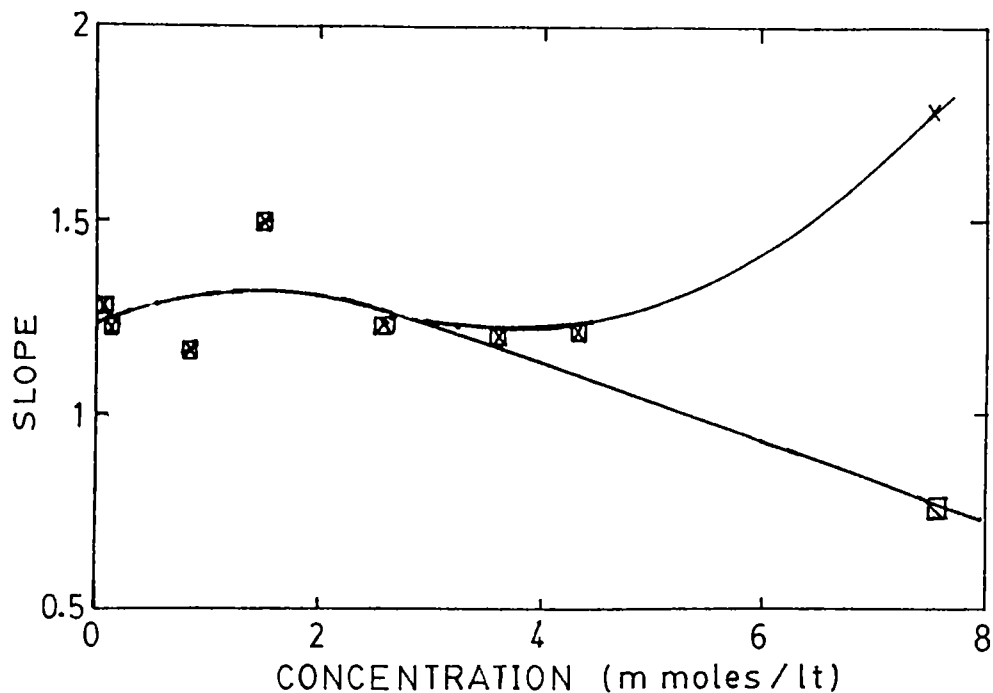
Z - 4.3 milli moles/lt, A - 2.59 milli moles/lt, A₁ - 1.5 milli moles/lt, D - 0.13 milli moles/lt, E - 0.069 milli moles/lt



(b) Unfocussed

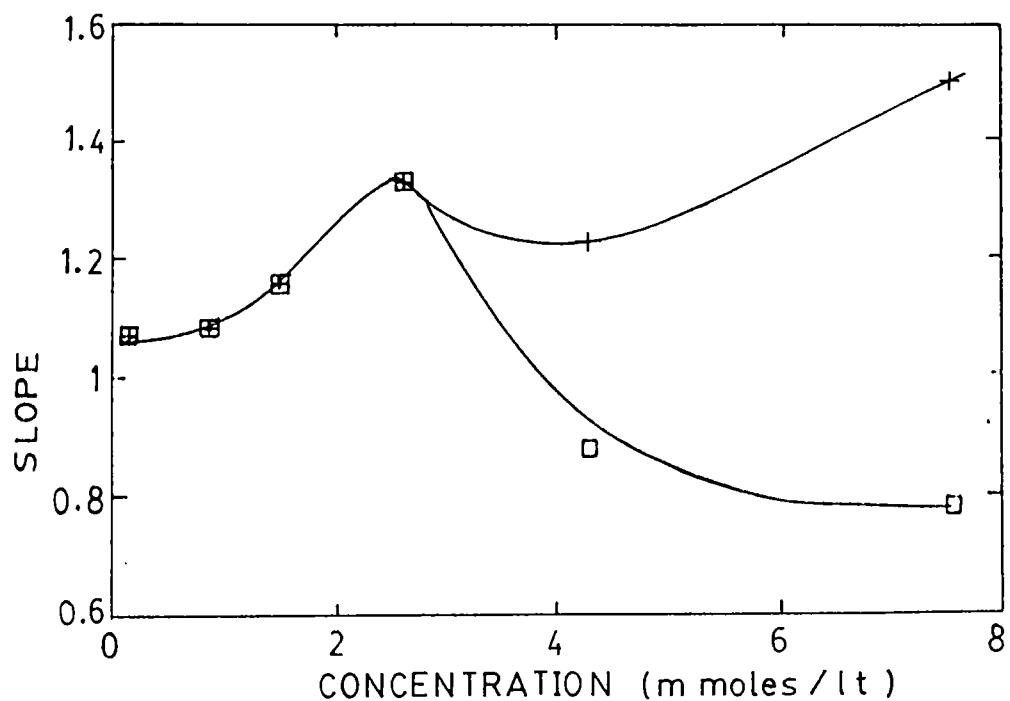
Z1 - 7.25 milli moles/lt, Z - 4.3 milli moles/lt, B - 0.86 milli moles/lt, C - 0.414 milli moles/lt, D - 0.138 milli moles/lt

g.4.11. Variation of the slope of log-log plots with the concentration in methanol solutions of Fluorescien.



(a) Focussed

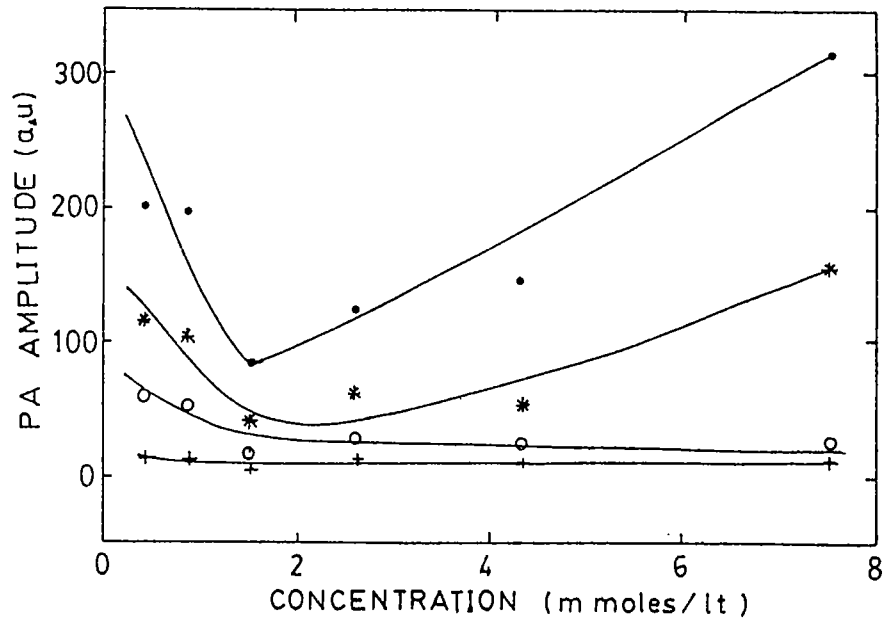
□ - laser pulse energy < 12.5 mJ, X - laser pulse energy > 12.5 mJ



(b) Unfocussed

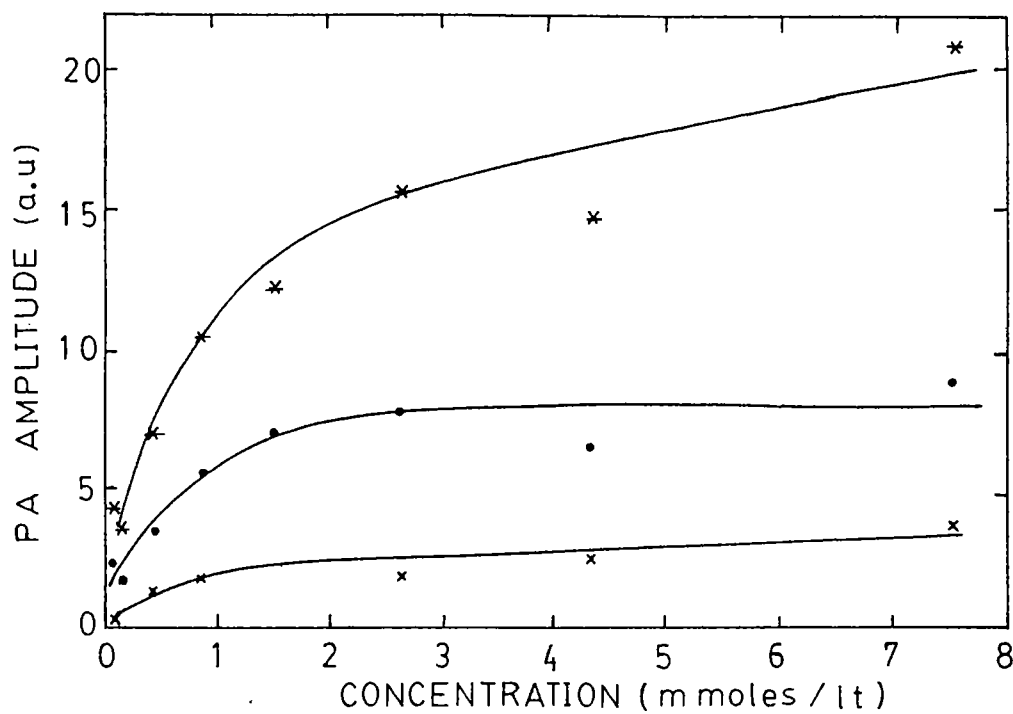
□ - laser pulse energy < 20 mJ, + - laser pulse energy > 20 mJ

Fig.4.12. Concentration dependence of photoacoustic signal, in methanol solutions of Fluorescien. Measured at various laser pulse energies.



(a) Focussed

+ - 6.25 mJ, o - 12.5 mJ, * - 25 mJ, • - 43.75 mJ



(b) Unfocussed

x - 6.25 mJ, • - 18.75 mJ, * - 37.5 mJ

variation in the results of fluorescien:methanol system is, the distinct pump power dependence of the slope. At higher concentrations the "slope curve" splits into two branches, corresponding to the high and low pump intensity regimes similar to that obtained in the case of Rhodamine 6G (chapter 3). The increase in slope for high power - high concentration case in comparison with low power - high concentration case can be attributed to the enhancement of two step excitation process ($S_0 \rightarrow S_1 \rightarrow S_n$) at higher pump intensities. Results show that such enhancement in two step excitation process is more probable in methanol solutions as compared to aqueous solutions.

Figs.4.9 and 4.12 respectively show the variation of the absolute PA signal with concentration in the fluorescien:water and fluorescien:methanol systems. These figures have been included here to emphasize the importance of the beam geometry in PA measurements where a change in the optical density of the sample is involved. In the focussed configuration, the acoustic source is a point slightly away from the detector as compared to the unfocussed case. The attenuation of the acoustic signal would be greater in the former case reducing the PA signal. But as the concentration is increased enhancement in PA signal occurs due to enhanced excited state absorption and TPA at higher laser powers.

4.3 PA GENERATION IN FLUORESCIEN : PUMPING BY 1060 NM

The log-log plots corresponding to the PA signals produced in the above concentrations of fluorescien solutions on irradiation with the 1060 nm laser radiation are given in figs.4.13 and 4.14. The slope is found to be one in all cases, indicating that the observed PA signal is generated from OPA

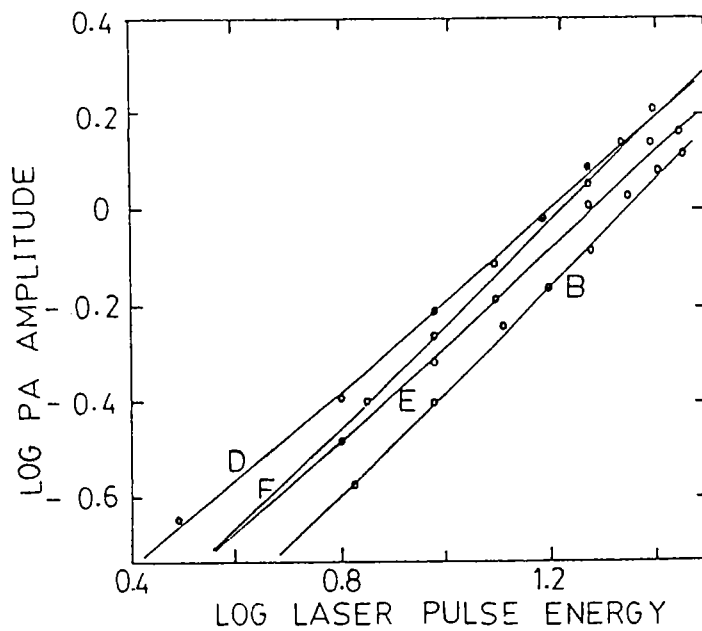


Fig.4.13. Log photoacoustic signal amplitude vs log laser pulse energy plot for Fluorescien in water, on 1060 nm excitation

B - 0.86 milli moles/lt, D - 0.137 milli moles/lt,
E - 0.068 milli moles/lt, F - 0.034 milli moles/lt

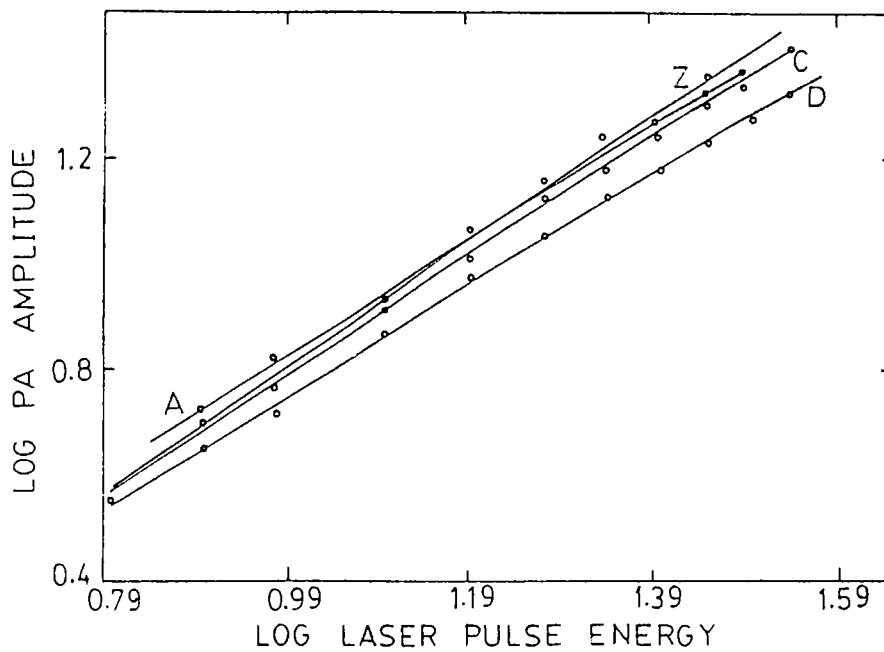


Fig.4.14. Log photoacoustic signal amplitude vs log laser pulse energy plot for Fluorescien in methanol, on 1060 nm excitation

Z - 4.3 milli moles/lt, A - 2.59 milli moles/lt,
C - 0.414 milli moles/lt, D - 0.138 milli moles/lt

process. Overtone absorption and subsequent vibrational relaxation of the solvent molecules are contributing here to the PA process in the samples. In general, the other means of PA generation are $S_1 \rightarrow S_0$ internal conversion resulting from an $S_0 \rightarrow S_1$ TPA and $S_n \rightarrow S_1$ nonradiative relaxations subsequent to multiphoton absorption. However these signals, if at all present, are so weak that they are masked by the signal from the solvent as observed in the case of various R6G solutions reported in chapter 3.

4.4 CONCLUSIONS

Photoacoustic investigations of two-photon absorption phenomena in aqueous and methanol solutions of fluorescein have been carried out at the pump wavelength of 532 nm. Experiments have been conducted in two different configurations, (focussed and unfocussed) and the results obtained are in mutual agreement. In aqueous solutions of the dye, TPA probability does not show a strong dependence on the pump intensity whereas in methanol solutions the pump power dependence is obvious at higher concentrations. Maximum probability for TPA is found to be around the concentration of 10^{-3} moles/lit in both solutions. The present studies also reveal the positions of some of the vibronic levels of the ground state of the dye fluorescein.

REFERENCES

- [1] Drexhage K H, in Dye lasers, 2nd edition p.143-193, ed. F P Schafer, Springer-Verlag, New-York, 1977
- [2] Myer J A, Johnson C L, Kierstead E, Sharma R D and Itzkan I, Appl.Phys.Lett., 16, 3, 1970
- [3] Chan M S and Bolton J R, Solar energy, 24, 561, 1980
- [4] Shen T, Huaxue Tongbao (Chem.), 6, 34, 1984
- [5] Gollnick K and Schenck G O, Pure appl.Chem., 9, 507, 1964
- [6] Usui Y and Enokido H, Bull.chem.Soc.Japan, 46, 2741, 1973
- [7] Xu H J and Shen S Y, Acta Chim.Sinica, 2, 148, 1985
- [8] Soep B, Kellmann A, Martin M and Lindqvist L, Chem.Phys.Lett., 13, 241, 1972
- [9] Schafer F P (ed) Topics in Applied Physics, vol 1, Springer-Verlag, New-York, 1977
- [10] Putcha Venkateswarlu, George M C, Rao Y V, Jagannath H, Chakrapani G and Miahnahri A, Pramana J.Phys., 28, 59, 1987
- [11] Orner G C and Topp M R, Chem.Phys.Lett., 36, 295, 1975

CHAPTER - 5

MULTIPHOTON ABSORPTIONS IN XANTHENE DYES USING 1060 nm RADIATION :



5.0 INTRODUCTION

Multiphoton absorption (MPA) is one of the nonlinear optical phenomena which has been investigated by various research workers [1-7]. Currently there are two experimental methods being generally used for identifying higher order nonlinear optical absorptions. One is the observation of radiative pathways of de-excitation, resulting in the antistokes fluorescence (ASF), and the other is the recently introduced photoacoustic (PA) technique which monitors the non radiative relaxation processes. As described in chapter 3, PA technique is not suitable to detect multiphoton absorptions resulting from infrared absorption in dye solutions. The conventional ASF technique suits us better here, and this chapter describes the investigation of multiphoton infrared absorptions carried out in two xanthene dyes (Rhodamine 6G and Fluorescein) by means of the ASF technique.

In antistokes fluorescence technique, a pump laser beam of longer wavelength is absorbed by the sample, and a weak fluorescence emitted at a shorter wavelength is detected. One of the causes of ASF is two-photon absorption. There are two methods of monitoring the radiative relaxation process for the study of two-photon absorption : the first is based on a direct measurement of the light absorbed due to two photon excitation

using an absorption spectrophotometer [8,9]. In the second method the ASF emission is monitored as a function of excitation intensity and wavelength [5,10,11].

Fluorescein and Rhodamine 6G are two important laser dyes belonging to the family of xanthene dyes. In this chapter, details of the present studies on two photon excitation to the S_1 level and subsequent de excitations in these dyes in various solvents are described. In the dyes selected, $S_0 \rightarrow S_1$ absorption bands are at the right wavelength region for two photon absorption of the pump radiation (1060 nm) and hence these dyes are potential candidates for efficient third harmonic generation of the pump laser frequency [12-14]. Two photon absorption data are necessary for the analysis of third harmonic generation process in nonlinear media.

5.1 THEORY

Earlier investigations on the molecular structure of laser dyes have given reliable models for the transitions occurring between the vibrational manifolds of various electronic energy states. A level diagram for the $S_0 \rightarrow S_1$ transition is given in fig 5.1. The dyes under consideration have $S_0 \rightarrow S_1$ absorption levels matching with 532 nm radiation. When pumped by 1060 nm radiation molecules are excited by TPA from the ground state S_0 (level 1) to the Franck Condon level 2 in the first excited singlet manifold S_1 , followed by a fast relaxation to level 3. Three photon absorption from S_0 can occur as well, to the excited state S_2 . Generally de-excitation to S_0 occurs through spontaneous emission, stimulated emission and

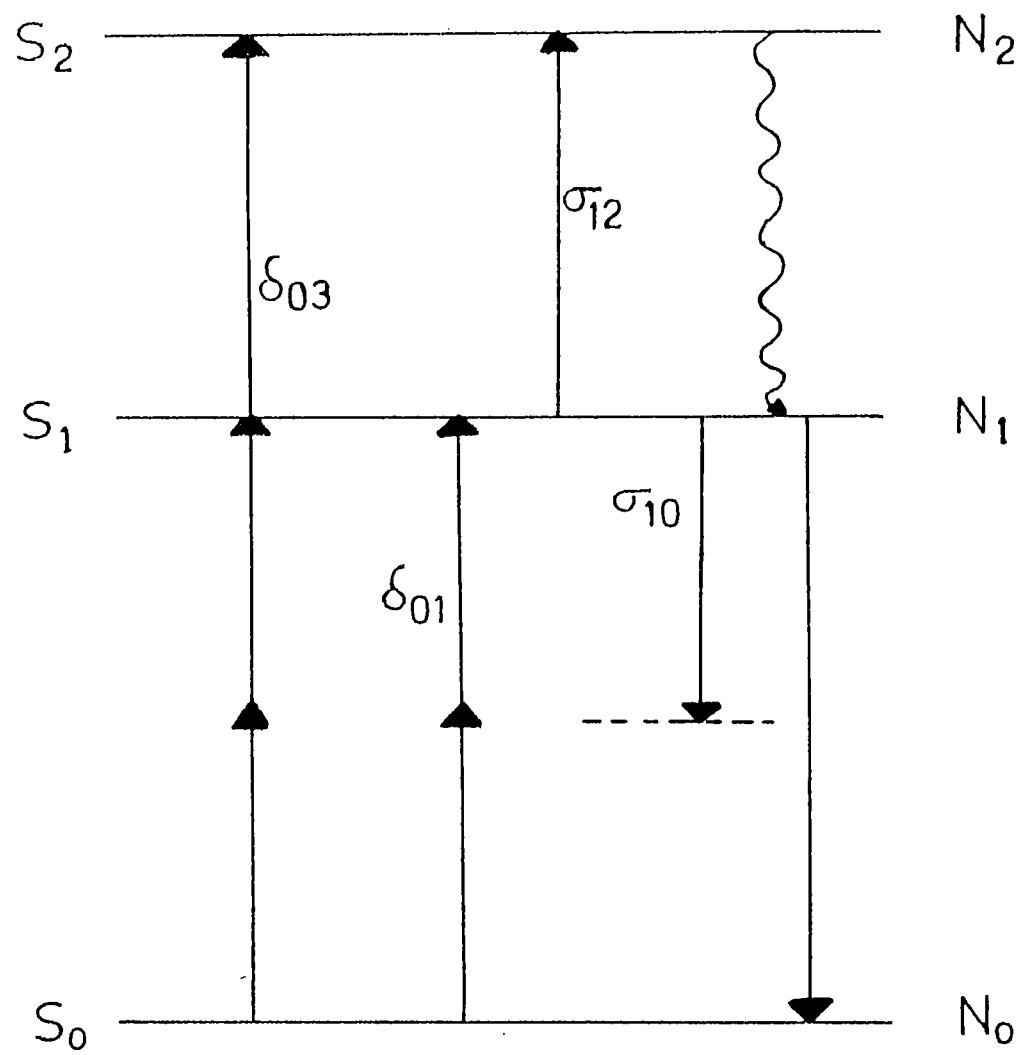


Fig.5.1. Energy level diagram for $S_0 \rightarrow S_1$ transition

radiationless transition. Relaxation by stimulated emission will be at the pump frequency, ν_L . The pump laser may induce excited state absorption also, from S_1 to higher levels as shown in fig.5.1. The PA signals are generated from non radiative relaxations between different levels. In this model, the non radiative pathways are (a) transitions from $S_n \rightarrow S_1$ ($n > 1$), (b) relaxation within the vibronic manifold of S_1 and (c) relaxation from the Franck Condon state to the lowest vibrational level in S_0 . Another channel for non radiative relaxation is the internal conversion from S_1 to S_0 . Intersystem crossing from singlet to triplet levels is neglected since the pump pulses are short here (≈ 10 ns).

The cross section δ for an n-photon absorption process can be defined as [15],

$$\delta = I_{FM} / q_{FM} N I_0^n \quad (5.1)$$

where I_{FM} is the fluorescence intensity (photons $\text{cm}^{-3} \text{sec}^{-1}$), I_0 is the excitation intensity (photons $\text{cm}^{-2} \text{sec}^{-1}$), N is the number of molecules per unit volume and q_{FM} is the fluorescence quantum efficiency which is assumed to be the same as that for one-photon absorption. The parameter δ is expressed in units of $\text{cm}^{2n} \text{s}^{n-1} \text{photons}^{-(n-1)} \text{molecule}^{-1}$.

We note that if N_0 is the number of ground state molecules before excitation, then the S_1 state population (N_1) can be expressed (for 1060 nm irradiation) by the rate equation

$$\frac{dN_1}{dt} = N_0 \delta_{01} F^2 + N_0 \rho \delta_{03} F^3 + N_2 \tau_{21}^{-1} - N_1 \sigma_{12} F - N_1 \sigma_{10} F - N_1 \tau_{10}^{-1} \quad (5.2)$$

where F is the laser flux, δ_{01} and δ_{03} are the molecular absorption cross-sections for $S_0 \rightarrow S_1$ (two-photon) and $S_0 \rightarrow S_2$ (three-photon) transitions respectively, σ_{12} and σ_{10} are the one photon cross-sections shown in the figure, and ρ is the fraction of molecules relaxing to S_1 from S_2 level, subsequent to $S_0 \rightarrow S_2$ three-photon absorption.

$N_0 \delta_{01} F^2$ is the no. of molecules /unit volume/sec, getting excited to the S_1 level,

$N_0 \rho \delta_{03} F^3$ is the no. of molecules /unit volume/sec, getting excited to the S_2 level, and relaxing from there to N_1 ,

$N_1 \sigma_{12} F$ is the no. of molecules /unit volume/sec, getting excited from S_1 to S_2 ,

$N_1 \sigma_{10} F$ is the no. of molecules /unit volume/sec, undergoing stimulated emission from S_1 ,

$N_2 \tau_{21}^{-1}$ is the no. of molecules /unit volume/sec, relaxing radiatively from S_2 to S_1 , and

$N_1 \tau_{10}^{-1}$ is the no. of molecules /unit volume/sec undergoing spontaneous emission from S_1 to S_0 .

The terms $N_2 \tau_{21}^{-1}$ and $N_1 \sigma_{10} F$ can be neglected being very small [16], and the equation (5.2) now becomes

$$\frac{dN_1}{dt} = N_0 (\delta_{01} F^2 + \rho \delta_{03} F^3) - N_1 (\sigma_{12} F + \tau_{10}^{-1}) \quad (5.3)$$

Assuming the pump pulse to be square shaped, and long in comparison with τ_{10} , we can write the steady state equation

$$\frac{dN_1}{dt} = 0, \quad (5.4)$$

giving

$$N_0 (\delta_{01} F^2 + \rho \delta_{03} F^3) = N_1 (\sigma_{12} F - \tau_{10}^{-1}) \quad (5.5)$$

such that the S_1 state population becomes

$$N_1 = \frac{N_0 (\delta_{01} F^2 + \rho \delta_{03} F^3)}{\sigma_{12} F + \tau_{10}^{-1}} \quad (5.6)$$

The ASF intensity (I_F) will be proportional to N_1 . Hence as seen from equation (5.6) we expect cubic and quadratic dependences of I_F on the laser flux F . The values of δ_{01} and δ_{03} clearly depend on the nature of the medium [2] whereby it becomes obvious that for different solvents and pump fluxes, the dependence of I_F on F can vary.

5.2 EXPERIMENTAL SET UP

For preparing the samples, stock solutions are initially made by dissolving R6G (Exciton) in doubly distilled water, methanol (spectroscopic grade) and ethylene glycol (analar grade); and Fluorescien Sodium in water and methanol. All samples used in the experiments (covering the range of 10^{-3} moles/lit to

G 5366 .

10^{-6} moles/lit) are prepared by subsequent dilution with the respective solvents. The experimental set up for recording ASF from the dyes is as described in chapter 2. Radiation (1060 nm) from a pulsed Q-switched Nd:YAG laser with pulse repetition rate of 10 Hz and pulsewidth 10 ns is used as the excitation source. The sample taken in a quartz cuvette is irradiated with the unfocussed laser beam. The ASF is observed at the right angle geometry and is focussed using a convex lens ($f = 5$ cm) to the entrance slit of a 0.3 meter Mcpherson monochromator attached with PMT assembly. The PMT signal is gated and averaged over 30 samples using a gated integrator and boxcar averager system. For all concentrations of R6G and fluorescien in various solvents ASF spectra have been recorded. The spectra are corrected for the spectral response of the detector. The laser energy dependence of the ASF emission is also measured.

Laser energies are measured with a commercial laser power meter. The absorbance spectra of the samples also have been recorded using a Hitachi Spectrophotometer.

5.3 RESULTS

5.3.1 Rhodamine 6G

The ASF spectra recorded for various concentrations of R6G in water, methanol and ethylene glycol solutions are shown in figs.5.2a, 5.2b & 5.2c respectively. It is observed that for R6G in water the emission peak apparently shifts from 560 nm to 600 nm as the concentration varies from 3.4×10^{-5} moles/lit to 2×10^{-3} moles/lit whereas in methanol, the peak shifts from 560 nm to

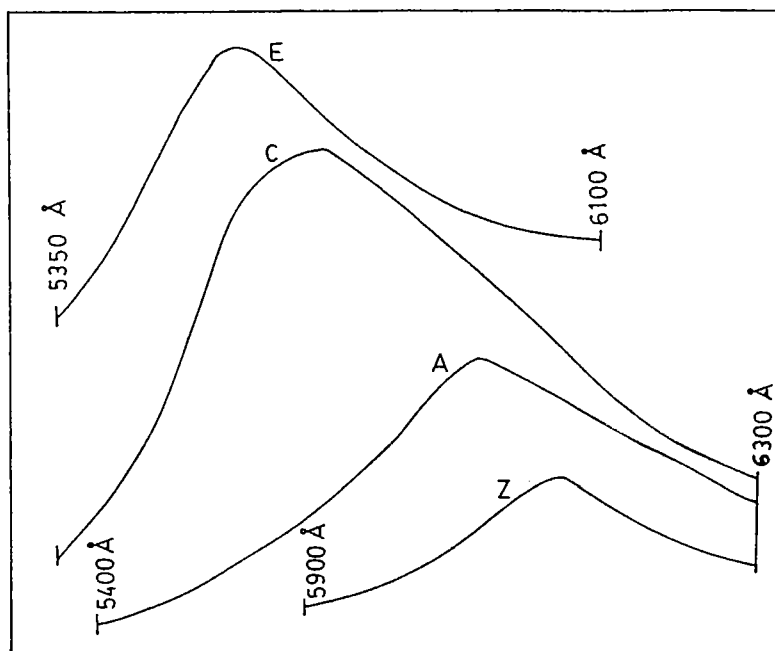


Fig.5.2a. Antistokes fluorescence spectra of Rhodamine 6G in water obtained on 1060 nm excitation. Peaks are given in brackets.

Z - 1.29 milli moles/lt (605 nm), A - 1.08 milli moles/lt (590 nm)
 C - 0.69 milli moles/lt (570 nm), E - 0.44 milli moles/lt (560 nm)

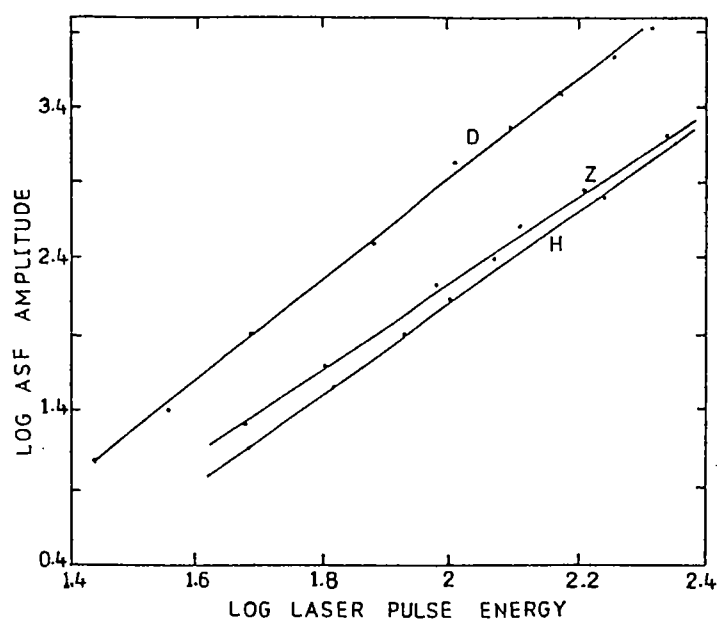


Fig.5.3a. Log ASF signal amplitude vs log laser pulse energy plot for Rhodamine 6G in water

Z - 1.29 milli moles/lt, D - 0.53 milli moles/lt, H - 0.25 milli moles/lt

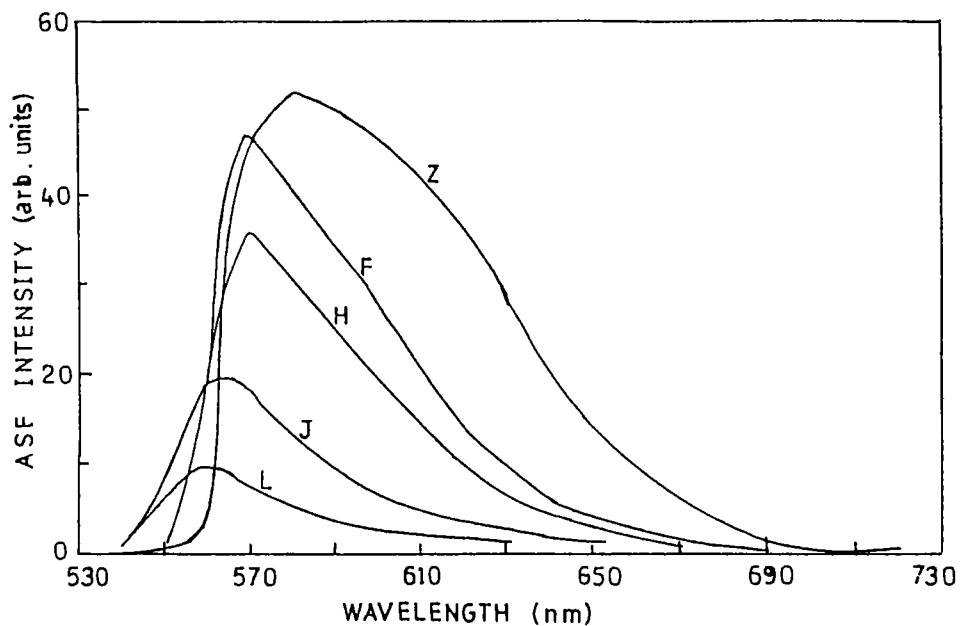


Fig.5.2b. Antistokes fluorescence spectra of Rhodamine 6G in methanol on 1060 nm excitation. Peaks are given. Z - 2 milli moles/lt (580 nm), F - 0.52 milli moles/lt (570 nm), H - 0.34 milli moles/lt (570 nm), J - 0.114 milli moles/lt (565 nm), L - 0.034 milli moles/lt (560 nm)

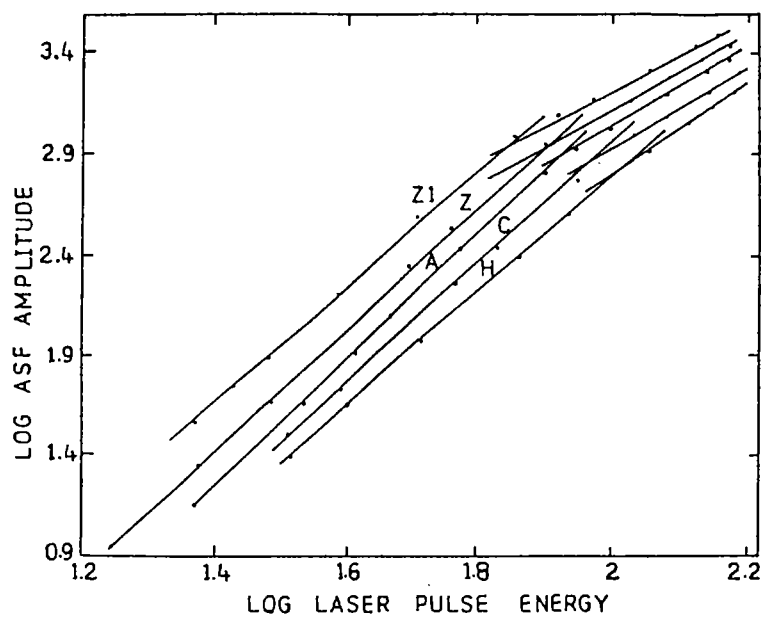


Fig.5.3b. Log ASF signal amplitude vs log laser pulse energy plot for Rhodamine 6G in methanol
 Z1 - 5.8 milli moles/lt, Z - 2.08 milli moles/lt, A - 1.25 milli moles/lt, C - 0.75 milli moles/lt, H - 0.376 milli moles/lt.

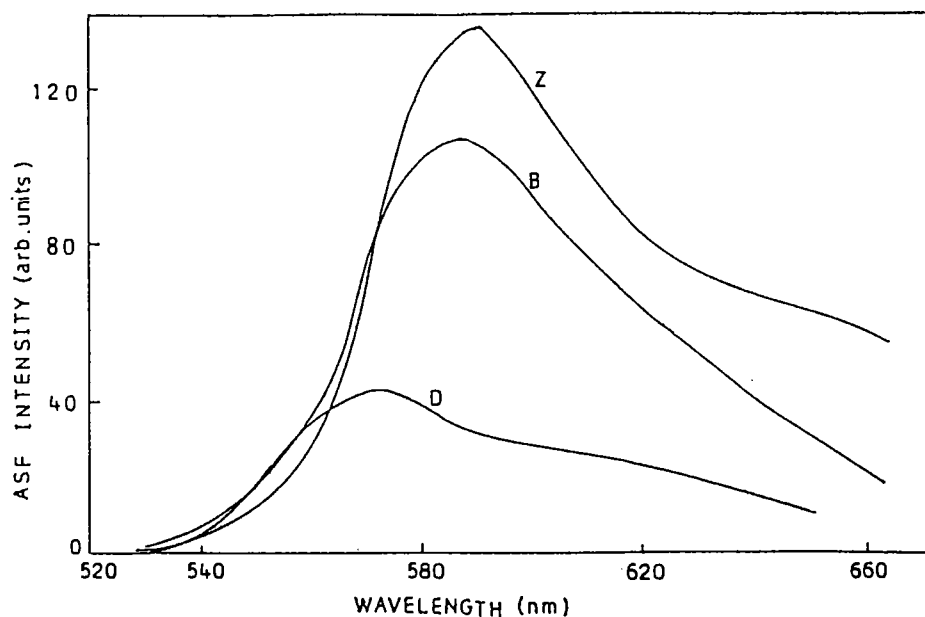


Fig.5.2c. Antistokes fluorescence spectra of Rhodamine 6G in ethylene glycol on 1060 nm excitation. Peaks are given in brackets.

Z - 1 milli mole/lt (590 nm), B - 0.53 milli moles/lt (585 nm),
 D - 0.071 milli moles/lt (570 nm)

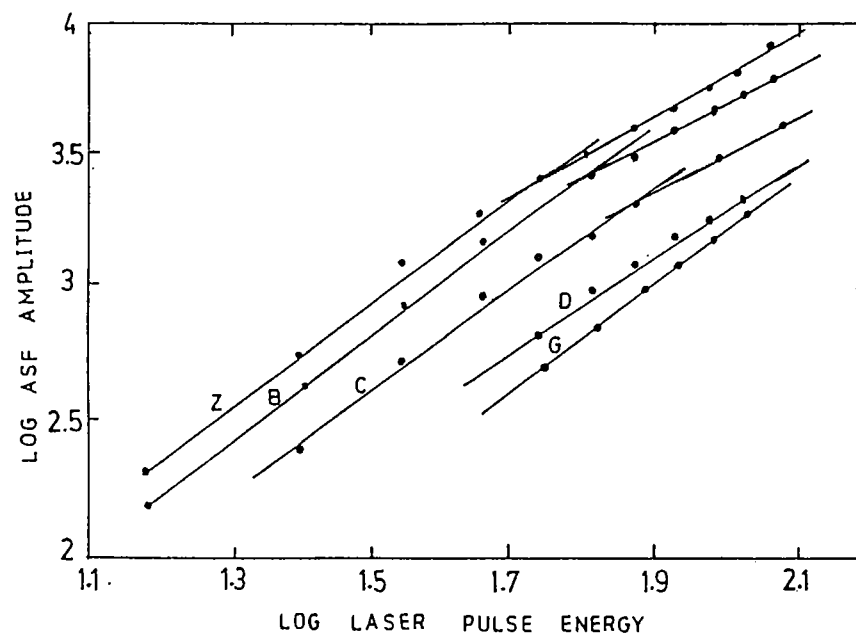


Fig.5.3c. Log ASF signal amplitude vs log laser pulse energy plot for Rhodamine 6G in ethylene glycol

Z - 1 milli mole/lt, B - 0.53 milli moles/lt, C - 0.178 milli moles/lt,
 D - 0.071 milli moles/lt, G - 0.0045 milli moles/lt

580 nm for the same concentration range. In the case of R6G in ethylene glycol The peak shifts from 555 nm to 590 nm in the concentration range of 1.8×10^{-6} moles/lt to 1×10^{-3} moles/lt.

Figs 5.3a, 5.3b & 5.3c show the plots of log ASF signal vs log laser pulse energy for R6G in water, methanol and ethylene glycol respectively, at various concentrations. In the case of R6G in water, at a high concentration (10^{-3} moles/lt) the slope is found to be 2.7. However, as concentration is decreased to 10^{-5} - 10^{-6} moles/lt the slope increases to 3. The values 2 & 3 of the slopes in these curves indicate that ASF emission occurs subsequent to two- and three- photon absorptions in the dye solutions. For R6G in methanol, the slope has a value of 2.8 at the concentration of 5×10^{-3} moles/lt and 3 in the lower concentrations (3×10^{-3} to 7×10^{-4} moles/lt) studied. In methanol solutions, predominance of three photon absorption is found to occur. For R6G in ethylene glycol solutions, slope of ≈ 2 is shown for all concentrations (10^{-3} to 10^{-6} moles/lt) studied. In this case two photon absorption is found to dominate.

5.3.2 Fluorescien Sodium

The ASF spectra recorded for various concentrations of Fluorescien in water:NaOH and methanol:NaOH solutions are shown in figs. 5.4a & 5.4b respectively. It is observed that for Fluorescien in water:NaOH the emission peak apparently shifts from 517 nm to 560 nm as the concentration varies from 3.4×10^{-5} moles/lt to 7.5×10^{-3} moles/lt. For Fluorescien in methanol, the peak varies from 526 nm to 550 nm for concentrations ranging from 6.9×10^{-5} moles/lt to 7.5×10^{-3} moles/lt.

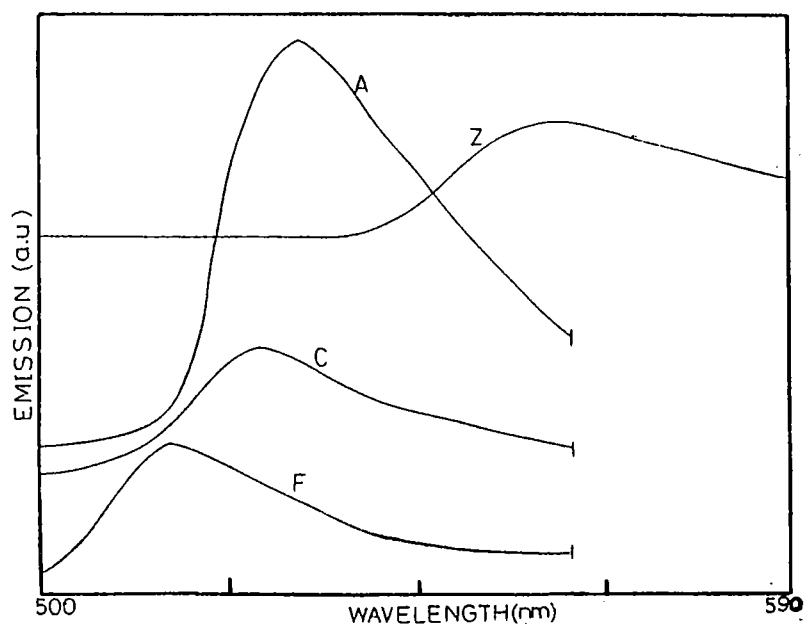


Fig.5.4a. Antistokes fluorescence spectra of Fluorescein in water on 1060 nm excitation. Peaks are given in brackets. Z - 4.3 milli moles/lt (559 nm), A - 2.58 milli moles/lt (536 nm), C - 0.413 milli moles/lt (530 nm), F - 0.034 milli moles/lt (517 nm)

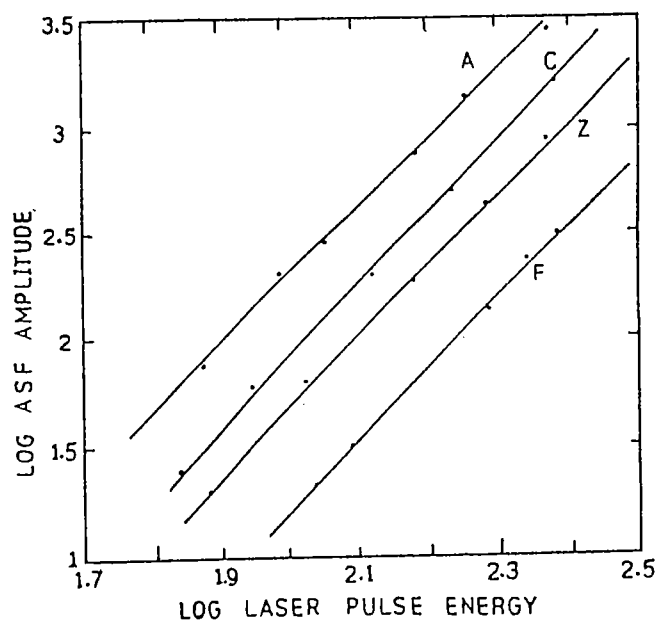


Fig.5.5a. Log ASF signal amplitude vs log laser pulse energy plot for Fluorescein in water

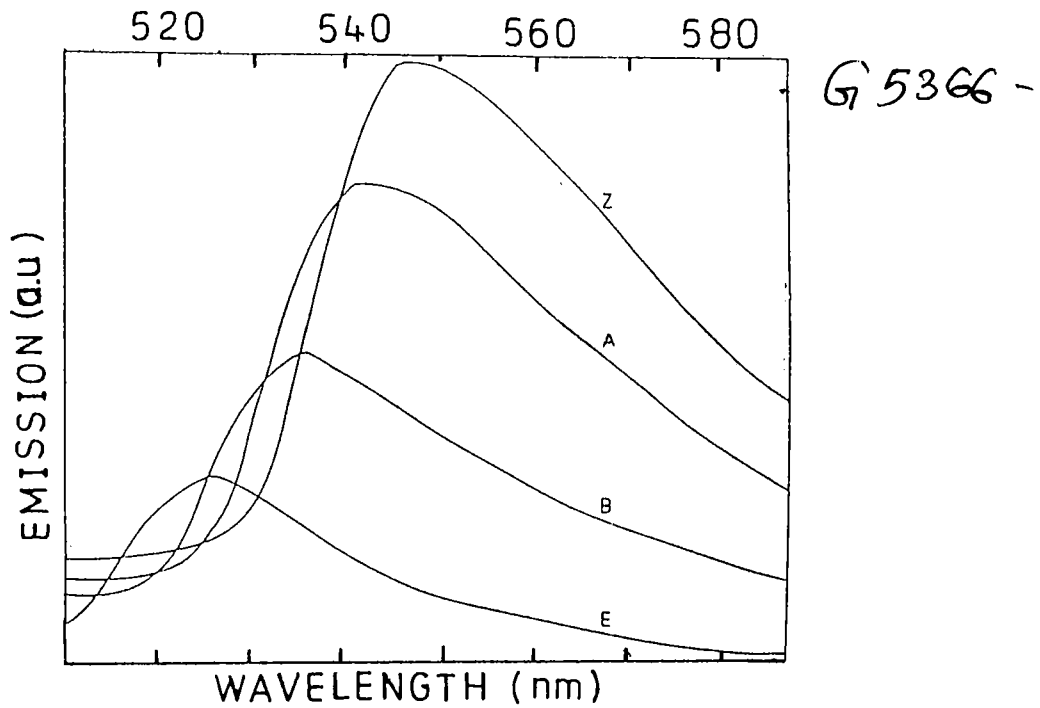


Fig.5.4b. Antistokes fluorescence spectra of Fluorescien in methanol on 1060 nm excitation. Peaks are given in brackets.

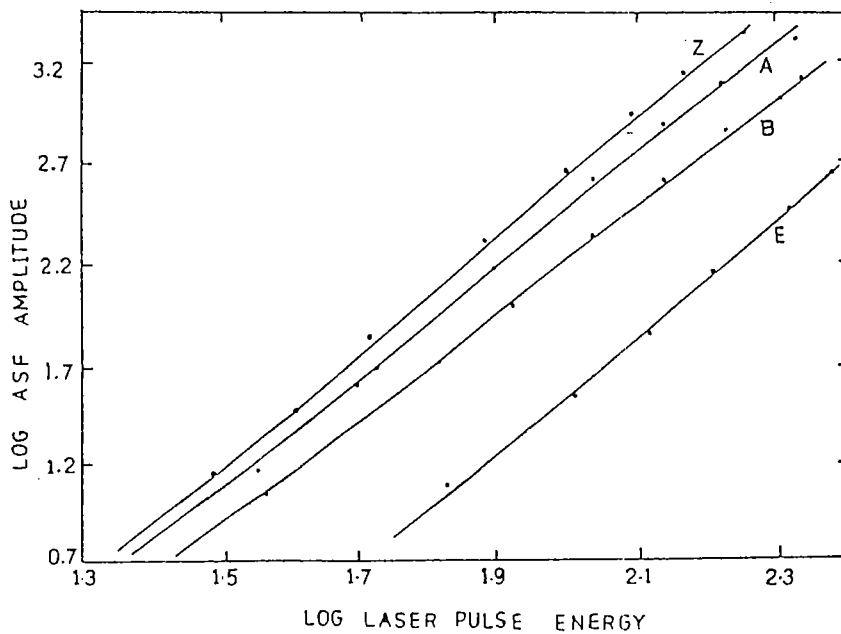


Fig.5.5b. Log ASF signal amplitude vs log laser pulse energy plot for Fluorescien in methanol

Z - 4.3 milli moles/lt (548 nm), A - 2.58 milli moles/lt (543 nm),
 B - 0.86 milli moles/lt, (536 nm), E - 0.069 milli moles/lt, (526 nm)

Figs 5.5a & 5.5b show the plots of log ASF signal vs log laser pulse energy respectively for Fluorescien in water:NaOH and methanol:NaOH solutions of different concentrations. In the case of Fluorescien in water:NaOH the slope has a value of ≈ 3.3 in the concentration range of 7.5×10^{-3} moles/lt to 3.4×10^{-4} moles/lt. In methanol:NaOH solutions the slope has a value of ≈ 2.9 in the concentration range of 7.5×10^{-3} moles/lt to 6.9×10^{-5} moles/lt.

5.4 DISCUSSION

The peak shift due to change in concentration results from the reabsorption of ASF emission within the medium. The overlap of the $S_0 \rightarrow S_1$ absorption band on R6G emission becomes significant at higher concentrations, thus leading to greater chances of radiation trapping and subsequent peak shifting [17]. (It has been observed that [18] the average reabsorption cross section is approximately equal to the ground state absorption cross section at the emitting wavelength for R6G in ethanol). Other reasons for this behaviour are the concentration dependence of fluorescence lifetime that affects the gain coefficient $r(\lambda)$ [19], biasing of stimulated emission cross section towards longer λ as compared to spontaneous emission [20] etc. In any case, the peak shift behaviour shown by ASF is similar to that exhibited by the usual fluorescence emission from dyes. The shift is found to be maximum for R6G:water system ($\Delta\lambda = 40$ nm) and minimum for R6G:methanol system ($\Delta\lambda = 20$ nm). Similarly in the case of fluorescien:(water:NaOH) system the shift ($\Delta\lambda = 40$ nm) is larger than in methanol:NaOH system ($\Delta\lambda = 30$ nm).

In conformity with the respective schematic energy level diagram (figs.5.6 & 5.7) for R6G and fluorescein to be discussed below, the observed multiphoton absorptions at 1060 nm radiation will excite the molecule to the S_1 and S_2 states. These energy level diagrams are drawn following the method described in chapter 4 (sec.4.2.1).

Following the interpretation of Hermann [21] the Rhodamine molecule in the ground state has practically C_{2v} symmetry. The S_0 ground state of the π electrons belongs to the totally symmetric representation A_1 , whereas the excited states belong to either A_1 or B_2 . The two possible classes of two photon transitions are both symmetry allowed. It has been shown [21] that $A_1 \rightarrow A_1$ transition moments are large for two photon transitions and weak for one photon transitions. The opposite situation occurs for $A_1 \rightarrow B_2$ transitions. Experimental evidences [5,22] show that S_1 belongs to B_2 symmetry and S_2 to A_1 symmetry. A large dispersion in the values of TPA cross-sections (δ) for R6G in ethanol has been observed and δ at 680 nm is found to be approximately 27 times greater than δ at 1060 nm [21]. This dispersion is in agreement with the above symmetry assignment.

According to our results in R6G:Methanol systems three photon absorption is evident in all the samples studied. We believe that along with direct three photon absorption from S_0 to S_2 , a two step process involving the intermediate level S_1 is also probable. In most solvents this scheme should be quite efficient according to the previous symmetry assignments. It is interesting to note that in R6G:ethylene glycol system the slope is 2 for all the samples indicating a strong two photon absorption rather than three photon absorption. It is known that because of the Franck-Condon effect excitation from a solvated

In conformity with the respective schematic energy level diagram (figs.5.6 & 5.7) for R6G and fluorescein to be discussed below, the observed multiphoton absorptions at 1060 nm radiation will excite the molecule to the S_1 and S_2 states. These energy level diagrams are drawn following the method described in chapter 4 (sec.4.2.1).

Following the interpretation of Hermann [21] the Rhodamine molecule in the ground state has practically C_{2v} symmetry. The S_0 ground state of the π electrons belongs to the totally symmetric representation A_1 , whereas the excited states belong to either A_1 or B_2 . The two possible classes of two photon transitions are both symmetry allowed. It has been shown [21] that $A_1 \rightarrow A_1$ transition moments are large for two photon transitions and weak for one photon transitions. The opposite situation occurs for $A_1 \rightarrow B_2$ transitions. Experimental evidences [5,22] show that S_1 belongs to B_2 symmetry and S_2 to A_1 symmetry. A large dispersion in the values of TPA cross-sections (δ) for R6G in ethanol has been observed and δ at 690 nm is found to be approximately 27 times greater than δ at 1060 nm [21]. This dispersion is in agreement with the above symmetry assignment.

According to our results in R6G:Methanol systems three photon absorption is evident in all the samples studied. We believe that along with direct three photon absorption from S_0 to S_2 , a two step process involving the intermediate level S_1 is also probable. In most solvents this scheme should be quite efficient according to the previous symmetry assignments. It is interesting to note that in R6G:ethylene glycol system the slope is 2 for all the samples indicating a strong two photon absorption rather than three photon absorption. It is known that because of the Franck-Condon effect excitation from a solvated

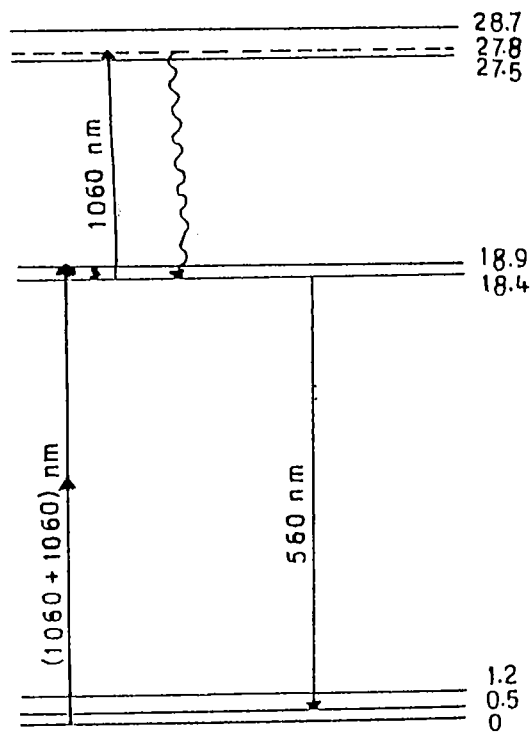


Fig.5.6. The energy level diagram for Rhodamine 6G.

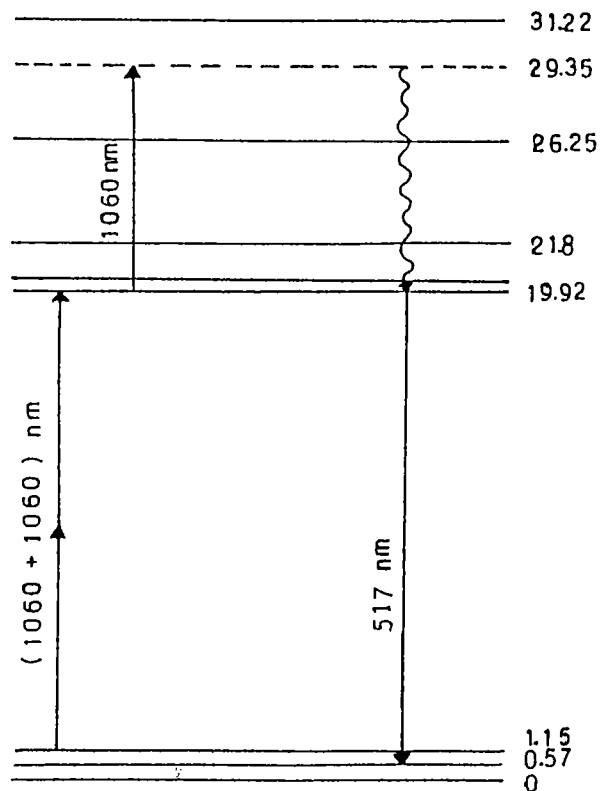


Fig.5.7. The energy level diagram for Fluorescien.

Energies given in 10^3 cm^{-1}

ground state leads not to the energetically most stable solvated conformation of the excited state, but to a conformation (the FC state) geometrically identical to the ground state [22]. Due to the high viscosity of ethylene glycol (19.9 cp as compared to 0.58 cp for methanol) the orientational relaxation time of R6G molecules will be much larger in the S_1 state, being in the order of the S_1 state lifetime. (For eg., for cresyl violet molecules the orientational relaxation times are 100 ps and 2 ns respectively in methanol and ethylene glycol solutions [25]). It is not known whether the large orientational relaxation times are affecting the level symmetry in such a way as to reduce the $S_1 \rightarrow S_2$ ESA. This conjecture is supported from our observation that in the least viscous solvent (methanol) three photon absorption is found to occur completely and in water which is more viscous than methanol both effects are observed. However more experiments are necessary to confirm this assumption.

In fluorescein:methanol systems TPA and three photon absorptions are found to occur but three photon absorptions predominate, as indicated by slopes ≈ 2.9 . In fluorescein:water solutions three photon absorption is found to occur as observed from the slopes ≈ 3.3 .

As seen in fig.5.3b a tendency of ASF quenching at higher laser powers is observed. Various reasons suggested for the quenching of ASF at higher powers are stimulated emission from S_1 , and absorption from S_1 to higher excited states followed by intersystem crossing [16]. Eichler et al [24] have shown that stimulated anti-stokes Raman scattering can also quench ASF intensity at high powers. However in our case the first process seems to be negligible [16] and the pump induced quenching may be attributed to $S_1 \rightarrow S_n$ transitions. It has also been seen that at

higher concentrations quenching occurs at lower pump energies, due to the enhancement in excited state absorption resulting from the increased S_1 state population.

5.5 CONCLUSIONS

Multiphoton absorption in solutions of R6G:water, R6G:methanol and R6G:ethylene glycol; and Fluorescien:water and Fluorescien:methanol has been achieved by pumping with 1060 nm laser radiation. The subsequent ¹nonlinear fluorescence is investigated. Reabsorption of fluorescence and emission peak shifting are observed at higher dye concentrations. Maximum peak shift is seen in aqueous solutions. ASF quenching is found to occur at higher pump powers and concentrations. The predominance of two photon absorption in the solvent ethylene glycol is discussed in connection with the large solvation times of dye molecules in viscous media.

REFERENCES

- [1] Orner G C and Topp M R, Chem.Phys.Lett., 36, 295, 1975
- [2] Catalano I M and Cingolani A, Opt. Commun., 32, 159, 1980
- [3] Vabnits Kh, Gaisenok V A, Slobodyanyuk A I and Shubert D, Opt. Spektrosk., 61, 201, 1986
- [4] Hermann J P and Ducuing J, Phys.Rev. A, 5, 2557, 1972
- [5] Rulliere C and Kottis P, Chem. Phys. Lett., 1980, 75, 478
- [6] Lin H B and Topp M R, Chem.Phys.Lett., 47, 442, 1977
- [7] Penzkofer A and Leupacher W, Optical and Quantum Electronics, 19, 327, 1987
- [8] Monson P R and McClain W M, J. Chem. Phys., 53, 29, 1970
- [9] Penzkofer A, Falkenstein W and Kaiser W, Appl.Phys.Lett., 28, 319, 1979
- [10] Mikami N and Ito M, Chem. Phys. Lett., 31, 472, 1975
- [11] Tang H L B, Thrash R J and Luo G E, Chem. Phys. Lett., 57, 59, 1978
- [12] Bey PP, Galbraith J F and Rabin H, IEEE J.Quantum.Electron., QE - 7, 86, 1971
- [13] Diels J C and Schafer F P, Appl. Phys. B, 5, 197, 1974
- [14] Leupacher W, Penzkofer A, Runde B and Drexhage K H, Appl. Phys. B, 44, 1987
- [15] John B.Birks, Photophysics of Aromatic molecules, Wiley -Interscience, London, 1970
- [16] Bradley D J, Hutchinson M H R, Koetser H, Marrow T, New G H C and Petty M S, Proc. R. Soc. Lond. A, 328, 97, 1972
- [17] Hammond P R and Nelson R, IEEE J.Quantum.Electron., QE - 16, 1161, 1980
- [18] Falkenstein W, Penzkofer A and Kaiser W, Opt.Comm., 27, 151, 1978

- [19] Tsuneo Urisu and Kenji Kajiyama, J.Appl.Phys., 47, 3559, 1976
- [20] Magde D, Gaffney S T and Campbell B F, IEEE J.Quantum.Electron., QE - 17, 48, 1981
- [21] Hermann J P and Ducuing J, Opt.Comm., 6, 101, 1972
- [22] Jaffe H H and Milton Orchin, Theory and applications of Ultraviolet Spectroscopy, John Wiley and Sons, Inc., New York, 1964
- [23] Dye Lasers , ed. F.P.Schafer, Springer Verlag, New York, 1977
- [24] Eichler H J, Langhans D and Klein U, Appl.Opt., 18, 1383, 1979

CHAPTER - 6

MULTIPHOTON ABSORPTIONS IN XANTHENE AND MEROCYANINE DYES :



6.0 INTRODUCTION

Since the first observation of a two-photon absorption process in $\text{Ca F}_2:\text{Eu}^{2+}$ by Kaiser and Garrett [1], this nonlinear optical phenomenon, postulated a long time ago by Goppert-Mayer [2], has been the subject of detailed investigations of many workers. Organic molecules are especially suited to the study of this process due to their large number of energy levels implying the possibility of relatively large cross-sections for two photon transitions. When certain aromatic crystals [3,4] and liquid solutions of aromatic compounds [5] were excited using ruby laser, such two-photon excitations were found to generate anti-stokes fluorescence (ASF). Similar observations have been made with aqueous solutions of certain organic dyes [6] also. Values of two-photon absorption cross-sections for these substances lie between 10^{-48} and $10^{-50} \text{ cm}^4 \text{ sec}^{-1}$. Investigations of the fluorescence of such complex molecules under strong photoexcitation enable one to determine the characteristics of nonlinear absorption and the interaction of light with excited molecules.

Multiphoton excitations of dyes which absorb radiation in the visible region may lead to the emission of weak Antistokes fluorescence in the uv and blue regions. This luminescence has been interpreted as emission associated with transitions from the

higher singlet states (S_n) to the ground state (S_0) of the dye molecule. (Triplet molecules [7], photoproducts and impurities [13] also can be sometimes responsible for short wavelength luminescence of solutions of organoluminophores). Collisional energy transfer between two excited molecules, represented by $S_1 + S_1 \rightarrow S_n + S_0$, is one process by which higher excited singlet states can be populated. The population of the S_n state may be brought about by a transition from the first excited state (S_1) of the molecule as well at high pump intensities, with the absorption of visible [8] or infra red [8,9] quanta. In general, such step-wise excitations can also occur along with direct multiphoton transitions if the molecular electronic energy states are resonant with the pump radiation. In step-wise or excited state absorptions (ESA), the initial excitation by the absorption of one photon places the molecule in an excited state, and the subsequent absorption of a second photon raises the molecule to a still higher energy level. One may note that whereas a multiphoton absorption process is a 'single' act, step-wise absorption is characterized by distinct acts of absorption, separated in time from each other.

6.1 EXCITED STATE ABSORPTION (ESA)

The ESA process of singlet excited complex molecules when pumped at a frequency that matches with the $S_0 \rightarrow S_1$ absorption band occurs according to the scheme $S_1 + h\nu \rightarrow S_n$ where S_1 and S_n are respectively the ground state, first excited and higher excited ($n > 1$) singlet states. For ESA to occur, the pump frequency should match with one of the $S_1 \rightarrow S_n$ transitions. The result of ESA of singlet molecules is the quenching of

fluorescence from the S_1 state and the appearance of Antistokes fluorescence from the S_n states.

Eventhough direct excitation by uv radiation is good enough to study singlets higher than the first excited state in most of the absorbing organic compounds, it is advantageous to use ESA for the same, due to certain specific reasons. The first attraction of this technique is its unconventional nature itself. In ESA we have the excitation into S_1 as the primary step, and the second photon may be absorbed at anytime during the S_1 state lifetime [10]. The second photon may be generated by a second source as well, and by properly adjusting the time delay between the pump photons, it is possible to populate the target levels to different degrees. Since a real intermediate state is involved and the two photons need not be coincident, a further degree of photoselective discrimination is available. In certain cases one may reflect upon the difficulties involved in the unambiguous assignment of $S_m \longrightarrow S_{n>m}$ absorption spectra of highly excited levels S_m , since in condensed systems absorption spectra of higher excited states are generally not very well resolved. However in comparison with TPA the ESA method has several advantages: (a) Since the process occurs by two allowed single-photon transitions, the extent of excitation is comparable to mono-photon excitation and considerably exceeds that obtained in an unenhanced direct two-photon experiment, (b) The shape of the fluorescence spectrum and the coherence and polarisation properties of the emission are subject to variation in experimental coincidence of the light pulses, especially if they are of different wavelengths so that one can extract valuable information about excitation level lifetimes [11] and the

relaxation route, and (c) The excited state fluorescence intensity is determined by the number of photons incident per unit fluorescence decay time of S_1 . Since simultaneous two-photon absorption by impurities relies on large absolute intensities, it is possible to discriminate against this by spreading the total intensity over a period of nanoseconds rather than by a single ultrashort pulse.

In most cases, the observed luminescence quantum yield (Φ_F) of the higher excited singlets is low, since these states are rapidly depopulated after fluorescing for only a small fraction of their natural radiative lifetimes, $(k_F)^{-1}$:

$$\Phi_F = k_F \left[k_F + \sum_i k_i \right]^{-1}$$

(where k_i represents all other processes resulting in deactivation of a potentially fluorescent state). For levels other than thermal levels in S_1 , $\sum_i k_i \gg k_F$, and hence $\Phi_F \ll 1$. For example, the quantum yield of fluorescence in the 300-450 nm region for an ethanol solution of R6G is estimated to be $(2 \pm 1) \times 10^{-5}$ [13]. The principal difference between high and low quantum-yield fluorescence (Stokes fluorescence and ASF respectively in our case) is thus in the decay time $(k_F + \sum_i k_i)^{-1}$. One may also note that the fluorescence radiative lifetimes $(k_F)^{-1}$ are usually comparable in both cases such that integration over sufficiently short times will yield comparable amounts of emission from both high - and low quantum-yield states [12].

Since according to previous estimates [9] the lifetime of the S_n state is about 10^{-13} sec, it would be expected that the ASF is appreciably polarized even in liquid solutions.

Investigation of the polarization of ASF will yield information on the mutual orientation of dipole moments of $S_n \longleftrightarrow S_0$, $S_1 \longleftrightarrow S_n$, and $S_1 \longleftrightarrow S_0$ transitions. On the basis of these, conclusions can be drawn regarding the nature of the emitting states in each particular case. Studies on polarization of the ASF during multistage excitation of a solution of R6G by linearly polarized light with $\lambda = 530$ nm and 1060 nm has been reported by Aristov and Shevandin [13]. It is worthwhile here to notice the possibility of separating the components of ASF connected with ESA and TPA by using short duration (picosecond) light pulses. The lifetime of the higher electronic states being very short, ASF induced by direct TPA practically disappears instantly after cessation of excitation. On the other hand ASF due to ESA under the same conditions will exist down to the total decay time of the S_1 state. Thus ESA must lead to the appearance of a comparatively long-lived component in the ASF.

One may use upper state fluorescence as a self-probe of subpicosecond lifetime phenomena and since emission spectra are characteristic of both upper and lower levels, they can be used directly to determine the level of excitation. Observation of the variation of the fluorescence spectrum as a function of excitation pathway, coupled with quantum yield data may then be used to estimate the rates of radiationless conversion.

This chapter describes the details of the application of TPA and ESA for the population of higher excited singlets in certain organic dyes (R6G, Fluorescien and DCM), and the measurement of the resultant low-quantum yield fluorescence spectrum.

6.2 EXPERIMENTAL SET UP

The experimental arrangement for recording ASF spectra is as described in chapter 2. The samples studied include R6G in water,

Fluorescien in water:NaOH and DCM in Ethylene glycol : Benzyl alcohol taken at various concentrations. Radiations at 1060 nm (ω_1), 532 nm (ω_2) and (1060 + 532) nm ($\omega_1 + \omega_2$) separately available from a pulsed Nd:YAG laser are used to irradiate the sample solutions contained in a quartz cuvette. (For obtaining (1060 + 532) nm radiation at the cuvette we simply remove the harmonic separator from the experimental set up. Since the conversion efficiency of the KD*P second harmonic crystal used in our system is well below unity, if we remove the harmonic separator from the beam path we will in fact get a mixture of 532 nm and 1060 nm wavelengths at the cuvette. Spatial and temporal overlap of the two beams also will be automatically achieved). The weak ASF emission is focused by a convex lens into a 0.3 m McPherson monochromator. The emission is wavelength scanned in the region 300-500 nm and detected by a photomultiplier tube. The signal from the PMT is amplified, gated and averaged over 100 pulses by employing a gated integrator and boxcar averager system. The output is fed to a chart recorder.

The absorption spectra of the samples are recorded on a spectrophotometer. The normal dye fluorescence upon excitation with 532 nm also is recorded.

6.3 RESULTS

The following results have been obtained from these investigations:

(1). Irradiation of the dyes with ($\omega_2 + \omega_1$) gives an ASF band in the shorter wavelength region in all cases. In aqueous solutions of R6G, the emission peak changes from 367nm to 387 nm as the concentration is increased from 4×10^{-6} moles/lt to 2×10^{-3} moles/lt (fig.6.2a). In aqueous solutions of fluorescien, fluorescence peak is found to vary from 364 nm to 397 nm for a

change of concentration from 3×10^{-5} moles/lit to 2.5×10^{-3} moles/lit (fig.6.3a). In DCM (solvent : ethylene glycol + benzyl alcohol) a band that peaks at $\lambda \approx 400$ nm independent of the concentration is obtained in the range 4×10^{-5} moles/lit to 2.3×10^{-3} moles/lit (fig.6.4a).

(2). Irradiation of the samples by ω_1 alone gave no measurable signal at the sensitivity of the above experiments.

(3). Irradiation by ω_2 alone gives a weaker fluorescence signal than that obtained for $(\omega_1 + \omega_2)$. For aqueous solutions of R6G the peak variation was from 378 to 393 nm (fig.6.2b) and the change is from 362 to 377 nm for aqueous fluorescein solutions (fig.6.3b). For DCM in (ethylene glycol + benzyl alcohol) the peak is rather unshifted at $\lambda \approx 410$ nm (fig.6.4b).

(4). The normalised fluorescence $Q(\lambda) / Q_{(\max)}$ and the normalised absorption $\epsilon(\lambda) / \epsilon_{(\max)}$ in the region for DCM and fluorescein solutions are as shown in figs.6.5 and 6.6. The point of intersection of these spectra represents the position of the lowest vibrational level of the first excited singlet state S_1 above that of the ground state S_0 [14]. Once fixing this level, the energy level diagrams can be drawn from the absorption and emission data as discussed before (sec.4.2.1).

(5). The calculated energy level diagrams for DCM and fluorescein molecules are given in fig (6.8) and (6.9) respectively. In fig.6.7 the same is given for R6G taken from Orner and Topp [8].

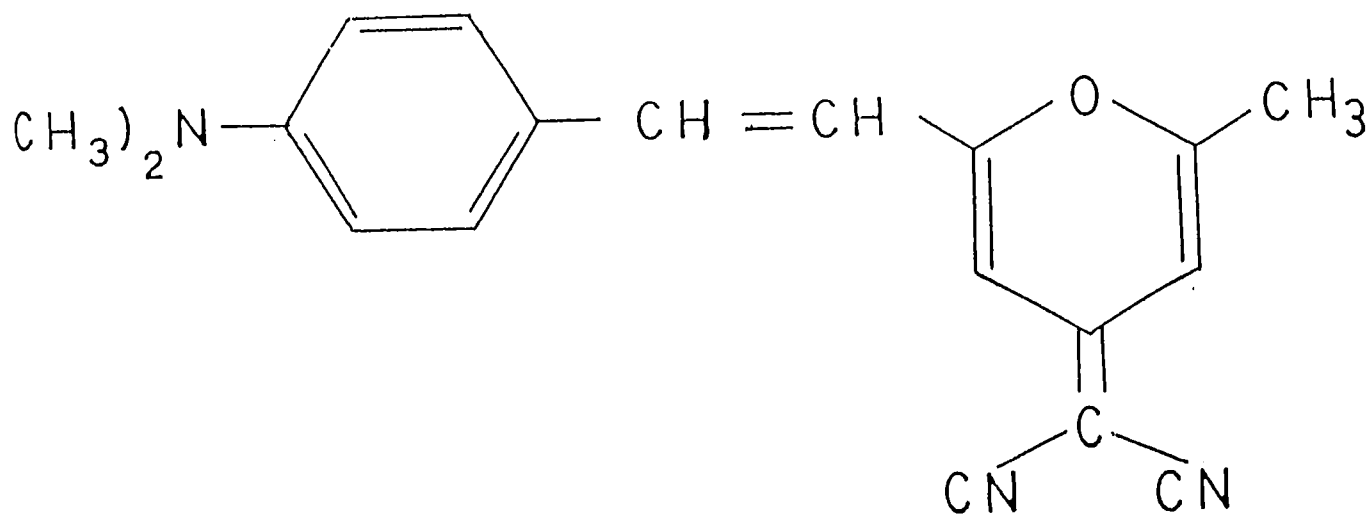


Fig.6.1a. Structure of DCM (4 - Dicyanomethylene - 2 -methyl - 6 - p - dimethyl aminostyryl-4H-pyran) dye

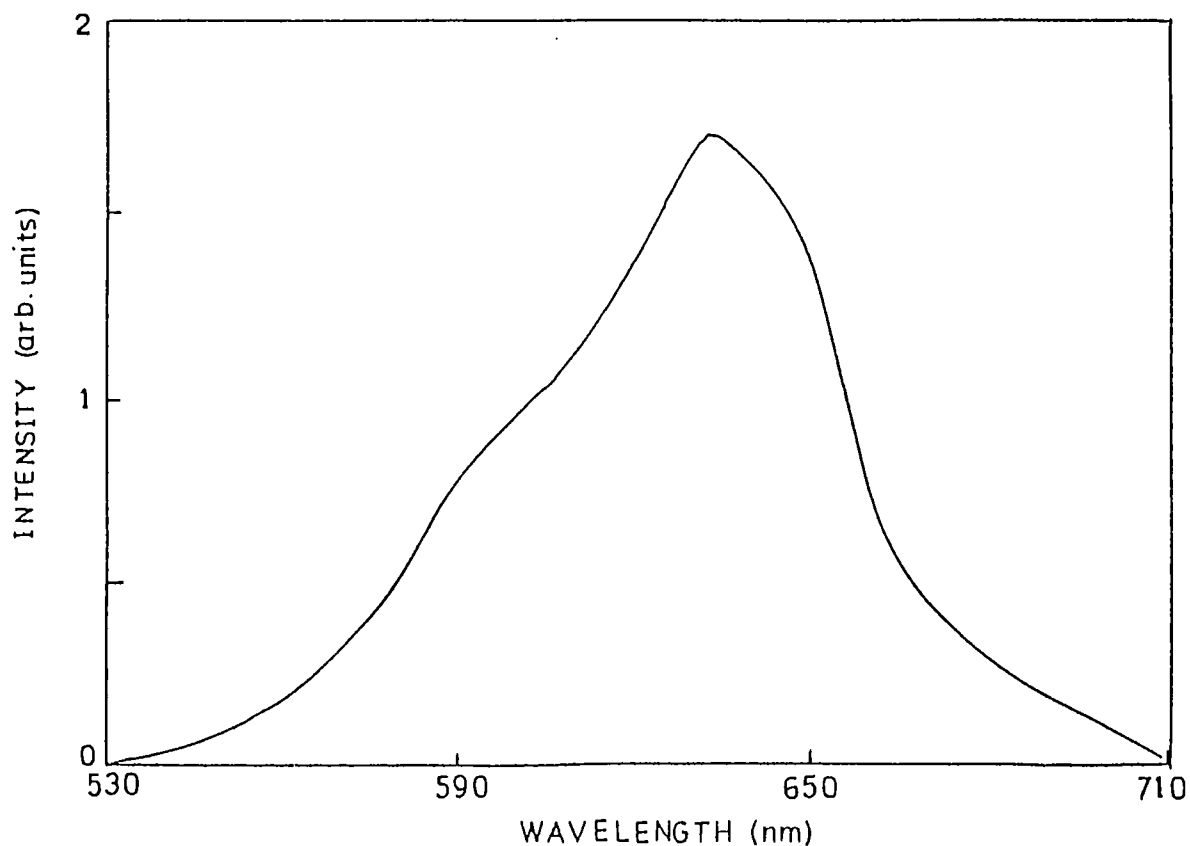


Fig.6.1b. Fluorescence emission spectra of DCM in (Ethylene glycol + Benzyl alcohol) obtained on 532 nm excitation. Concentration - 0.008 m moles/lt, Peak at 635 nm

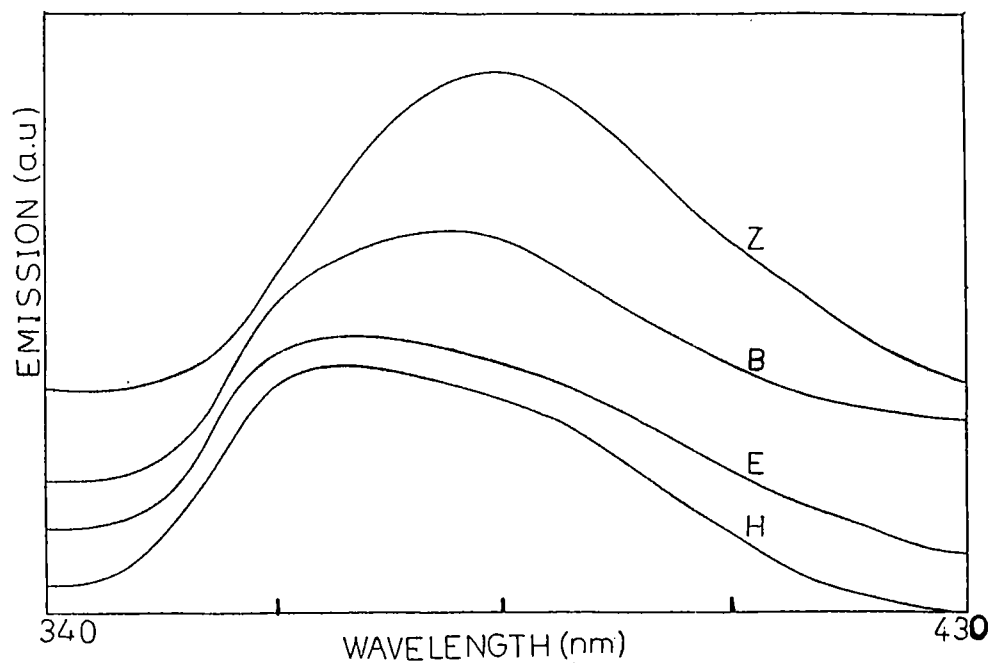


Fig.6.2a. Antistokes fluorescence spectra of Rhodamine 6G in water obtained on (532 nm + 1060 nm) excitation. Peaks are shown in brackets.

Z - 1.29 milli moles/lt (387 nm), B - 0.899 milli moles/lt (383 nm),
 E - 0.44 millimoles/lt (367 nm), H - 0.25 milli moles/lt (367 nm)

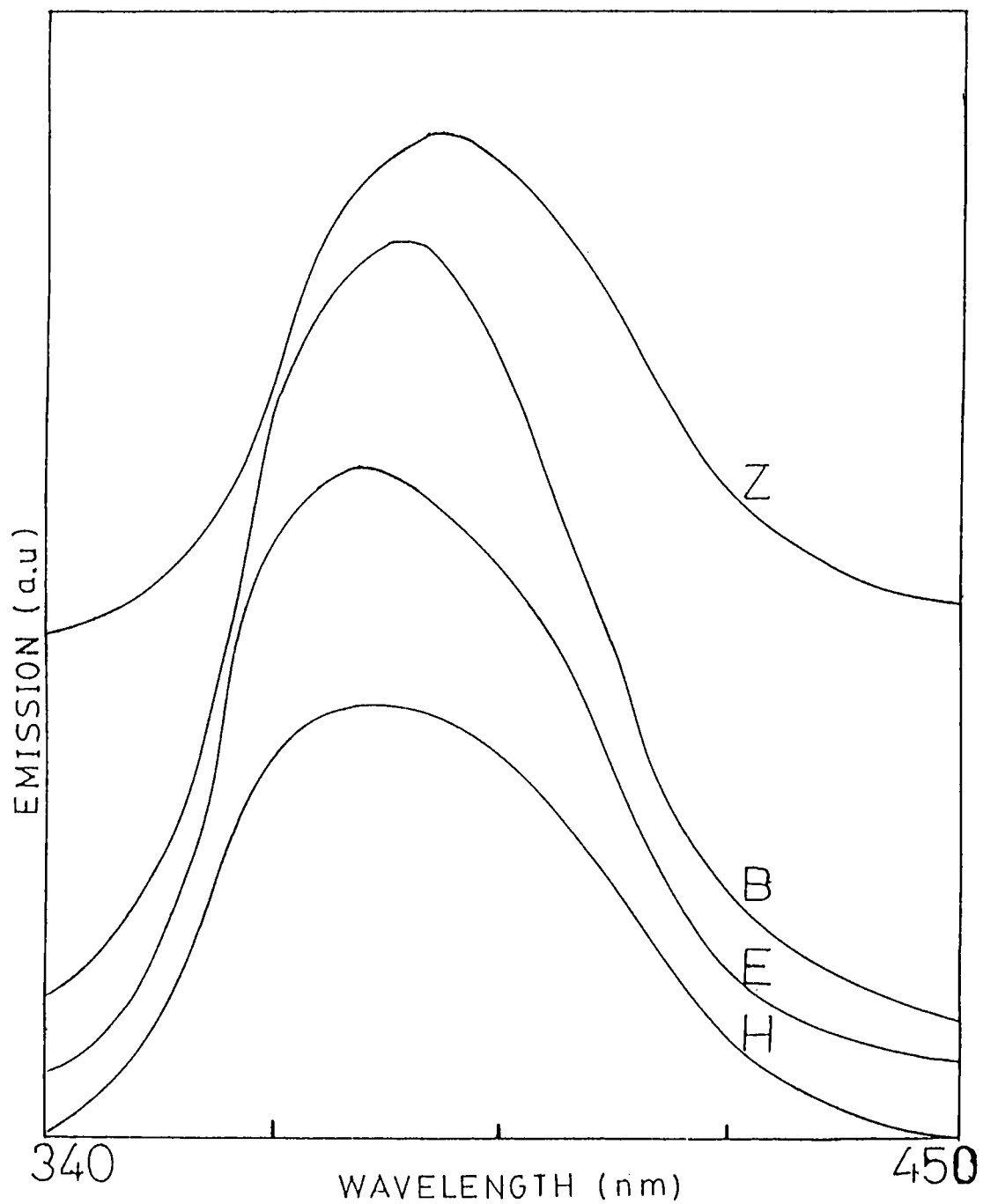


Fig.6.2b. Antistokes fluorescence spectra of Rhodamine 6G in water obtained on 532 nm excitation. Peaks are shown in brackets.

Z - 1.29 milli moles/lt (393 nm), B - 0.899 milli moles/lt (386 nm),
 E - 0.44 milli moles/lt, (380 nm), H - 0.25 milli moles/lt (378 nm)

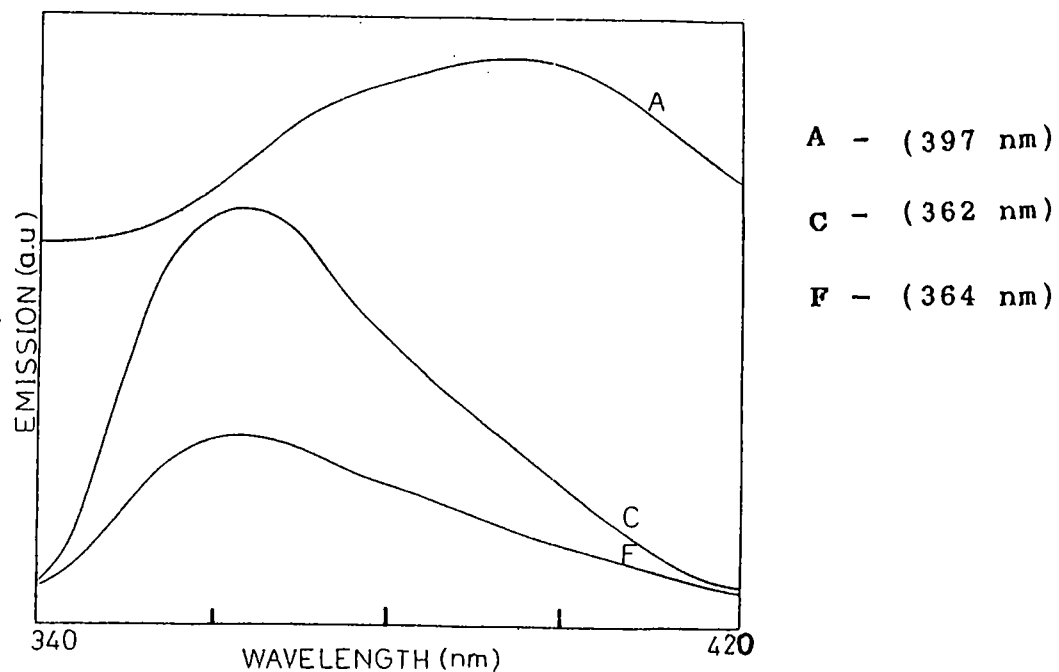


Fig.6.3a. Antistokes fluorescence spectra of Fluorescein in water obtained on (532 nm + 1060 nm) excitation. Peaks are shown in brackets.

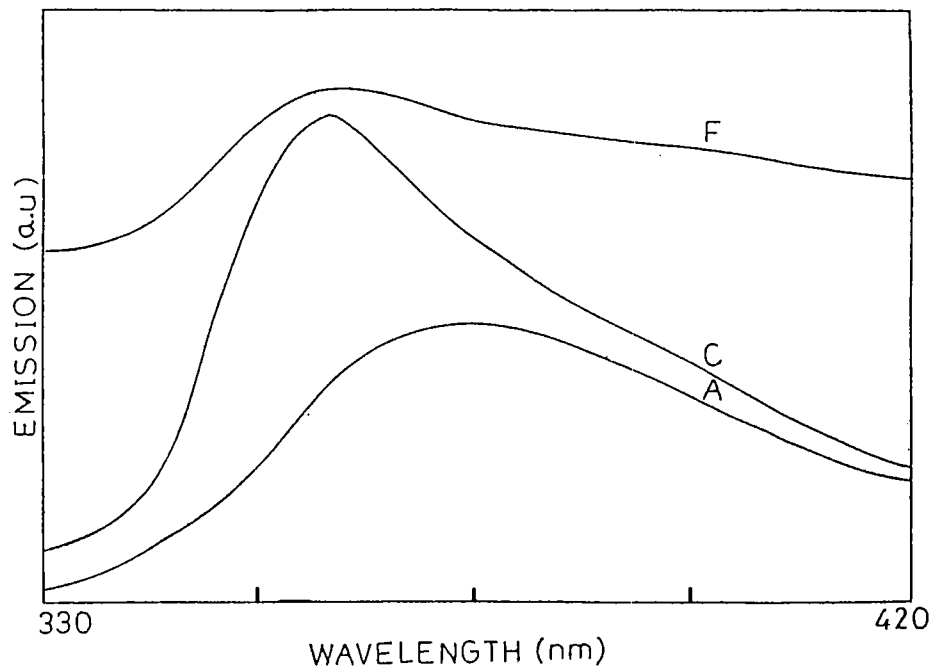


Fig.6.3b. Antistokes fluorescence spectra of Fluorescein in water obtained on 532 nm excitation. Peaks are shown in brackets.

A - 2.5 milli moles/lt (377 nm), C - 0.413 milli moles/lt (362 nm),
 F - 0.034 milli moles/lt (362 nm)

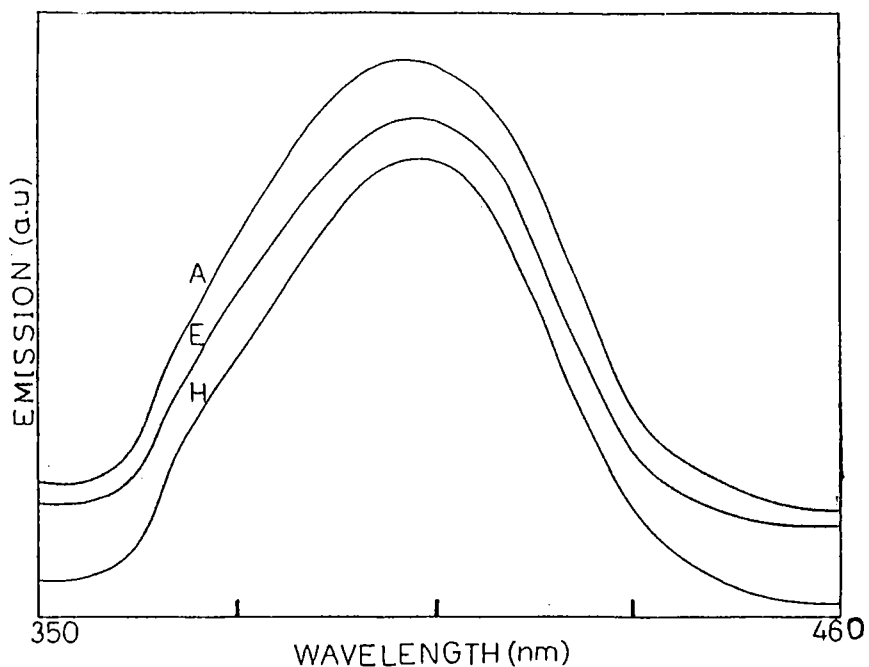


Fig.6.4a. Antistokes fluorescence spectra of DCM in (Ethylene glycol + Benzyl alcohol) obtained on (532 nm + 1060 nm) excitation. Peaks are shown in brackets.

A - 2.3 milli moles/lt (403 nm), E - 0.374 milli moles/lt (402 nm),
 H - 0.04 milli moles/lt (404 nm)

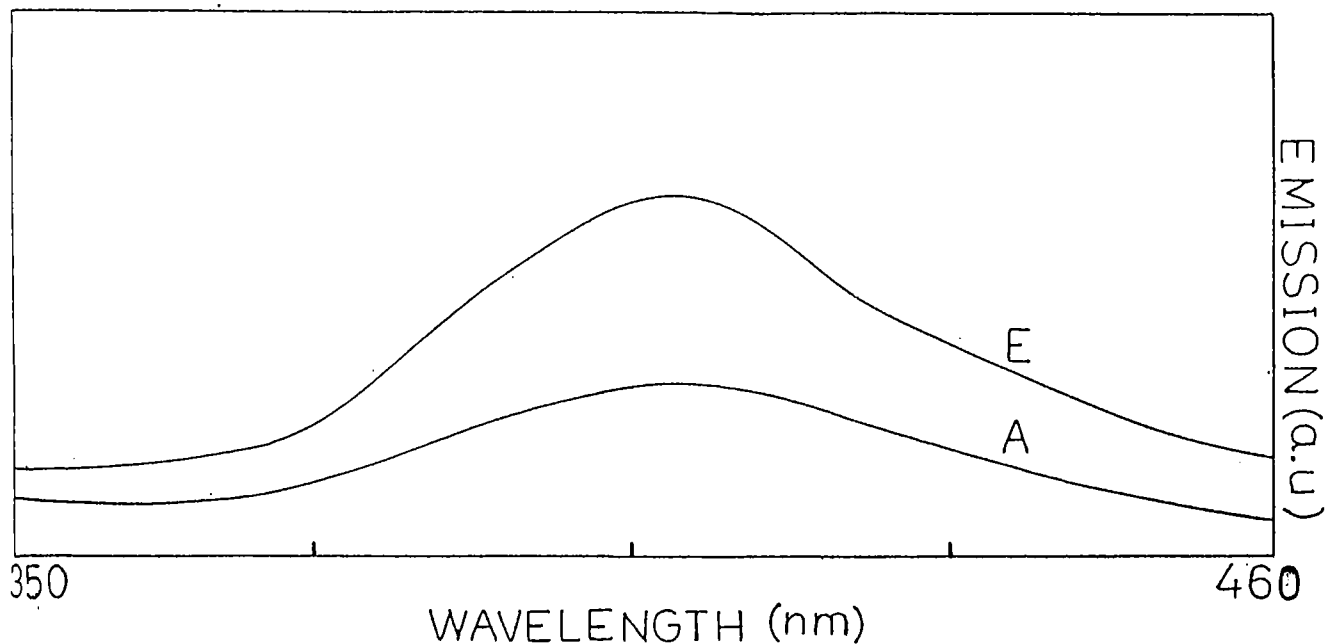


Fig.6.4b. Antistokes fluorescence spectra of DCM in (Ethylene glycol + Benzyl alcohol) obtained on 532 nm excitation. Peaks are shown in brackets.

A - 2.3 milli moles/lt (409 nm), E - 0.374 milli moles/lt (408 nm)

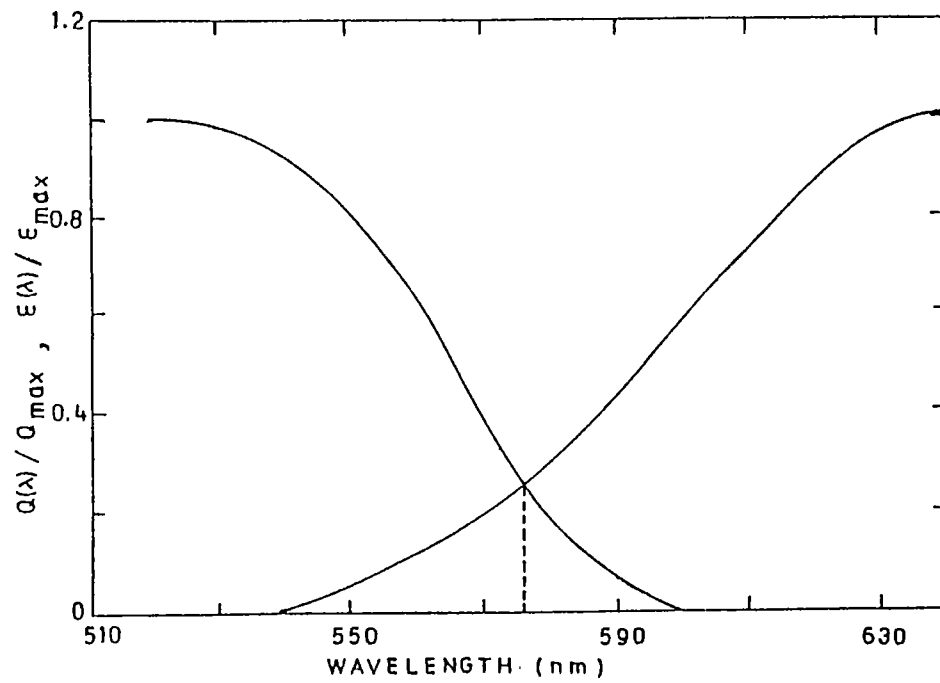


Fig.6.6. The normalised absorption and fluorescence spectra of DCM in (Ethylene glycol + Benzyl alcohol)

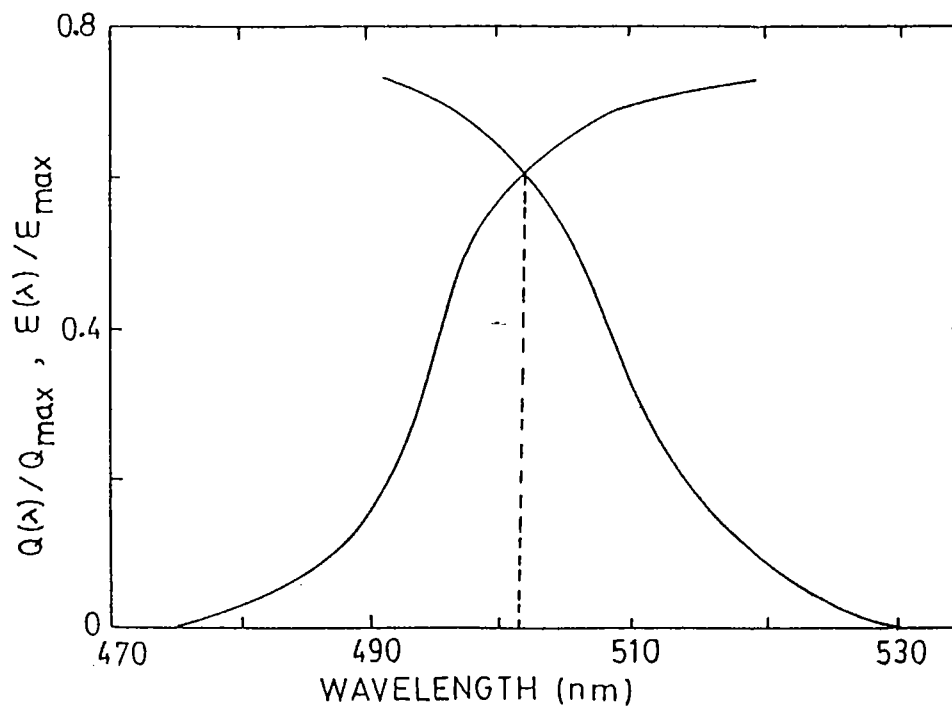


Fig.6.5. The normalised absorption and fluorescence spectra of Fluorescein in water

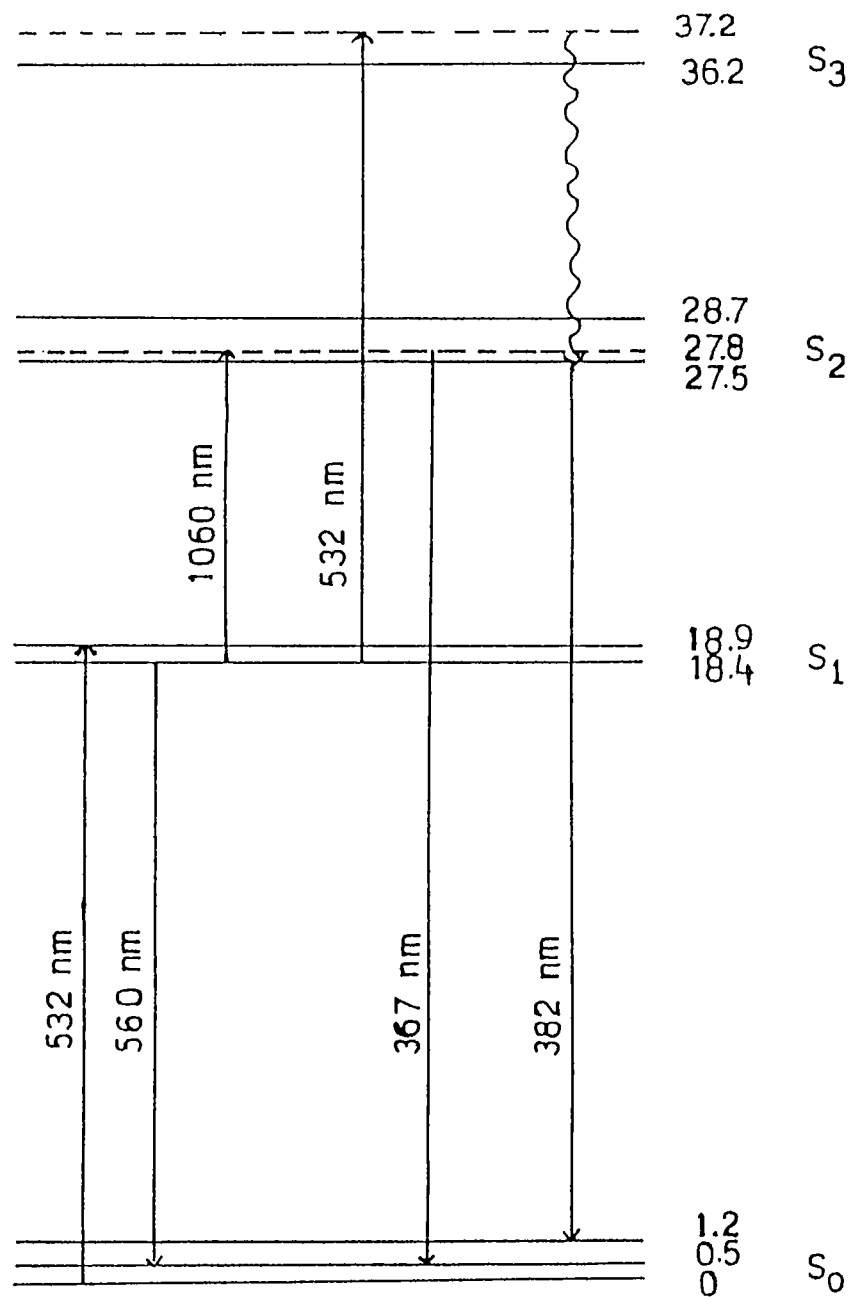


Fig.6.7. Energy level diagram of Rhodamine 6G, calculated from the absorption and fluorescence data. — energy levels corresponding to Franck-Condon maximum radiative transitions; ---- energy levels reached by available laser frequencies. Energy given in 10³ cm⁻¹.

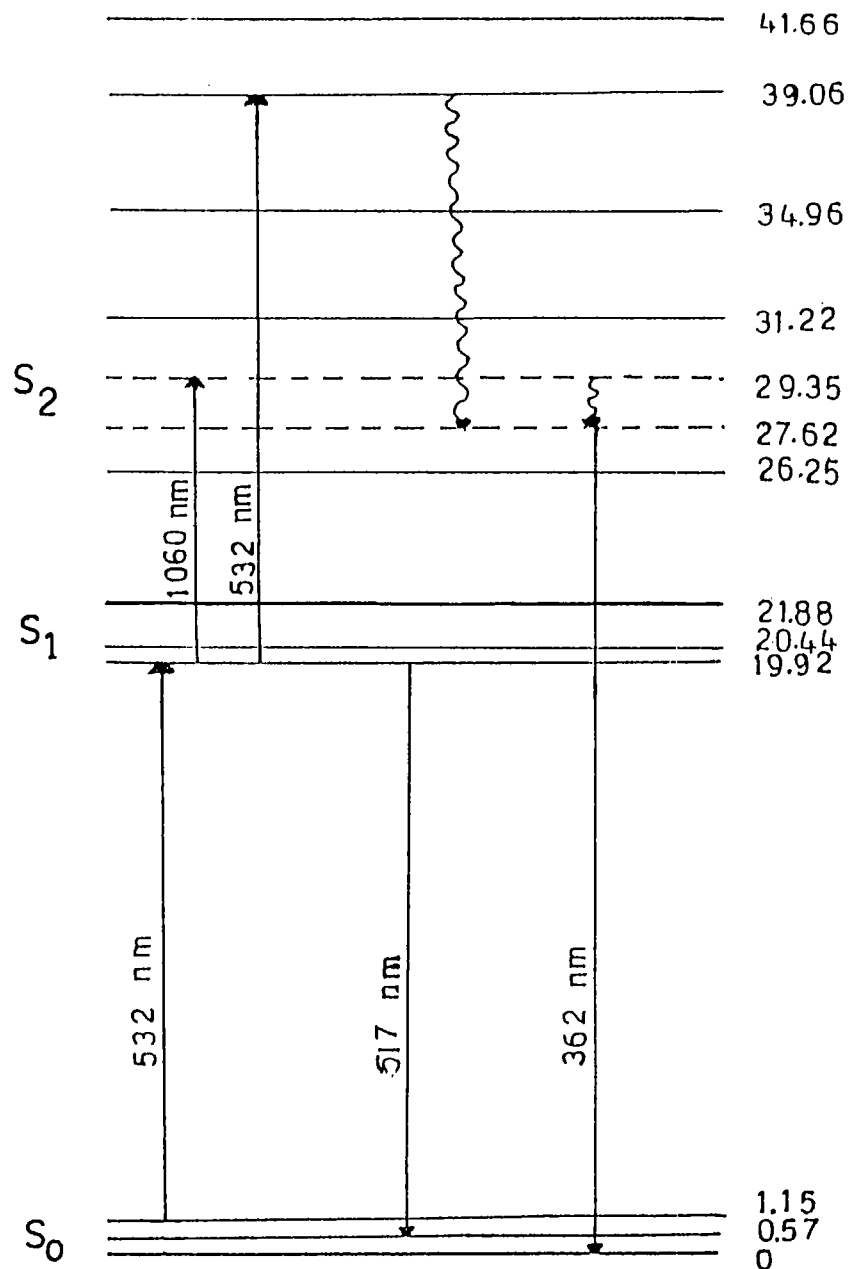


Fig.6.8. Energy level diagram of Fluorescein, calculated from the absorption and fluorescence data. — energy levels corresponding to Franck-Condon maximum radiative transitions; ---- energy levels reached by available laser frequencies. Energy given in 10³ cm⁻¹.

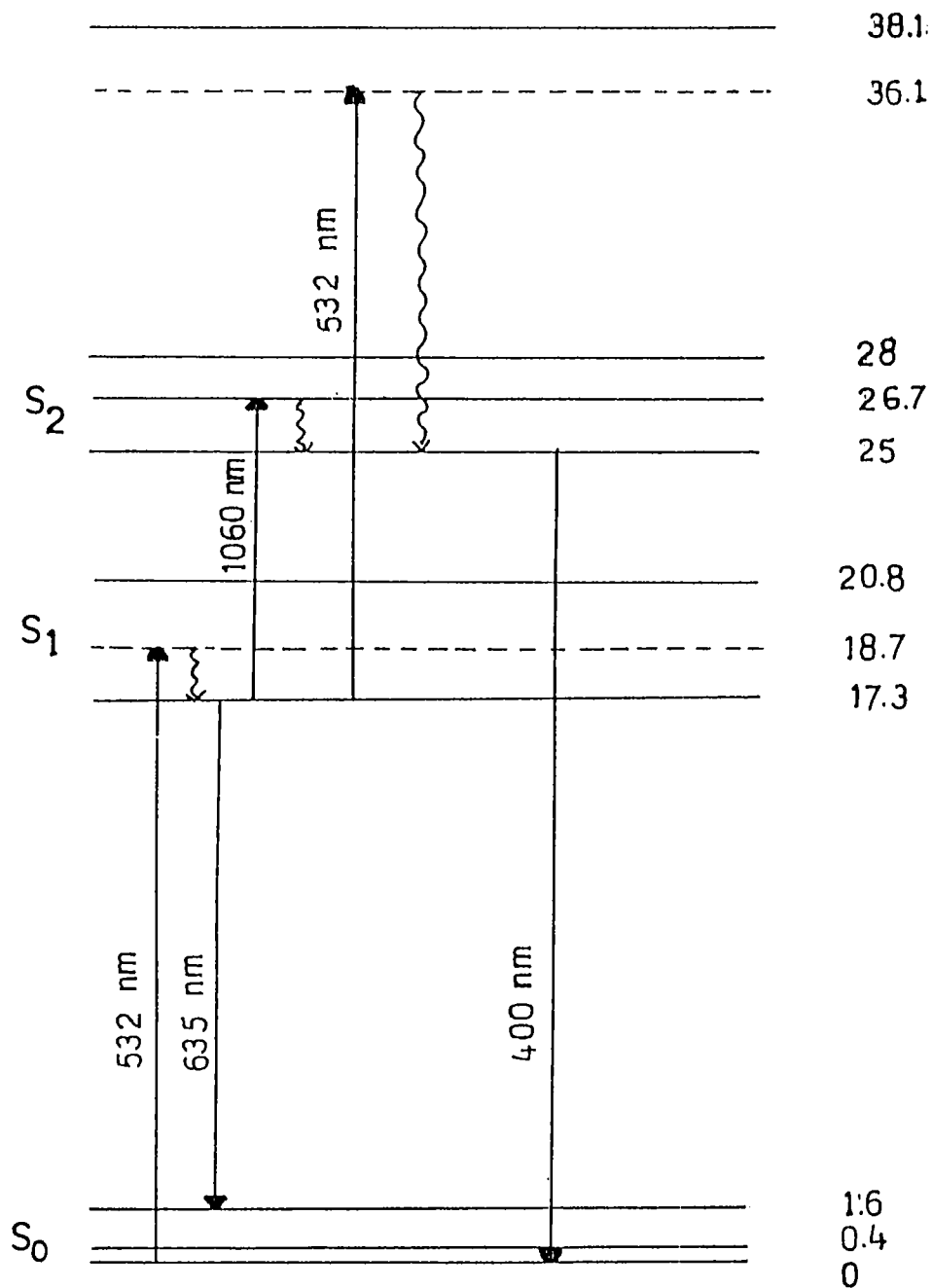


Fig.6.9. Energy level diagram of DCM, calculated from the absorption and fluorescence data. — energy levels corresponding to Franck-Condon maximum radiative transitions; ---- energy levels reached by available laser frequencies. Energy given in 10^3 cm^{-1} .

6.4 DISCUSSION

In all three dyes investigated the $S_0 \rightarrow S_1$ absorption matches with ω_2 excitation to various degrees. Whereas for R6G there is a perfect resonance, for DCM and fluorescien we have effectively a partial pumping only (especially at low concentrations) as seen from the absorbance spectra. Taking the case of usual one-photon absorption at ω_2 frequency, a Franck-Condon "vertical transition" occurs, and vibrational relaxation in S_1 results in a state of lowest energy in that level. The high quantum yield transition from S_1 to the ground state has a lifetime $\approx 10^{-9}$ sec [15]. The difference in energy between the excitation and fluorescence emission maxima results in the observed Stokes shift. The Stokes shift in the case of R6G + water is ≈ 30 nm, that for DCM + (EG:BA) is ≈ 130 nm (fig.6.1b) and for fluorescien + water it is negative in our case, being ≈ 12 nm.

6.4.1. ω_2 excitation

When the pumping is by ω_2 alone, two possibilities exist : one is the direct $S_0 \rightarrow S_3$ TPA and the other is the ESA channel $S_0 \rightarrow S_1 \rightarrow S_3$. From the energy level scheme we note that ESA and two-photon absorption will be enhanced by resonance in R6G as compared to DCM and Fluorescien. However, for R6G it is known that the $S_0 \rightarrow S_1$ and $S_0 \rightarrow S_3$ transition dipole moments are not parallel to each other [13]. (There are no reports in the case of DCM and Fluorescien). To account for the ASF emission at the observed wavelength we assume that from the terminal level S_3 the molecule nonradiatively decays through collisional deactivation and vibrational coupling to one of the vibronic levels of S_2 . In this case S_2 forms an intermediate state during

the relaxation of S_3 . The observed fluorescence is due to $S_2 \rightarrow S_0$ radiative relaxation. (It may be noted that the possibility of $S_3 \rightarrow S_1$ internal conversion also does exist [16].) At high concentrations the emission peaks are found to shift to higher wavelengths for R6G (fig.6.10) and fluorescien (fig.6.11), with the exception of DCM (fig.6.12). Further, the emission peak for DCM is at 410 nm, whereas the average peaks are at 385 nm for R6G and 369 nm for fluorescien. It is interesting to note that in the case of usual fluorescence also, the minimum shift of emission peak from the absorption peak is exhibited by fluorescien and the maximum shift by DCM. The increase in emission wavelength peak with concentration can be understood in terms of reabsorption of emitted ASF quanta and increased collisional deactivation, both prominent at high concentrations. From the curves obtained it is to be concluded that for DCM, these effects are less prominent.

6.4.2. $(\omega_1 + \omega_2)$ excitation

Here most of the pump energy ($\approx 90\%$) comes from ω_1 radiation. The dye molecules are first excited by ω_2 radiation into a vibrational level of the first excited state S_1 . ESA of ω_1 radiation in the S_1 state excites the molecule to a higher vibronic level in S_2 , from which transient ASF occurs to the ground state S_0 . (This ESA process will be most efficient if the transition dipole moments $S_0 \rightarrow S_1$ and $S_1 \rightarrow S_2$ are mutually parallel. For R6G this is known to be so [13]). In the $(\omega_1 + \omega_2)$ excitation case, the average emission peaks are found to be shifted to the shorter wavelength side as compared to ω_2 excitation for R6G (fig.6.10) and DCM (fig.6.12). For fluorescien (fig.6.11), however, the shift is to the longer wavelength side. The emission still corresponds to $S_2 \rightarrow S_0$ transition, but the non-radiative losses are reduced here in R6G and DCM whereas that

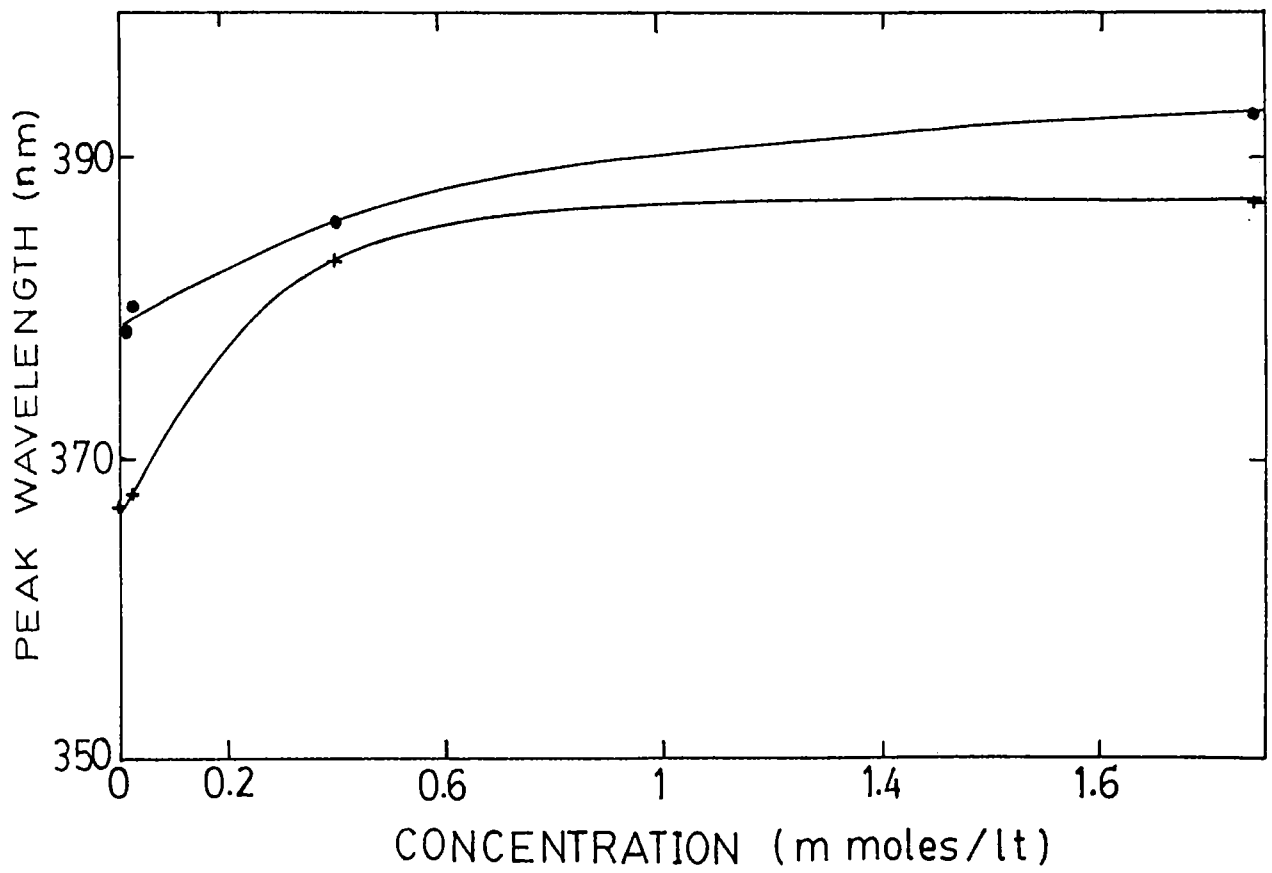


Fig.6.10. Variation of antistokes fluorescence peak wavelength with concentration in Rhodamine 6G

● - 532 nm excitation, + -(532 nm + 1060 nm) excitation

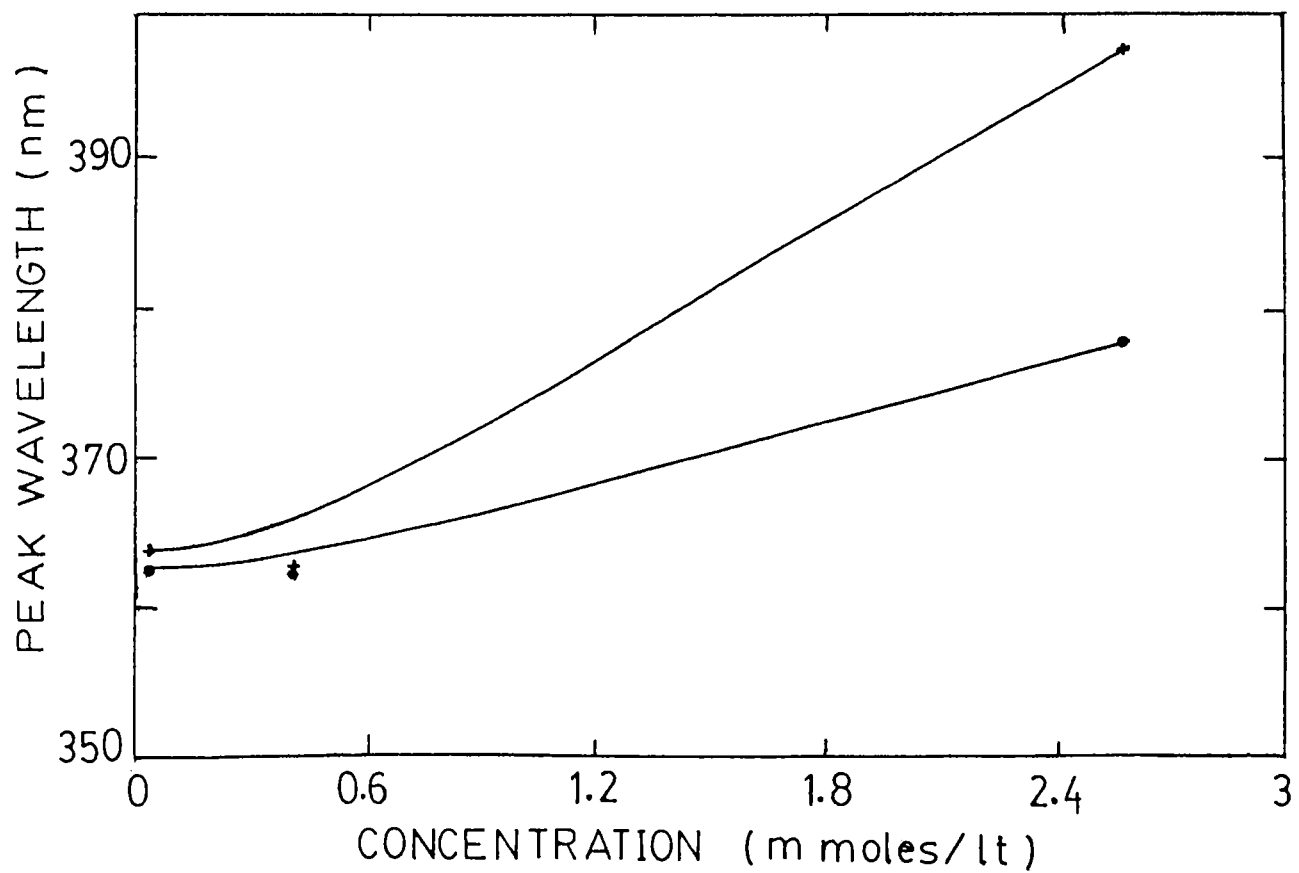


Fig.6.11. Variation of antistokes fluorescence peak wavelength with concentration in fluorescein
+ - 532 nm excitation, • - (532 nm + 1060 nm) excitation

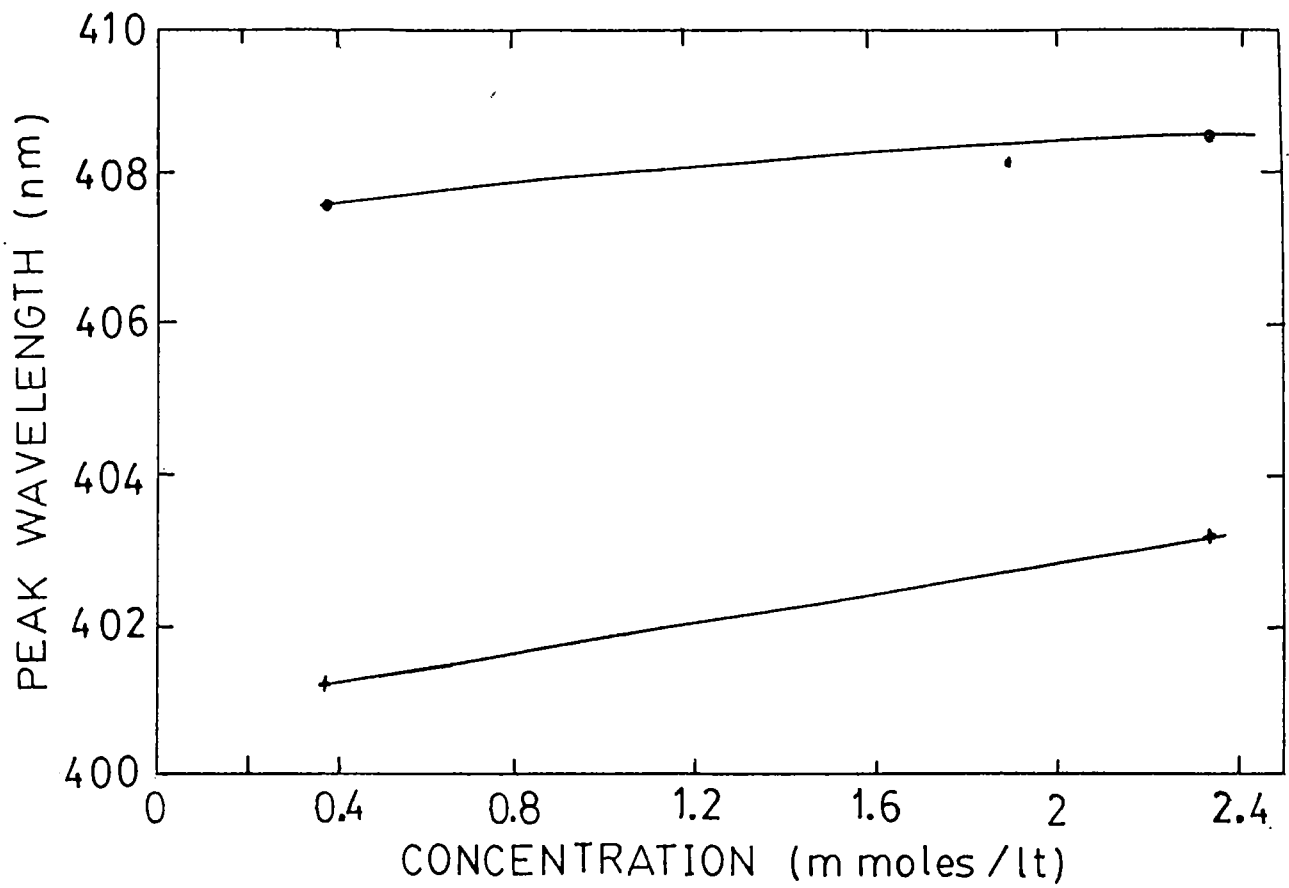


Fig.6.12. Variation of antistokes fluorescence peak wavelength with concentration in DCM

• - 532 nm excitation, + - (532 nm + 1060 nm) excitation

increases for fluorescien. For an exact explanation of this behaviour, further experiments and studies have to be carried out.

6.5 CONCLUSIONS

The dyes R6G, Fluorescien and DCM have been excited to the higher singlet states by multiphoton absorption and ESA at 532 nm and (532 + 1060) nm wavelengths. These phenomena did not show up with pure 1060 nm irradiation. $S_2 \rightarrow S_0$ antistokes fluorescence is observed in both cases. It is seen that the addition of 1060 nm beam to the 532 nm beam increases the intensity of $S_2 \rightarrow S_0$ transition. This may be due to a parallel orientation of the $S_0 \rightarrow S_1$ and $S_1 \rightarrow S_2$ transition dipole moments in DCM and fluorescien, as in R6G. In the case of R6G and Fluorescien, for higher concentrations spectral shifts towards higher wavelengths are seen which are attributed to collisional quenching and reabsorption. For DCM this spectral shift is not observed, indicating a low profile for these effects. The higher excited singlet levels responsible for low quantum yield fluorescence have been calculated for DCM and fluorescien from the recorded absorption and emission spectra. $S_3 \rightarrow S_0$ radiative emission, if at all present, is extremely weak and could not be recorded at the sensitivity of our present experimental set up.

Picosecond time-resolved fluorescence studies will be required for distinguishing the strongly resonance enhanced two-photon absorption from the ESA process. However it is expected that this difference in the excitation pathway will not be manifest in the ASF spectrum, unless the rate of internal conversion greatly exceeds that of vibrational relaxation.

REFERENCES

- [1] Kaiser W and Garrett C G B, Phys.Rev.Lett., 7, 229, 1961
- [2] Goppert-Meyer M, Ann.Physik 9, 273, 1931
- [3] Peticolas W L, Goldsborough J P and Rieckhoff K E, Phys.Rev.Lett., 10, 43, 1963
- [4] Singh S and Stoicheff B P, J.Chem.Phys. 38, 2032, 1963
- [5] Peticolas W L and Rieckhoff K E, J.Chem.Phys., 39, 1347, 1963
- [6] Schafer F P and Schmidt W, IEEE J.Quant.Electron., QE - 2, 357, 1966
- [7] Gillispie G and Lin E, J.Chem.Phys., 65, 2022, 1976
- [8] Orner G C and Topp M R, Chem.Phys.Lett., 36, 295, 1975
- [9] Galanin M D and Chizhikova Z A, Kratk Soobshch.Fiz. 4, 35, 1971
- [10] Porter G and Topp M R, Proc.Roy.Soc.A., 315, 163, 1970
- [11] Rentzepis P M, Chem.Phys.Lett., 2, 117, 1968
- [12] Topp M R, Rentzepis P M and Jones R P, Chem.Phys.Lett., 9, 1, 1971
- [13] Aristov A V and Shevandin V S, Opt.Spectrosc., 44, 276, 1978
- [14] Putcha Venkateswarlu, George M C, Rao Y V, Jagannath H, Chakrapani G and Miahnri A, Pramana J.Phys., 28, 59, 1987
- [15] Strickler S J and Berg R A, J.Chem.Phys., 37, 814, 1962
- [16] Huang C S and Lim E C, J.Chem.Phys., 62, 3826, 1975

CHAPTER - 7

MEASUREMENT OF FLUORESCENCE QUANTUM YIELD USING PHOTOACOUSTIC TECHNIQUE

The knowledge of fluorescence quantum efficiency of organic dyes is essential in selecting efficient dye laser media. The fluorescence quantum yield of a compound is defined as the fraction of photons emitted to that absorbed by the compound. Information about the absolute quantum yield of a material allows one to assess the sensitivity of a proposed fluorimetric determination of materials and the extent of interferences [1,2], judge the suitability of materials as wavelength shifters in optical pumping experiments [1,3] etc. Quantum yields coupled with luminescence data can be used to evaluate the purity of materials [1]. Theoretically, absolute yields are of central importance for studies of radiationless processes in molecules [1,3-5], for correlation of predicted luminescence lifetimes with the observed lifetimes [6], for making assignments of electronic transitions [7] etc.

In this chapter, after a brief discussion of the various techniques employed for the measurement of fluorescence quantum yields, the relative advantages of the recently introduced PA technique are outlined, and results obtained from our experiments in the dye Rhodamine 6G are given.

7.1 CONVENTIONAL METHODS FOR THE MEASUREMENT OF FLUORESCENCE QUANTUM YIELDS

7.1.1 The use of standard scatterers

The modern era of luminescence quantum yield measurements began in 1924 with an article by Vavilov [8]. Basically, Vavilov's technique is a substitution method employing a magnesium oxide scatterer as a standard. The experimental set up (fig.7.1) is as described below. Light from a mercury arc is monochromatised by a filter (F) and focussed to a small spot on an element (C) by a lens. Either a cuvette containing the luminescent material or a plate coated with a freshly prepared layer of magnesium oxide serves as the element. A detector views the scatterer or cuvette normal to the front surface.

First, the cuvette containing the sample is placed at C, and the signal strength of sample luminescence is recorded by the detector. The concentration of the material is normally selected so that 99 % or more of the exciting light is absorbed within a few mm. Then the cuvette is replaced by MgO which scatters the exciting beam and a second detector reading is obtained. One assumes the scatterer to be an ideal diffuse reflector obeying Lambert's cosine law, which states that the intensity of scattered light $I(\phi)$ at an angle ϕ from the normal to the surface is given by

$$\begin{aligned} I(\phi) &= I_0 \cos(\phi) & (0 \leq \phi \leq \pi/2) \\ &= 0 & (\pi/2 \leq \phi \leq \pi) \end{aligned} \tag{7.1}$$

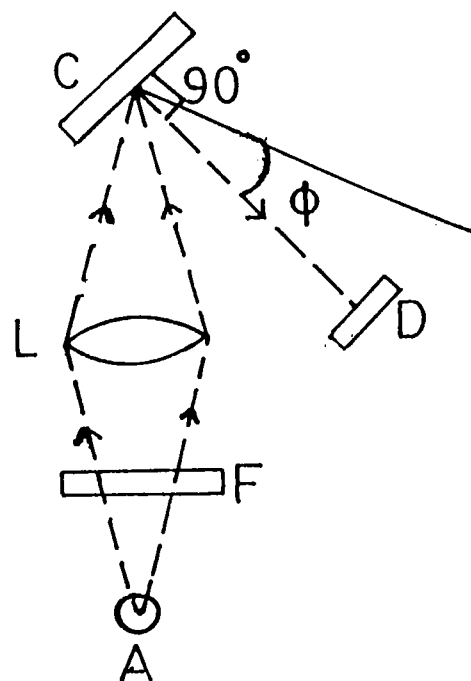


Fig. 7.1. Quantum yield apparatus for use with a magnesium oxide standard (after Melhuish [27,28]).

A - Light source, C - Sample cuvette or magnesium oxide screen,
 D - Detector, F - Filters, L - Focussing lens.
 Dashed lines represent light paths.

$I_0 = I(\phi = 0)$ has units of quanta/sec-steradian. From these data and some additional information the absolute quantum yield can be calculated.

An important development in quantum yield measurement occurred when Weber and Teale [9] introduced solution scatterers instead of substances like magnesium oxide and anthracene. They employed optically dilute colloidal solutions which behave as almost ideal dipole scatterers. The ideal scatterer behaves as if it is a substance which re-emits all the absorbed photons without changing the wavelength, so that it has a scattering efficiency of one.

7.1.2 Comparison with compounds of known quantum yields :

Here a compound of known quantum yield is substituted in the place of a standard scatterer as the reference. The relative measurements mainly fall into two convenient classes; the optically dense and optically dilute methods. At intermediate concentrations the two methods overlap and with suitable corrections yield the same results.

(a). Optically dense measurements :

For this method, the Vavilov configuration (fig.7.1) is adopted, but the scatterer is replaced with a cuvette containing an optically dense solution of a standard compound. The expression for the quantum yield is

$$Q_x = Q_r \left[\frac{K_r}{K_x} \right] \left[\frac{D_x}{D_r} \right] \left[\frac{n_x^2}{n_r^2} \right] \quad (7.2)$$

where Q is the quantum yield of the solution, K is the average detector output per photon over the emission spectrum, D is the detector response and n is the refractive index of the solution. The subscripts x and r refer to the unknown and the standard reference solution respectively. However the use of this equation is restricted to a comparison of compounds which can be excited at a common wavelength. Also, a geometrical correction in the collection of fluorescence emission is necessary to compensate for the changes in the amount of light collected from the cuvette as the sample's optical density varies. The high concentration necessary to obtain total absorption enhances the possibility for concentration-quenching and reabsorption-reemission phenomena, which will significantly distort the calculated quantum yield values.

(b). Optically dilute measurements:

The determination of quantum yields using optically dilute solutions is the most common method employed now-a-days. The technique is relatively simple and the accuracy is better than the other methods.

This measurement rests on Beer's law

$$I_0 B = I_0 \left[1 - 10^{-AL} \right] \quad (7.3)$$

where B is the fraction of light absorbed by the sample, I_0 (quanta/sec) is the intensity of the incident light, A is the absorbance /cm and L (cm) is the path length. If the luminescence intensity for each compound is proportional to $I_0 B$, then the expression for quantum yield becomes [10,11]

$$Q_x = Q_r \left[\frac{B_r}{B_x} \right] \left[\frac{D_x}{D_r} \right] \left[\frac{n_x^2}{n_r^2} \right] \left[\frac{I(\lambda_r)}{I(\lambda_x)} \right]. \quad (7.4)$$

The luminescence intensity is normally proportional to the fraction of light absorbed (B) over a relatively large range (depending upon the geometry) but for high optical densities the luminescence may be confined to the front surface of the cuvette., thereby altering this proportionality.

7.2 CALORIMETRIC METHODS

In addition to the photometric methods described above, calorimetry also has been applied to estimate the fluorescence quantum yields, where the absolute energy yields are obtained from temperature changes during irradiation. The temperature rise of an irradiated luminescent sample is compared with the rise in temperature of a nonluminescent material of similar optical density subjected to the same optical pumping. Since the nonluminescent sample has a zero radiative energy yield, the ratio of the heating of the two samples gives the fraction of the absorbed energy which is lost by nonradiative processes in the luminescent sample, that is, the complement of the luminescence

energy yield. To convert energy yields to quantum yields one needs the emission spectrum of the sample and the frequency distribution in the exciting beam. The two yields are related by,

$$Q_q = Q_e \frac{\int \bar{\nu} E(\bar{\nu}) d\bar{\nu} / \int E(\bar{\nu}) d\bar{\nu}}{\int \bar{\nu} F(\bar{\nu}) d\bar{\nu} / \int F(\bar{\nu}) d\bar{\nu}} \quad (7.5)$$

where Q_q is the quantum yield, Q_e is the energy yield, and $E(\bar{\nu})$ and $F(\bar{\nu})$ are the unnormalised spectral distributions of the exciting and emitted light (quanta/sec cm^{-1}) respectively. Highly accurate spectra are not necessary, since relatively large errors in these spectra produce only small errors in the quantum yield. If the exciting light extends over a wide wavelength range and the solution does not absorb all of the exciting light, then the absorption spectrum of the sample also is needed.

Among the problems of the calorimetric method, reabsorption is one of the worst, for the relative insensitivity of the usual temperature sensors and the large blanks force one to choose a strongly absorbing sample. The problem is especially critical when absorption-emission overlap is pronounced. Advantages of the method are that corrections for experimental geometry, refractive index changes (the refractive index affects the measured yield indirectly by its effect on the amount of reabsorption in the cuvette) and polarization effects are largely eliminated.

7.3 PHOTOACOUSTIC METHOD

Even after the various corrections for system geometry, re-absorption, polarization etc., the accuracy of the quantum yield values obtained from photometric and calorimetric measurements is rather poor [12]. Photoacoustic (PA) and thermal lens techniques which are variations of the calorimetric technique have been recently applied very successfully for the determination of absolute quantum yields [13-17]. This techniques are free from the complications of photometry, and fast measurement is possible. Further, very weak to very strong absorbers can be identically treated in the experimental set-up.

When a material is optically excited it decays to the ground state by fluorescence and/or by heat generation. The measurement of the absolute optical energy absorbed W_0 and the absolute heat energy generated W_{heat} provides the fluorescence quantum efficiency ϕ for a simple two-level system,

$$\phi = [W_0 - W_{\text{heat}}] / W_0 \quad (7.6)$$

In measuring quantum yield by equation (7.6) the absolute heat energy is involved; however, the PA signal is only proportional to the modulated heat generated, with the proportionality constant usually poorly known. To avoid this difficulty the PA measurement is made twice, first with the desired luminescence quantum yield ϕ_f and secondly with the quantum yield altered in a known way. This provides two equations with two unknowns and so ϕ_f can be solved.

There are two methods for evaluating ϕ_f . The first is a quenching method, which has been employed by several workers [18-20]. Here, after taking the PA reading on the pure fluorescing sample first, its fluorescence is quenched by the addition of a small concentration of an efficient 'quencher' molecule, and the second reading is taken. In this method care should be taken such that only ϕ_f , and no other physical or chemical property of the sample is affected by the addition of the quencher.

The second method relies on the possibility of optically exciting higher excited states S_n that decay non radiatively to the lowest state in S_1 . This higher excitation method was first proposed and demonstrated by Rockley and Waugh [21]. Depending on the wavelength of excitation, a dye molecule can be excited to the lowest excited singlet state (S_1) with energy E_1 or to higher singlet states S_n , with energies E_n . For every absorbed photon of energy E_n the fraction of energy corresponding to $\frac{E_n - E_1}{E_1}$ will appear as heat coming from the sample. A fraction $(1 - \phi_f)$ of all the energy absorbed by $S_0 \rightarrow S_1$ transitions also will appear as heat, where ϕ_f is the fluorescence quantum yield. PA can be used to measure the heat signals. The following equations are used in the evaluation of quantum yield :

$$I^{PAS}(S_n) = K \left[E_n - E_1 + E_1 (1 - \Phi_f) \right] \quad (7.7)$$

$$I^{PAS}(S_1) = K \left[E_1 (1 - \Phi_f) \right] \quad (7.8)$$

where E_n and E_1 are known quantities, and $I^{\text{PAS}}(S_n)$ and $I^{\text{PAS}}(S_1)$ are the measured quantities.

7.4 FLUORESCENCE QUANTUM YIELD MEASUREMENT OF RHODAMINE 6G USING PULSED PHOTOACOUSTIC TECHNIQUE

Due to the mutual complementarity of PA and luminescence phenomena, the photoacoustic signal is sensitive to the total fluorescence in laser dyes which means that any change in the emission characteristics will influence the PA signal. The variations in quantum yield of highly fluorescent dyes can hence be effectively studied by this method because of the relatively large changes occurring in PA signal compared to that in fluorescence output [22].

According to the discussion of Malkin and Cahen [23], for fluorescent samples with quantum yield ϕ_f , the PA signal $P(\lambda)$ can be written as

$$P(\lambda) = \alpha(\lambda) \left[1 - (\phi_f / \lambda_f) \lambda \right] \quad (7.9)$$

where λ and λ_f are the excitation wavelength and the fluorescence peak wavelength respectively. α is the fraction of light absorbed in that part of the sample that participates in the generation of the PA signal. In the case of a totally fluorescence quenched sample we can consider the entire excitation energy to be converted to non-radiative relaxation processes and hence

$$P(\lambda) = P_{\alpha}(\lambda) \stackrel{-}{=} \alpha(\lambda) \quad (7.10)$$

such that

$$\frac{P}{P_{\alpha}} = 1 - (\phi_f/\lambda_f)\lambda \quad (7.11)$$

and if λ_f is known, ϕ_f can be obtained directly using the equation

$$\phi_f = \frac{\lambda_f}{\lambda} \left[1 - \frac{P}{P_{\alpha}} \right] \quad (7.12)$$

7.5 EXPERIMENTAL SET UP

The schematic experimental set up for PA measurement is as given in chapter 2. The IR eliminated second harmonic output (532 nm) of the frequency doubled Q-switched pulsed Nd:YAG laser is the exciting light source. A stock solution (10^{-3} moles/lit) is prepared by dissolving commercial laser grade R6G (exciton) in doubly distilled water and samples of lower concentration (10^{-4} - 10^{-6} moles/lit) prepared by subsequent dilution. The laser beam is allowed to pass through the PA cell containing the sample solution. (The description of the PA cell and the transducer is given in chapter 2) The PA signal generated in the sample solutions is detected by the transducer, and fed to a digital storage oscilloscope. The amplitude of the first peak of the PA profile is averaged over thirty successive pulses each time, and measurements are taken. The time delay between the laser pulse and the first peak is found to be 16 μ s.

To record the fluorescence, the laser beam is allowed to fall on a cuvette that contains the same solutions as in the PA cell. Fluorescence is collected by a convex lens ($f=5$ cm) and directed into a 0.5 m Jarrell-Ash monochromator. A filter checks the entry of the scattered laser radiation into the monochromator. The emission is wavelength scanned in the region 530 - 630 nm and the optical intensity is detected by a photomultiplier tube. The signal from the photomultiplier tube is suitably gated (gate width= $10 \mu\text{s}$, gate delay= $40 \mu\text{s}$) and averaged using a gated integrator and boxcar averager system, and the output is fed to a chart recorder. The integrated fluorescence intensity is calculated from the area under the curve of the emission spectrum for each sample.

7.6 RESULTS AND DISCUSSION

The amplitudes of PA signal and fluorescence emission are plotted against concentration in the range of 10^{-6} moles/lit to 10^{-4} moles/lit in fig.7.2. Fig.7.3 shows the variation of the calculated quantum yield with concentration of the R6G solutions.

From fig.7.2 it is seen that at the highest concentration used here the PA signal shows a saturation behaviour. Correspondingly, the fluorescence emission is very weak due to concentration quenching. PA signal corresponding to this concentration gives the value of $P(\alpha)$. The calculated value of the quantum yield at the lowest concentration studied (3.2×10^{-6} moles/lit) is 0.9 ± 0.02 and the yield decreases rapidly with concentration. Earlier estimates have shown that for selected concentrations, aqueous solutions of R6G has a quantum efficiency of 92 % [24], 96 % \pm 2 % [18] etc. The quantum yield intimately depends on the environment of the fluorescing molecule, and

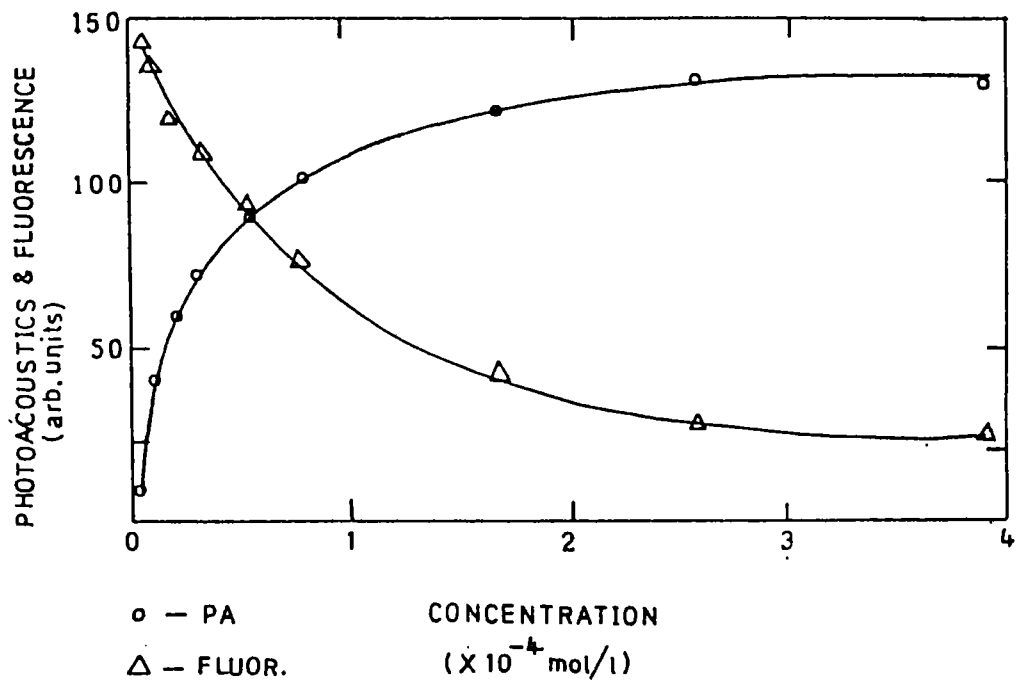


Fig.7.2. Variation of fluorescence intensity and PA signal amplitude with concentration for rhodamine 6G in water.

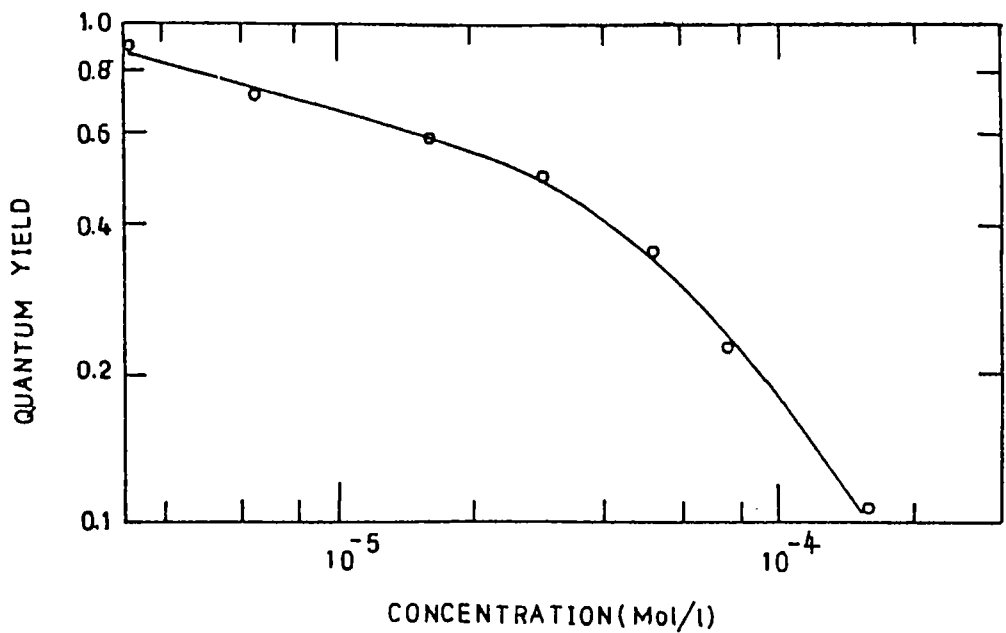


Fig.7.3. Variation of quantum yield of Rhodamine 6G in water with concentration

processes like internal non radiative conversion ($S_1 \longrightarrow S_0$), intersystem crossing ($S_1 \longrightarrow T_1$), excited singlet state absorption and aggregation of dye molecules are strongly dependent on the solvent characteristics as well as on concentration [25]. The role of excitation source also is important in this respect, as many of the above phenomena become significant in the medium when the input energy exceeds a certain critical value. It has been known that R6G forms stable ground state dimers and higher aggregates in aqueous solution, and the decrease of R6G fluorescence quantum efficiency at higher concentrations is caused by Forster-type energy transfer (electric dipole-electric dipole interaction) to dimers [26]. The equilibrium between monomers and dimers shifts to the side of the latter with increasing concentration and at 10^{-4} moles/lit, the dimerization of dyes like RhB and R6G is severe enough to prevent laser action [25] unless a deaggregating agent like hexafluoroisopropanol or ammonyx LO is added to the solution. In the present case no such deaggregating agents were added. Apart from a small variation, the quantum yield is almost independent of concentration in the 10^{-6} moles/lit region, and the rapid decrease in ϕ_f at higher concentrations (fig.7.3) can be attributed mainly to the formation of dimers and higher aggregates which have zero or small fluorescence quantum yield.

7.7 CONCLUSIONS

The fluorescence quantum yield in aqueous solutions of the dye R6G of various concentrations has been measured using the pulsed photoacoustic technique. The technique is very sensitive

for evaluating absolute fluorescence quantum yield in cases where the fluorescence efficiency is very low. This enables one to extend the dynamic range of the measurement of fluorescence quantum yield as a function of concentration. The simplicity of instrumentation, ease of measurement and the unambiguous nature of results clearly establish the PA technique as an accurate method for the estimation of fluorescence quantum yields.

REFERENCES

- [1] Parker C A, "Photoluminescence of Solutions," Elsevier Publishing Co., New York, N.Y., 1968
- [2] Dagnall R M, Pratt S J, Smith R and West T S, *Analyst*, 93, 638, 1968
- [3] Calvert J G and Pitts J N Jr., "Photochemistry," Wiley, New York, 1966
- [4] Henry B R and Kasha M, *Ann.Rev.Phys.Chem.*, 19, 161, 1968
- [5] McGlynn S P, Azumi T, and Kinoshita M, "Molecular Spectroscopy of the Triplet State," Prentice-Hall, Inc., Englewood Cliffe, N.J., 1969
- [6] Strickler S J and Berg R A, *J.Chem.Phys.*, 37, 814 1962
- [7] Lytle F E and Hercules D M, *J.Amer.Chem.Soc.*, 91,233, 1969
- [8] Vavilov S I, *Z.Phys.*, 22, 266, 1924
- [9] Weber G and Teale F W J, *Trans.Faraday Soc.*, 53, 64, 1957
- [10] Drushel H V, Sommers A L and Cox R C, *Anal.Chem.*,35,2166,1963
- [11] Parker C A and Rees W T, *Analyst*, 85, 587, 1960
- [12] Demas J N and Crosby J A, *J.Phys.Chem.*, 75, 991, 1971
- [13] Adams M J, Highfield J G and Kirkbright G F, *Anal.Chem.* 49, 1850, 1977
- [14] Adams M J, Highfield J G and Kirkbright G F, *Analyst*, 106,850, 1981
- [15] Krashennnikov A A and Shablya A V, *Opt.Spectrosc.*, 52, 159, 1982
- [16] Brannon J H and Magde D, *J.Phys.Chem.*, 82, 705, 1978
- [17] Shen J and Snook R D, *Chem.Phys.Lett.*, 155, 583, 1989
- [18] Lahmann W and Ludewig H J, *Chem.Phys.Lett.*, 45, 177, 1977.
- [19] Hall L M, Hunter T F and Stock M G, *Chem.Phys.Lett.*, 44, 145, 1976

- [20] Starobogatov I O, Opt.Spectrosc., 42, 172, 1977
- [21] Rockley M G and Waugh K M, Chem.Phys.Lett., 54, 597, 1978
- [22] David Cahen, Halm Garty and Ralph S Becker, J.Phys.Chem., 84, 3384, 1980
- [23] Malkin S and Cahen D, Photochem.Photobiol., 29, 803, 1979
- [24] Snavely B B in Dye lasers, 1973 ed. F.P.Schafer (Berlin:Springer)
- [25] Drexhage K H in Dye lasers, 1973 ed. F.P.Schafer (Berlin:Springer)
- [26] Penzkofer A and Leupacher W, J.Lum., 37, 61, 1987

CHAPTER -8

GENERAL CONCLUSIONS

Tunable, monochromatic light sources of the conventional type have been powerful tools in the study of the energy spectrum of matter for a long time. From measured quantities such as the oscillator strength, lifetime of excitations, polarization states of emitted radiation etc. many properties of stationary eigenstates of matter have been explored by optical techniques in the past. Most of this work was performed in the realm of "linear optics" which in general refers to the situation where only one photon interacts with an electron of the system at a time. Although linear optics was tremendously successful in helping to understand matter, its limitations were equally obvious. The discovery of laser in 1960 brought about a change in the understanding of light-matter interactions because the striking phenomena of nonlinear optics could be observed only at high power density levels.

The field of nonlinear optics embodies those physical phenomena which are based on the nonlinear response of a medium to applied electromagnetic fields, with some of the frequencies lying in the infrared, visible, ultraviolet or x-ray region of the spectrum. The electric polarization or the induced electric current density may, for example, be a quadratic, cubic or even an exponential function of the electric field amplitudes. From the study of such optical nonlinearities in matter a branch of research has emerged which is generally referred to as nonlinear

spectroscopy, which is associated with the behaviour of the nonlinear susceptibilities in the different regions of the spectrum of the system under investigation.

This thesis is the outcome of an attempt to identify and characterize one of the nonlinear optical phenomena, viz. higher order absorptions (with emphasis to two-photon absorption) stimulated in organic media under high energy laser excitation. The choice of laser dyes for our investigations rests on the importance of these materials in dye laser physics and technology. The large dye molecules possess broad absorption and emission bands and the matching of energy levels with the available laser wavelengths (532 nm and 1060 nm) make them particularly suitable for the present studies. We have successfully combined the recently developed technique of high sensitivity pulsed photoacoustics to higher order absorptions taking place in dye solutions, for directly observing nonradiative relaxations from higher excited states in dye media. For verifying the relative merits and demerits of the PA technique, experiments have been conducted to observe the same by recording the nonlinear fluorescence emitted by the samples. From the present studies we have arrived at the following conclusions:

(a). In a typical dye laser, multiphoton absorptions ($S_0 \longrightarrow S_n$) occur in the dye during optical excitation at the pump wavelength, in addition to the $S_0 \longrightarrow S_1$ OPA. This in turn results in the generation of nonlinear fluorescence and PA signals in the medium.

(b). The transitions $S_n \longrightarrow S_1$ occurring in a typical dye molecule are strongly non-radiative in nature, and the S_n state lifetimes are extremely small (\approx ps). Consequently the fluorescence emitted by higher excited states will be very weak and submerged in the strong $S_1 \longrightarrow S_0$ dye fluorescence, requiring high sensitivity fluorescence instrumentation for observing this antistokes emission. Further, various higher excited states emit in different wavelength regions, thereby necessitating more sophistication and complexity of the equipment.

(c). On the other hand, most of the energy of the S_n states is dissipated through the nonradiative channel leading to large PA signals, and a relatively simple PA set up can readily detect and measure these signals which show a nonlinear dependence on the pump intensity. With the help of absorption spectra and the calculated nonlinearity parameter, the levels of emission also can be immediately identified. The same acoustic detector can be used for observing different orders of nonlinear absorption. Because of the mutual complementarity of PA and fluorescence, as fluorescence gets weaker, PA will become correspondingly stronger.

(d). Depending on the pump wavelength and the sample under analysis, either PA or ASF can act as a zero background technique. For example, in the 532 nm excitation case the background acoustic noise from the solvents is negligible and in the 1060 nm excitation case the ASF signal is practically free of a noise background. Hence ASF is preferred for higher order absorption analysis at infrared wavelengths where the solvent is

^ G 5366 -

nonfluorescing. However PA is obviously better when the pump wavelength is sufficient enough to raise the molecule to its fluorescence level or higher.

(e). The unique advantages offered by the PA technique in the estimation of fluorescence quantum yields have been demonstrated by measuring the same in various concentrations of Rhodamine 6G dye.

(f). In spite of its various inherent difficulties, ASF still has the advantage that it gives the spectrum of emission on the energy (wavelength) scale, whereas in PA this information is not available. Hence it is the discretion of the experimenter to decide in favour of either of these techniques. Of course the choice will depend on various factors like the laser wavelengths one can use, nature of the samples to be analyzed etc.

The investigation of higher order absorptions forms a potential branch of nonlinear optics. The relatively young subject of nonlinear optics, the study of how light interacts with and propogates through matter, is so scientifically fertile and technologically promising that it is destined to be one of the most important areas of science in the years to follow.